

2018-04-18

Design and Implementation of a Magnitude Only Bio-Impedance Analyzer

Al-Ali, Abdulwadood Abdullah Abdulwadood

Al-Ali, A. A. (2018). Design and Implementation of a Magnitude Only Bio-Impedance Analyzer (Master's thesis, University of Calgary, Calgary, Canada). Retrieved from <https://prism.ucalgary.ca>. doi:10.11575/PRISM/31812

<http://hdl.handle.net/1880/106525>

Downloaded from PRISM Repository, University of Calgary

UNIVERSITY OF CALGARY

Design and Implementation of a Magnitude Only Bio-Impedance Analyzer

by

Abdulwadood Abdullah Abdulwadood Al-Ali

A THESIS

SUBMITTED TO THE FACULTY OF GRADUATE STUDIES
IN PARTIAL FULFILLMENT OF THE REQUIREMENTS FOR THE
DEGREE OF MASTER OF SCIENCE

GRADUATE PROGRAM IN ELECTRICAL AND COMPUTER ENGINEERING

CALGARY, ALBERTA

APRIL, 2018

© Abdulwadood Abdullah Abdulwadood Al-Ali 2018

ABSTRACT

The increasing interest in the bio-impedance analysis in various fields has increased the demand for portable and low-cost impedance analyzers that can be used in the field. Simplifying the hardware is crucial to maintaining low-cost and portability, but this is not an easy task due to the need for accurate phase and magnitude measurements.

This thesis proposes a new measurement technique that replaces the need to measure the phase by using a software algorithm to extract the phase from the magnitude information.

The algorithm which is based on a modified Kramers-Kronig transforms was implemented and tested first using MATLAB, where error and noise analysis on the algorithm were done. Furthermore, the algorithm was written using a python code, and a full Bio-impedance measurement system was proposed to be used for fruit quality control which is receiving increasing attention as an important application of bio-impedance measurements, for being a non-invasive technique.

The Final design which was implemented on a printed circuit board (PCB), had a final cost of around \$95 CAD and drew a maximum current of around 88mA which satisfies the requirement of a low-cost and low-power device respectively. The device was then tested with passive components and several fruit samples to show that it can effectively monitor fruit samples impedance in the range $100\Omega - 280k\Omega$, and a frequency range 1 Hz-10 MHz which is higher than any other work in the literature. The proposed portable bio-impedance analyzers were then used to study the ageing effect of some strawberries samples on their bio-impedance, and the results showed that the device could be used in such an application.

ACKNOWLEDGMENTS

This thesis has been possible because of the guidance and support offered by many people. I would like to take this opportunity to give my sincere thanks, first and foremost, to my supervisor Prof. Brent Maundy. Thank you for giving me the chance to pursue this work and to contribute something to this field. It wouldn't have been possible without your time and guidance. I couldn't have asked for a better supervisor, and I will always be grateful for the chance of working with you.

I would also like to take this moment and thank Prof. Ahmed Elwakil from the Department of Electrical and Computer Engineering at the University of Sharjah. Thank you for believing in me and my abilities and introducing me to Prof. Brent Maundy. Your enthusiasm and advice have definitely shaped my approach to research and how important I view this field. I will always be grateful for all the discussions we had since the days when I was doing my BSc at the university of Sharjah.

I will be always indebted to my parents, whose constant and unwavering support made my pursuit of this all possible. Thank you for allowing me the chance to complete my graduate studies and never making me doubt my decision of traveling to study abroad.

I cannot thank my cousin and her husband, Marwa Kassim and Ehab Hussain enough. Your hospitality and support during the course of my graduate studies made me feel like I was home.

I would also like to thank the Natural Sciences and Engineering Research Council (NSERC, Canada). This work wouldn't have been possible without their financial support.

For my parents and my grandparents

Thank you.

TABLE OF CONTENTS

Abstract	i
Acknowledgments	ii
Dedication	iii
Table of Contents	iv
List of Tables	vii
List of Figures	vii
List of Abbreviations	xi
 1 Introduction	 1
1.1 Research Objective	1
1.2 Thesis Overview	3
 2 Impedance measurement	 4
2.1 Introduction	4
2.2 Electrochemical Impedance Spectroscopy (EIS)	5
2.3 Bio-Impedance Analysis	6
2.4 Bio-Impedance Analysis Applications	6
2.4.1 Biomedical	7
2.4.2 Agriculture	7
2.4.3 Food Characterization	7
2.5 Electrical modelling of Biological Tissues	8
2.6 EIS Measurement techniques	9
2.6.1 Transient Measurements	10
2.6.2 Mixed/White Noise Signals	11
2.6.3 Frequency Sweep	11
2.7 Impedance Analysis Instruments	12
2.7.1 Commercial Impedance Analyzers	12
2.7.2 Impedance Analyzers Designs in the Literature	13
2.8 Summary	16

3	Phase Extraction Algorithm	18
3.1	Introduction	18
3.2	Background	19
3.3	The proposed algorithm	21
3.4	Algorithm testing	23
3.4.1	Simulated Data	23
3.4.1.1	Parameter tuning	25
3.4.1.2	The Tails Problem	27
3.4.1.3	Noise analysis	31
3.4.2	Cherry Tomato Experimental Data	31
3.5	Summary	37
4	Proposed Impedance Analyzer Design and Implementation	38
4.1	Introduction	38
4.2	The magnitude detection	38
4.2.1	Signal generation	39
4.2.2	DC Cancellation	40
4.2.3	Amplitude control	41
4.2.4	Magnitude Sensing Amplifier	42
4.2.5	Analog to digital conversion (ADC)	43
4.3	Processing and Control	44
4.3.1	Microcontroller code	44
4.3.2	Python Code	44
4.3.3	Calibration Process	48
4.4	Implementation	49
4.4.1	Analog and Digital Components	51
4.4.2	Printed Circuit Board (PCB)	52
4.4.3	Power Consumption	54
4.4.4	Total Cost	55
4.5	Summary	56
5	Experimental Results	57
5.1	Introduction	57
5.2	Breadboard Tests	57
5.2.1	Passive Components Measurements	58
5.2.2	Apple Measurements	61
5.3	PCB Testing	64

5.3.1	Passive Components Measurements	64
5.3.2	Strawberry Measurements	68
5.4	Application to Strawberry Ageing	68
5.5	Summary	70
6	Conclusions and future work	73
6.1	Conclusion	73
6.2	Future Work	74
6.3	System Vision	75
	BIBLIOGRAPHY	77
A	Appendix 1	89

LIST OF TABLES

2.1	The precision N4L PSM 1735 Impedance analyzer models	13
3.1	Comparison of the parameters of a double-dispersion Cole-Cole model fitting of two tomato samples. Reprinted by permission from [Springer Nature and Copyright Clearance Center]: [Springer Nature] [Circuits, Systems, and Signal Processing] [Extraction of phase information from magnitude-only bio-impedance measurements using a modified Kramers–Kronig transform, A. Al-Ali, A. Elwakil, B. Maundy, and T. Freeborn], [2017].	37
4.1	Power consumption	55
4.2	Cost of a single unit	56
5.1	Comparison of the parameters of a double-dispersion Cole-Cole model fitting of the two Apple samples	61
5.2	Comparison of the parameters of a double-dispersion Cole–Cole model fitting of sample 4 results over the 3 days	72
6.1	Proposed design specifications	74

LIST OF FIGURES

1.1	Block diagram of the experimental setup	2
2.1	Electrode configurations (a) two electrodes, (b) three electrodes and (c) four electrodes	9
2.2	Commercial Impedance Analyzers (a) N4L PSM 1735 (b)BAS-Zahner IM6	14
2.3	Portable commercial impedance analyzer PalmSens3	15
3.1	Classical Cole-Cole models involving resistors and Constant Phase elements (CPEs) (a) single-dispersion and (b) double-dispersion impedance models. Note that $0 < \alpha_{1,2} \leq 1$ are the dispersion coefficients. Reprinted by permission from [Springer Nature and Copyright Clearance Center]: [Springer Nature] [Circuits, Systems, and Signal Processing] [Extraction of phase information from magnitude-only bio-impedance measurements using a modified Kramers–Kronig transform, A. Al-Ali, A. Elwakil, B. Maundy, and T. Freeborn], [2017].	19
3.2	K-K modified transform algorithm flowchart	24
3.3	Comparison of computer simulated Cole-Cole impedance data original versus that obtained using the proposed modified K-K algorithm (a) Bode plot, (b) Nyquist plot and (c) relative error $\delta_\phi(\omega)$ in the extracted phase information. Reprinted by permission from [Springer Nature and Copyright Clearance Center]: [Springer Nature] [Circuits, Systems, and Signal Processing] [Extraction of phase information from magnitude-only bio-impedance measurements using a modified Kramers–Kronig transform, A. Al-Ali, A. Elwakil, B. Maundy, and T. Freeborn], [2017].	26

3.4	Relative error $\delta_\phi(\omega)$ analysis for (a) changing values of N , (b) changing values of s and (c) changing values of r . Reprinted by permission from [Springer Nature and Copyright Clearance Center]: [Springer Nature] [Circuits, Systems, and Signal Processing] [Extraction of phase information from magnitude-only bio-impedance measurements using a modified Kramers–Kronig transform, A. Al-Ali, A. Elwakil, B. Maundy, and T. Freeborn], [2017].	28
3.5	Demonstration of the tails problem in a double-dispersion Cole impedance model which has its critical frequencies located approximately at 20Hz and 1.6MHz when simulated for 2 different frequency ranges (10Hz-1MHz and 1Hz-10MHz) via (a) Bode Plot, (b) Nyquist plot and (c) relative error $\delta_\phi(\omega)$. Reprinted by permission from [Springer Nature and Copyright Clearance Center]: [Springer Nature] [Circuits, Systems, and Signal Processing] [Extraction of phase information from magnitude-only bio-impedance measurements using a modified Kramers–Kronig transform, A. Al-Ali, A. Elwakil, B. Maundy, and T. Freeborn], [2017].	30
3.6	Noisy magnitude data testing (a) the input magnitude with different SNR levels and (b) the computed phase compared to the ideal value (c) relative error $\delta_\phi(\omega)$. Reprinted by permission from [Springer Nature and Copyright Clearance Center]: [Springer Nature] [Circuits, Systems, and Signal Processing] [Extraction of phase information from magnitude-only bio-impedance measurements using a modified Kramers–Kronig transform, A. Al-Ali, A. Elwakil, B. Maundy, and T. Freeborn], [2017].	32
3.7	Results from the first (fresh) cherry tomato data set (a) phase information and (b) Nyquist plot. Reprinted by permission from [Springer Nature and Copyright Clearance Center]: [Springer Nature] [Circuits, Systems, and Signal Processing] [Extraction of phase information from magnitude-only bio-impedance measurements using a modified Kramers–Kronig transform, A. Al-Ali, A. Elwakil, B. Maundy, and T. Freeborn], [2017].	34
3.8	Results from cherry tomato second (aging) data set (a) phase information and (b) Nyquist plot. Reprinted by permission from [Springer Nature and Copyright Clearance Center]: [Springer Nature] [Circuits, Systems, and Signal Processing] [Extraction of phase information from magnitude-only bio-impedance measurements using a modified Kramers–Kronig transform, A. Al-Ali, A. Elwakil, B. Maundy, and T. Freeborn], [2017].	35

3.9	Comparison of data fitting to a double dispersion impedance model using precisely measured impedance data and the K-K constructed data for two tomato samples (a) sample #1 from the fresh tomatoe set and (b) sample #2 from the aging set. Reprinted by permission from [Springer Nature and Copyright Clearance Center]: [Springer Nature] [Circuits, Systems, and Signal Processing] [Extraction of phase information from magnitude-only bio-impedance measurements using a modified Kramers–Kronig transform, A. Al-Ali, A. Elwakil, B. Maundy, and T. Freeborn], [2017].	36
4.1	Magnitude detection hardware design	39
4.2	DC cancellation circuit design	40
4.3	Amplitude control circuit design	41
4.4	Magnitude sensing circuit design	43
4.5	Microcontroller code flowchart	45
4.6	Python code flowchart	46
4.7	Python code results (a) sampled v_{outA2} signal and (b) Magnitude and phase results	47
4.8	The saved CSV file	48
4.9	Calibration resistors actual values $R_c(f)$ measured using the precision N4L PSM1735 impedance analyzer	50
4.10	Calibration process done for $R_{f2} = 2.2k\Omega$ with $R_c = 2.2k\Omega$	50
4.11	Calibration process being applied while $Z_{unknown}$ is a $3.3k\Omega$ resistor	51
4.12	The teensy microcontroller module	52
4.13	The AD9850 DDS module	52
4.14	PCB schematics design	53
4.15	Double sided PCB layout (a) top (b) bottom layers	54
4.16	Manufactured PCB (a) top (b) bottom layers	54
4.17	Assembled PCB	55
5.1	Single-dispersion Cole-Cole model testing with passive components with the values $R_\infty = 470\Omega$, $R_1 = 2200\Omega$ and $C_1 = 1\mu F$. (a) Impedance magnitude plot (b) Impedance phase plot (c) Magnitude error and (d) Phase error.	59
5.2	Double-dispersion Cole-Cole model testing with on shelf components with $R_\infty = 470\Omega$, $R_1 = 2200\Omega$, $C_1 = 1\mu F$ $R_2 = 570\Omega$, $C_2 = 0.1\mu F$. (a) Impedance magnitude plot (b) Impedance phase plot (c) Magnitude error (d) Phase error.	60

5.3	Testing for bio-impedance using two different apples using the proposed hardware design. (a) Impedance magnitude plot (b) Impedance phase plot (c) Magnitude error (d) Phase error.	62
5.4	Comparison of data fitting to a double dispersion model using precisely measured impedance data and the proposed design for the two apples (a) Green Apple #1 and (b) Red Apple #2.	63
5.5	Testing with on shelf components double-dispersion Cole-Cole model with $R_{\infty} = 820 \Omega$, $R_1 = 68 k\Omega$, $C_1 = 0.12 \mu F$ $R_2 = 15 k\Omega$, $C_2 = 0.1 nF$. (a) Impedance magnitude plot (b) Impedance phase plot (c) Magnitude error (d) Phase error.	65
5.6	Testing with on shelf components double-dispersion Cole-Cole model with $R_{\infty} = 220 \Omega$, $R_1 = 47 k\Omega$, $C_1 = 15 nF$ $R_2 = 15 k\Omega$, $C_2 = 1 nF$. (a) Impedance magnitude plot (b) Impedance phase plot (c) Magnitude error (d) Phase error.	66
5.7	Day one results from the proposed design and the N4L impedance analyzer (a) Impedance magnitude plot (b) Impedance phase plot (c) Magnitude error (d) Phase error.	67
5.8	A picture of the portable device with one fruit sample being tested.	69
5.9	Nyquist plots for the five samples in (a) day 1 (b) day 2 (c) day 3	70
5.10	Nyquist plots for (a) sample#4 and (b) sample#5 with their fitted model results showing the ageing effect over the three days.	71

List of Abbreviations

Acronym	Definition
EIS	Electrochemical Impedance Spectroscopy
BIA	Bio-electrical Impedance Analysis
CPE	Constant-Phase-Element
WE	Working Electrode
CE	Counter Electrode
RE	Reference Electrode
WSE	Working Sensing Electrode
FRA	Frequency Response Analyzer
DSPs	Digital Signal Processors
K-K transform	Kramers-Kronig Transform
DDS	Direct Digital Synthesizer
ADC	Analog to digital Converter
PGA	Programmable Gain Amplifier
FPGA	Field-Programmable Gate Array
MCU	microcontroller unit
PCB	Printed Circuit Board
IDE	Integrated development environmen

CHAPTER 1

Introduction

In our modern world, and with the advancement in technology and sensors design, the automation of our life has taken all the attention in various fields. In fields like biomedical, agriculture and quality control, for example, the use of electrochemical sensors and tests has been getting a great interest. One of those tests is the Electrochemical Impedance Spectroscopy (EIS) which *is the small-signal measurement of the linear electrical response of a material of interest and the following analysis of the response to yield useful information about the physiochemical properties of the system* [1].

Although the work in the literature showed that EIS could be useful in many fields, it also showed the lack of a cheap, low-cost and low-power portable device that can be used to apply this technique on a wide scale. This need was caused by the fact that the commercial impedance analyzers suffer from being bulky and expensive, while most of the applications need a handy and portable device that can be used in the field. Several portable impedance analyzer designs have been proposed in the literature [2, 3]. Although, many different designs have been proposed the lack of a low-cost portable impedance analyzer still persist and we still can't find such a device in the market.

1.1 Research Objective

The ultimate goal of this work is to design a simple portable impedance analyzer that can be used to do continuous measurements in the field. The simplicity of the design was achieved by replacing the actual measurement of the phase by using a software algorithm based on

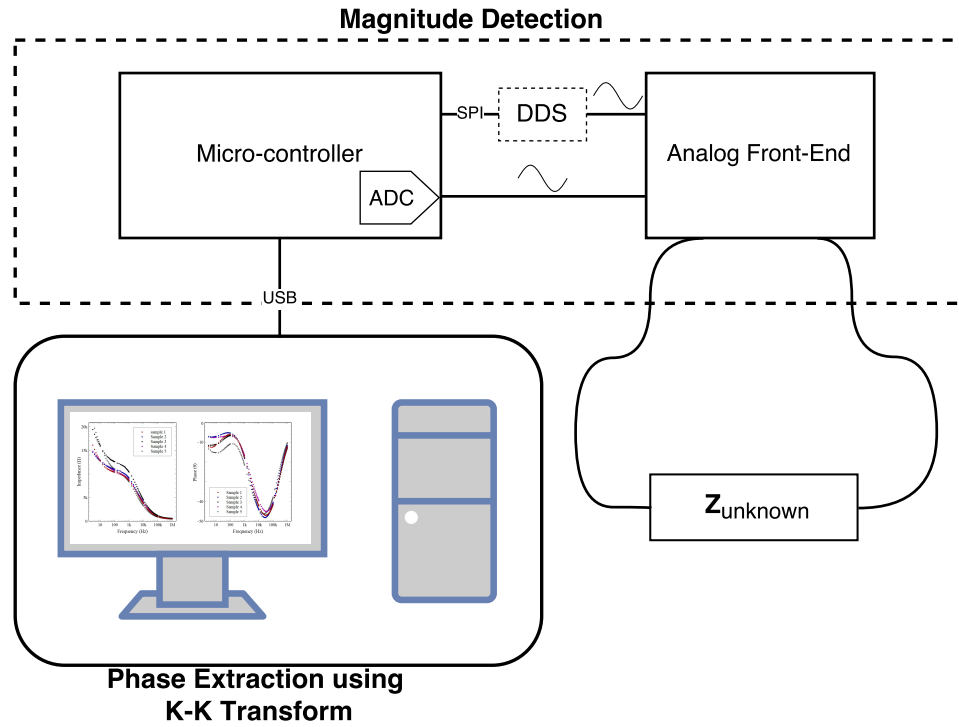


Figure 1.1: Block diagram of the experimental setup

a modified Kramers-Kronig transform to extract the phase from the impedance magnitude which is measured using simple hardware.

The block diagram of the portable impedance analyzer designed and used in this work is shown in Fig. 1.1. It is divided into two main parts, the magnitude detection hardware and the phase extraction algorithm based on a modified K-K transform. These two parts are linked using an ARM® Cortex®-M4F microcontroller, which controls the voltage excitation signal (generated from an external direct digital synthesizer (DDS)) and reads the output signal from the magnitude detection hardware through its internal ADC. The system is controlled by a computer with a Python code written to communicate with the microcontroller. The same Python code then applies the K-K transform to calculate the impedance phase.

1.2 Thesis Overview

This thesis is organized to present the design and implementation of the proposed portable impedance analyzer.

In chapter 2 the basics concepts of impedance are reviewed before going through the details of EIS measurements techniques and instruments that can be used. The chapter concludes with a literature review of the available impedance analyzers and their limitations.

The phase extraction technique is discussed in chapter 3, where the algorithm is discussed in details before being evaluated and tested. The algorithm was tested with simulated data to evaluate the error and optimize its parameters, before being finally tested with experimental magnitude data of some cherry tomato samples.

Chapter 4 then goes through the design of the entire system by first covering the magnitude detection technique in details before going through the software codes of both the python and the microcontroller. Finally the implementation process of the design was discussed and the final prototype is shown.

The system is finally tested in chapter 5 with some passive components and some fruits to show that the system produces accurate results in comparison with commercially available devices. The proposed design is then used to monitor the ageing of some strawberries brought from the local market; the results show a significant effect caused by the fruits ageing on their bio-impedance.

Chapter 6 concludes this work by some remarks and suggestions for future work.

CHAPTER 2

Impedance measurement

2.1 Introduction

The impedance $Z(j\omega)$ is the opposition presented by any material to the flow of the current when a voltage is applied across it. It is measured by the ratio of the voltage to the current at a particular frequency. The linear impedance is modelled as

$$Z(j\omega) = R(\omega) + j \cdot I(\omega) \quad (2.1)$$

and comprise of a real $R(\omega)$ and imaginary $I(\omega)$ parts taken at a certain angular frequency (ω). It can also take the following form

$$Z(j\omega) = |Z(\omega)| e^{j \cdot \phi(\omega)} \quad (2.2)$$

Where $|Z(\omega)|$ is the impedance magnitude which is the ratio of the voltage magnitude to the current magnitude across that material and $\phi(\omega)$ is the impedance phase which is the phase shift between the voltage and the current. In the case of resistive materials, the impedance will consist of a real part only and have a constant magnitude over the whole frequency range with zero phase since the current and the voltage across it will be in phase. However, the real life materials will never be purely resistive; they are usually a combination of resistive, capacitive and inductive materials.

2.2 Electrochemical Impedance Spectroscopy (EIS)

Electrochemical Impedance Spectroscopy (EIS), where the impedance of a specific object is measured over a suitable frequency range is a powerful technique [4], that is being used in a wide range of applications in medicine, agriculture, chemistry, and many others [4]. The properties that affect the flow of current in a certain material can be investigated and studied through EIS, “from mass transport, rates of chemical reactions, corrosion, and dielectric properties; to defects, microstructure, and compositional influences on the conductance of solids. EIS can predict aspects of the performance of chemical sensors and fuel cells, and it has been used extensively to investigate membrane behaviour in living cells. It is useful as an empirical quality control procedure, yet it can contribute to the interpretation of fundamental electrochemical and electronic processes” [4].

The impedance of a certain body can be determined by applying a certain voltage (of known magnitude and frequency) on the body and observing the resultant current flowing through. Thus, impedance (magnitude and phase) is affected by any property that affects the flow of charged particles (current) at a given voltage. *EIS* may be used to investigate the dynamics of bound or mobile charge in the bulk or interfacial (inner) regions of any solid or liquid material: ionic, semiconducting, mixed electronic–ionic, and even insulators (dielectrics) [4]. EIS measurements are usually carried out in the frequency domain, but it is sometimes carried out in the time domain and then Fourier transformed to the frequency domain. The process of EIS measurements requires electrical stimulation (usually with a known voltage signal), and the reading of the resulting electrical response (typically a current signal), which can be done using different methods and electrodes configuration as we will see further in section 2.6.

2.3 Bio-Impedance Analysis

Bio-impedance measurements have been widely used in the past 50 years. This technique introduced a great number of commercial devices and methods. It has been used to characterize solids, liquids, and suspensions, and, lately, to characterize biological tissues and fluids, either in extracellular (outside biological context) or in intracellular (inside biological context) [5], some of which having clinical applications [6]. Impedance spectroscopy is widely used in experimental studies to characterize tissue state [7]. The size, shape and density of cells in the tissue, as well as the conductivity of intra- and extra- cellular environment, are reflected in the impedance spectrum. This allows the distinction between different tissues and between different physiopathological (diseased and non-diseased) states of the same tissue. In biological plant tissues, for example, the proportion of current passing through the symplast and apoplast (the inner side of the cell membrane and the free space outside the cell membrane, respectively) varies with the frequency of the AC signal [8]. For low-frequency AC signals, the current flows only through the apoplast. As the cell membrane impedance decreases with increasing frequency, the amount of current passing through the symplast also increases [8]. Therefore, information about different tissue features may be revealed [8] and can be quantified using EIS by the analysis of the equivalent electric circuit [9]. With a proper equivalent electrical model, it is possible to study the effects of diverse factors on tissue properties, according to changes in the parameters of the model [9, 10].

2.4 Bio-Impedance Analysis Applications

Bio-impedance has been used in a lot of applications as it was mentioned earlier, but the three main fields where it has been extensively were the biomedical field, agriculture and food characterization as it will be shown in the following sections.

2.4.1 Biomedical

Bio-impedance is a widely used technique to estimate human body composition, as a quick non-invasive and low-cost method and it is usually called bio-electrical impedance analysis (BIA) [11]. Additionally, a non-invasive blood glucose measurement technique based on EIS has also been proposed, since the flow of the current in the blood was found to be affected by glucose levels [12, 13], but this technique is still not reliable enough to get an FDA approval and is not available on the market as of this writing. Bio-Impedance has also been proven to be a powerful non-invasive technique that can be used for skin cancer detection [14, 15].

2.4.2 Agriculture

In Agriculture, Bio-Impedance has proven to be a robust method for growth monitoring and quality control. Apple ageing effect on bio-impedance was studied in [16], while Strawberry ripeness was evaluated using Bio-impedance in [17]. Plant disease detection was also done using EIS in [18]. With a dedicated body of research publications studying different aspects of the plants using EIS, it has been proven that EIS is a great non-invasive tool that can be utilized in many different ways [11, 19–21].

2.4.3 Food Characterization

The increasing interest in food quality control has led to many application that utilizes Bio-impedance as a quick, low-cost quality assessment technique. In [22] it was shown that bio-impedance could be used to as a quality assessment tool for meat and fish. The work showed that EIS can be used to get some chemical compositions and Physicochemical properties that can be used for quality assessment. Also, in [23] and [24], wine and milk samples were tested respectively, and it was proven that the chemical compositions of these two products can be detected using EIS with the right electrical modeling of the data and the use of some statistical analysis. Additionally, in [25] the authors studied some

cow milk samples (full fat, skimmed, semi-skimmed and lactose reduced) to study the relationship between the milk composition and the electrical conductivity [11]. It was found that the milk salt and fat contents affects it's electrical conductivity. A detailed review on the use of bio-impedance in food characterization can be found in [11] where the authors provide a number of other applications.

For all of these applications the electrical modeling of the biological tissue using the collected EIS data is the main step which help us to understand whats happening inside the tissue or liquid or food and causing this change in this particular parameter in the model.

2.5 Electrical modelling of Biological Tissues

Electrical modelling of biological tissues is an excellent way of representing biological tissues and to study their behaviour using EIS. It is usually done by dealing with the Tissue as a black box where intensive testing is done then software algorithms are used to fit those results to the best model. The problem with the electrical modelling of biological tissues is that it is often not possible to mimic the electrical behaviour with typical and physically realizable components such as resistors, capacitors and inductors [26]. It has been found by the biochemists who worked on impedance measurement long ago that the impedance they are measuring is always related to the frequency as $Z(s) = 1/s^\alpha$, where α is a non-integer value between 0 and 1. This makes the phase angle between the excited voltage and the current equal to $\alpha\pi/2$, hence the widely used name Constant-Phase-Element (CPE) which is used to relate to this impedance. There are many ways to construct electrical impedance models of biological tissues, mainly utilizing CPEs, resistors and sometimes what is called the Warburg impedance is used. The Warburg impedance is a special case of the CPE where $\alpha = 0.5$ [27]. Models may vary in the number of components used for the equivalent circuits, the type of components used, the way those elements are connected to form the modelling circuit and the methods and theories used in evaluating those parts.

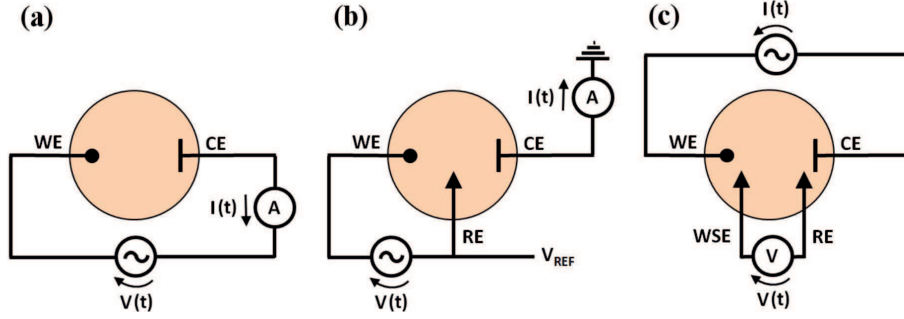


Figure 2.1: Electrode configurations (a) two electrodes, (b) three electrodes and (c) four electrodes

The oldest and most commonly used model with biological tissues is the Cole-Cole model presented in [28]. The Cole-Cole model is a famous model which has been found to fit many tissues [29]. According to this model, the impedance of a tissue can be given as

$$Z(s) = R_{\infty} + \frac{R_0 - R_{\infty}}{1 + (\tau s)^{\alpha}} \quad (2.3)$$

Where R_0 is the resistance at low frequency, R_{∞} is the resistance at very high frequency, τ is a characteristic time constant, and α is the so-called dispersion coefficient. This simple model thus contains two resistors and one CPE. Protein fibres, fruits and vegetable properties have been found to be adequately modeled using a combination of the Warburg impedance together with CPE elements [30, 31].

EIS modelling software can also be found in which each of them using different fitting algorithms and offer a different set of models. In this work, the freely available EIS software package which was proposed by Bondarenko and Ragoisha in [32] which is equipped with some optimization methods and models that the user can choose from will be used to extract the electrical parameters of the measured data.

2.6 EIS Measurement techniques

EIS measurements can be done in different electrode configurations as shown in Fig. 2.1 which was presented in [11]. The potentiostat EIS where a voltage $V(t)$ is excited and the

current $I(t)$ is measured the first two configurations are mostly being used. The first configuration two electrodes are used as in Fig. 2.1(a) with the working electrode (WE) and the counter electrode (CE) is the most used configuration, but in this setup, the contribution of the electrode will be visible in the measured impedance. In the second configuration Fig. 2.1(b), but in this setup, a reference electrode (RE) is added to limit the electrode contribution to WE since no current is drawn by RE and CE is used to measure the current. In galvanostat EIS where a current signal $I(t)$ is excited and the voltage $V(t)$ is measured, in this setup the last configuration is used by adding working sensing electrode (WSE) to be used with RE to sense the voltage while a current is being applied between WE and CE, this configuration ensures that the measured impedance is independent of the electrode interface. However, EIS is usually done using two electrode configuration shown in Fig. 2.1(a) since it is the simplest form and the electrode effect can be either modelled or neglected if it was the same in all the samples. In some cases like chemical sensors or living cells where the simple symmetrical geometry is not feasible other configurations might be used [4]. In this work, the two electrode configuration was adopted. With this configuration, there are many different methods of electrical stimuli that can be used. The three conventional techniques used in EIS measurements are discussed in the following subsections.

2.6.1 Transient Measurements

In transient measurements a step function of voltage [$V(t) = V_0$ for $t > 0$, $V(t) = 0$ for $t < 0$] may be applied at $t = 0$ to the system and the resulting time-varying current $i(t)$ measured. The ratio $V_0 / i(t)$, often called the indicial impedance or the time-varying resistance, which measures the impedance resulting from a step function voltage perturbation (of small amplitude). The result is then transformed using the Fourier or Laplace transform into the frequency domain. The non-periodicity of the excitation should be corrected by using windowing to avoid the distortion that happens if Fourier-transform is used. The system response has to be linear and V_0 should be sufficiently small for such a transformation

to work. The advantage of this method is that its experimental part is relatively easy and that the voltage controls the rate of the electrochemical reaction (which is represented in the flow of current) in the test subject. However, it has some disadvantages such as, the integral transformation which needs to be applied on the results and the fact the impedance may not be well determined over the desired frequency range because of the difference in the signal-to-noise ratio between different frequencies [4].

2.6.2 Mixed/White Noise Signals

In this technique a signal $n(t)$ composed of random (white) noise is applied to the system and the resulting current is measured. The Fourier-transform is again applied to the result to generate a frequency domain representation and obtain an impedance. The main advantage offered by this technique is the fast collection of the data because only one signal is applied to the test subject for a short time. Requiring a true white noise source and the need to carry out a Fourier analysis mark the main disadvantages of this technique [4]. The white noise signal is sometimes replaced by a sum of well-defined sine waves; this offers a better signal-to-noise ratio (SNR) for each desired frequency and the ability to analyze the linearity of the system response. This technique, in general, is suitable where a high throughput real-time data is needed. However, its intrinsic loss of accuracy because of the low SNR specially at high frequencies makes it a non-preferable technique over the other techniques [4] [33].

2.6.3 Frequency Sweep

The most commonly used technique to measure the impedance is by sweeping the frequency of a sinusoidal voltage or current to the interface and measuring the phase shift and amplitude, or the real and imaginary parts, of the resulting current/voltage at every single frequency in this sweep. This technique is used in most of the commercial instruments which measure the impedance as a function of frequency automatically in the frequency ranges of about $100\mu Hz$ to $50MHz$. This method has been popular because of the fact that

a high signal-to-noise ratio can be achieved in the frequency range of interest as well as its instruments ease of use. However, all of this occurs at the cost of a higher measurement time in comparison with other techniques and a more complicated hardware design [4, 33].

In this work, we use the basic idea of sweeping the frequencies from this technique, but we eliminate the need to measure the phase which results in a less complicated hardware design.

2.7 Impedance Analysis Instruments

In the old days before modern dedicated instruments were available, EIS was done by monitoring the current (I) that goes through the unknown impedance and the voltage (V) across it, and then manually measuring the magnitude (V/I) and the phase between them. The main disadvantage of this method was the very long measurement time needed to finish the measurements on all the frequencies and low accuracy introduced by the human error while measuring the voltage and current magnitude and the phase through the oscilloscope [11].

With today's advanced technologies and dedicated instruments there exist the ability to measure impedance using different methods, and electrode configurations from a few μHz up to around 50 MHz . However, the very high price of those instruments and the fact that they must be used in the lab has made researchers look for alternative portable designs. The need for portable impedance analyzers was raised in the last few years with the increasing interest in EIS that needs a device to be used in the field to do online measurements or continuous measurements.

2.7.1 Commercial Impedance Analyzers

Commercial impedance analyzers or what are so called LCR meters are available in different sizes from different companies. One of the new models is the precision N4L PSM

1735 Impedance analyzer [34] designed and manufactured by Newtons4th Ltd N4L (shown in Fig. 2.2a) which come with different models namely the IAI and the IAI2 impedance analyzer, with the specifications shown in Table. 2.1.

Table 2.1: The precision N4L PSM 1735 Impedance analyzer models

Spec	IAI Impedance Analyzer	IAI2 Impedance Analyzer
Connections	4 wire Kelvin connections	4 wire Kelvin connections
Interface needed	PSM17XX	PSM17XX
Signal level	$\pm 10V$	$\pm 10V$
Frequency range	Up to 35 MHz	Up to 50 MHz

Another model is the professional impedance analyzer BAS-Zahner IM6 [35]. This device which is shown in Fig. 2.2b can be used in 2, 3 and four electrode configuration in the range from $10\mu Hz$ to $8 MHz$ to measure an impedance range $30\mu\Omega - 1G\Omega$ with an error of around 3% which makes it one of the best available instruments.

Additionally, there have been some portable impedance analyzers commercially available like the PALmSense3 from PALMSENS as shown in Fig. 2.3. This portable model has a multifunction operation. It can work as a potentiostat, galvanostat, and impedance analyzer. The wide frequency range $100\mu Hz$ up to $50kHz$ makes it perfect for EIS and Frequency Response Analysis (FRA). However, the device's main disadvantage is the limited frequency range and the high price.

2.7.2 Impedance Analyzers Designs in the Literature

Increasing interest in bio-impedance analysis in different fields is fueling the demand for portable and affordable analyzers that can be deployed in field without having to take the samples for measurement to a laboratory [36–39]. Several designs for such portable impedance analyzers have been proposed in the literature, mainly employing at their heart the well-known single impedance chip AD5933 from Analog Devices [40] as the only chip that offers a complete, integrated system for impedance analysis.

In the work of [41] a design using the AD5933 was proposed. The design was limited



(a)



(b)

Figure 2.2: Commercial Impedance Analyzers (a) N4L PSM 1735 (b)BAS-Zahner IM6



Figure 2.3: Portable commercial impedance analyzer PalmSens3

and fixed at 10 Hz since it was used to conduct a specific study and the design was built just to serve that purpose with no error or impedance range mentioned. In [42], another design was proposed with a wide range of frequency and an acceptable error, however, the design again was built to serve a special purpose and to work in very specific applications of cell cultures. Using the other model from Analog Devices the AD5934 the design in [43] was concerned with single cell measurement and showed an error of 10% for cell measurements while covering the full impedance range and a wide frequency range. Another design for bio-sensor application was proposed in [44] with no information on error data, however, their design covered the widest impedance range between [41–44]. The designs in [44–46] were the only two papers published with a frequency range that exceeds the limits mentioned in the AD5933 datasheet. However, their designs showed a high error in measurement and that was due to the effect of the internal filter of the AD5933. A four-electrode design was proposed in [47] with a reasonable error, and a new measuring technique was proposed. A design for body composition was proposed in [48], but again the design was built with a fixed frequency which limits its use. The design proposed in [49, 50] used two AD5933, its low error made it the best design among all

. Based on two chips working synchronous together it had the ability to monitor both the voltage across the unknown impedance and the current flowing through it. Their design

was low power and featured low error. However, it wasn't portable due to the complexity of its design.

One of the latest proposed designs was the work in [51], where solutions for several of the design difficulties using the AD5933 were proposed. Covering the range from 10Ω to $1\text{ M}\Omega$ at frequencies from 1 Hz to 100 kHz with one chip and an error of 3.5% for the impedance modulus and 2.8 degrees for the impedance argument made their design among the best of all what's been accomplished with this chip. However, this single-chip solution has several limitations mainly imposed on the upper-frequency limit of 100 kHz and its unacceptable accuracy, particularly at the low frequencies, as previously outlined in [51] and [52]. These two drawbacks have led to alternative designs based on digital signal processors (DSPs) such as the one proposed in [53–55] where fitting algorithms were used to fit the digitized current and voltage. Additionally an ARM-based design with high accuracy and a wide frequency range $1\text{mHz} - 100\text{kHz}$ measuring an impedance range $1\Omega - 1\text{G}\Omega$ was proposed in [56]. Nevertheless, without a single chip solution, the hardware remains complicated; which is related primarily to the need for accurately measuring the phase shift between the electrical current flowing in the tissue under test to the applied voltage stimulus in potentiostatic-type impedance setups, which are the most common. Therefore, custom designed bio-impedance chip front ends have been proposed [57]. In all the mentioned solutions, simplifying the hardware is always the target either by changing the platform or through innovation in the circuit design itself [58, 59]. Nevertheless, a reliable low-cost device that can be used in the field for continuous measurements of the impedance is not currently available.

2.8 Summary

In this chapter, the basic concept of impedance was first presented. Then the Electrochemical Impedance Spectroscopy (EIS) and bio-impedance were discussed along with some of their applications. EIS modeling and measurement techniques were also briefly discussed.

Finally, some samples of the commercially available devices were presented, followed by a literature review of the portable impedance analyzers. The literature review showed that the main focus of the proposed designs was simplifying the hardware which is difficult with single-chip solutions having several limitations.

CHAPTER 3

Phase Extraction Algorithm

3.1 Introduction

At both very low and very high frequencies, phase measurements are highly affected by noise and hardware sampling/delay limitations while magnitude measurements are less affected and are easier to correct using a number of various methods. Examples of in-direct magnitude-only techniques were recently proposed in [60,61] which employ filter transfer functions (known a priori) to construct the phase response from the measured magnitude response. However, these techniques require numerical computation and a priori knowledge of the impedance model of the unknown tissue. These methods have used either a single or double dispersion Cole-Cole impedance model see Fig. 3.1 to fit the impedance under test. The equivalent circuit parameters of these models are determined by using measurements from the magnitude response to solve a set of nonlinear equations. Subsequently, having determined the circuit parameters, the phase response of these models can be obtained. Although these models are sufficient for a wide range of bio-impedance measurements, a general phase extraction method which is independent of the impedance fitting model is still needed for measurements that do not fit neither the single nor the double dispersion Cole-impedance models.

In this chapter we re-visit the signal processing concepts underlying bio-impedance measurements [62] and we propose a new method to extract the phase information from the measured impedance magnitude (in Ohms) using the Kramers-Kronig transform [63,64]. Hence, we shift the focus away from simply optimizing the hardware of bio-impedance

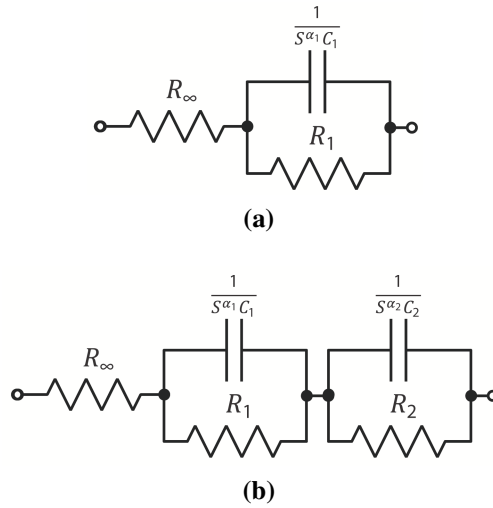


Figure 3.1: Classical Cole-Cole models involving resistors and Constant Phase elements (CPEs) (a) single-dispersion and (b) double-dispersion impedance models. Note that $0 < \alpha_{1,2} \leq 1$ are the dispersion coefficients. Reprinted by permission from [Springer Nature and Copyright Clearance Center]: [Springer Nature] [Circuits, Systems, and Signal Processing] [Extraction of phase information from magnitude-only bio-impedance measurements using a modified Kramers–Kronig transform, A. Al-Ali, A. Elwakil, B. Maundy, and T. Freeborn], [2017].

devices for portable applications. The method is validated using simulated datasets and measurements collected from cherry tomatoes purchased from the local market. The historical background of the method and its noise/error performance are clearly presented.

3.2 Background

Years ago, the Hilbert transform pair was proposed as a mathematical tool that can extend an analytic function into the complex frequency domain [65]. This transform takes several forms in continuous time and in discrete time domains. One of the first applications of the Hilbert transform was the study of the relationship between the refractive index and the absorption coefficient in light dispersion [66] where it was shown that they are related to each other by a pair of equations. These equations are now known as the Kramers-Kronig Transform (K-K transform) [67] and can be considered as a new form of the Hilbert

transform pair. Later, they were generalized to relate the frequency dependent real part " $R(\omega)$ " to the imaginary part " $I(\omega)$ " of any transfer function as long as this function is causal, linear, stable and band-limited in the form

$$I(\omega) = - \left(\frac{2\omega}{\pi} \right) \int_0^{\infty} \frac{R(x) - R(\omega)}{x^2 - \omega^2} dx \quad (3.1)$$

$$R(\omega) = R(\infty) - \left(\frac{2}{\pi} \right) \int_0^{\infty} \frac{x \cdot I(x) - \omega \cdot I(\omega)}{x^2 - \omega^2} dx \quad (3.2)$$

There are two conditions for accurate execution of (3.1) and (3.2) as proposed by [68] namely:

- 1) The data set should be taken over the range $x_{min} = 0$ to $x_{max} = \infty$.
- 2) The data set should have its points uniformly distributed over the frequency range.

The first condition cannot be satisfied in experimental data leading to what is known as "the tails problem" for systems which have poles or zeros located near the far ends of the frequency measurement points x_{min}, x_{max} (later demonstrated in this chapter). Truncation of the data can lead to significant errors if there are such critical poles or zeros. Although [63, 64, 68] proposed an algorithm to evaluate the K-K transform integrals, [69, 70] tested this algorithm on real data and concluded it had many limitations and restrictions. Therefore, the transform became employed mainly as a verification tool in commercial impedance measurement software packages, such as Z-Hit, which computes the impedance magnitude from the phase for data quality tests [71]. Using the transform to extract the impedance phase information out of its magnitude information was, to the best of the authors' knowledge, first reported in [72] for low frequency impedance data taken from a chemical reaction. However, not much can be found about their method or its extension for high frequencies as well as other types of data and therefore the K-K transform remained only as a validation tool [73] in the field of impedance measurement. The K-K transform

also received some interest in optical analysis where it is sometimes referred to as the Bode relations and is used to obtain the phase angle from the magnitude as in [74, 75]. Other applications of the K-K transform were reported in [76–79]. In this work which was originally published in [80], we propose a modified K-K algorithm and validate it on bio-impedance data experimentally collected in the range 1Hz-2MHz. Our conclusion is that the K-K transform can successfully be used to replace the need for actual phase measurements in low-cost portable impedance analyzers over this frequency band, as described in detail in the next section.

3.3 The proposed algorithm

Equations (3.1) and (3.2) arise from a linear impedance modeled as

$$Z(j\omega) = R(\omega) + j \cdot I(\omega) \quad (3.3)$$

In order to obtain the phase out of the magnitude we consider the impedance in the following form

$$\begin{aligned} Z(j\omega) &= |Z(\omega)| e^{j\phi(\omega)} \\ \ln(Z(j\omega)) &= \ln(|Z(\omega)|) + j \cdot \phi(\omega) \end{aligned} \quad (3.4)$$

where $|Z(\omega)|$ is the impedance magnitude and $\phi(\omega)$ is its phase angle. Equation (3.1) can therefore be modified to

$$\phi(\omega) = \left(\frac{2\omega}{\pi} \right) \int_0^\infty \frac{\ln(|Z(x)|) - \ln(|Z(\omega)|)}{x^2 - \omega^2} dx \quad (3.5)$$

where ω is the experimental angular frequency and x is the integration angular frequency. However, the existence of $x^2 - \omega^2$ in the denominator suggest that there could be a singularity when $x = \omega$. This issue was discussed in [64] by noting that

$$\frac{1}{x^2 - \omega^2} \Big|_{x < \omega} = -\frac{1}{\omega^2} \left\{ 1 + \left(\frac{x}{\omega} \right)^2 + \left(\frac{x}{\omega} \right)^4 + \left(\frac{x}{\omega} \right)^6 + \dots \right\} \quad (3.6)$$

$$\frac{1}{x^2 - \omega^2} \Big|_{\omega < x} = \frac{1}{x^2} \left\{ 1 + \left(\frac{\omega}{x}\right)^2 + \left(\frac{\omega}{x}\right)^4 + \left(\frac{\omega}{x}\right)^6 + \dots \right\} \quad (3.7)$$

From the above it is clear that each term tends to 1 as $x \rightarrow \omega$. However, in our case the terms are multiplied in the numerator by $\ln(|\hat{Z}(x)|) - \ln(|Z(\omega)|)$ which tends to zero under the same conditions, thereby making the function beneath the integral tend to zero too. Hence the singularity is avoided in our algorithm.

The integral in equation (3.5) can be numerically evaluated as

$$\phi(\omega) = \left(\frac{2\omega}{\pi}\right) \sum_{x_{min}}^{x_{max}} \frac{\ln(|\hat{Z}(x)|) - \ln(|Z(\omega)|)}{x^2 - \omega^2} \cdot \Delta x \quad (3.8)$$

where $\hat{Z}(x)$ is the fitted impedance after using linear interpolation. In particular, following the flowchart in Fig. 3.2 for the integration to be performed, the data should be segmented where each segment is taken over a small frequency range $[\omega_1, \omega_n]$ where n is the number of the points in this segment which can be calculated by *Total number of data points*/ s and then this segment is extrapolated to a wider frequency range where the numerical integration is performed from $x_{min} = \frac{\omega_1}{r}$ to $x_{max} = r \cdot \omega_2$ where r is a scaling factor. This segmenting idea was used in [64] to obtain a good fitting prior to integration, but it was noted that to use a polynomial-type fit, each segment should be fitted alone. This process of fitting each segment alone causes the order of the polynomial to be limited by the number of points. In our proposed algorithm we only utilize linear interpolation since it is not affected by the number of points per segment in the log-domain. Therefore, using Matlab's linear interpolation fitting algorithm, we fit $\ln(|Z(\omega)|)$ to $\ln(|\hat{Z}(x)|)$ and then divide it into s segments. The integration is then evaluated for N points from x_{min} to x_{max} for each segment with a step $\Delta x = (x_{max} - x_{min})/N$. This modified algorithm which evaluates the integral is given in (3.9) and requires the right choice of the parameters s , r and N .

$$\phi(\omega_i) = \left(\frac{2\omega_i}{\pi} \right) \sum_{\frac{\omega_{1,k}}{r}}^{r \cdot \omega_{n,k}} \frac{\ln(|\hat{Z}(x)|) - \ln(|Z(\omega_i)|)}{x^2 - \omega_i^2} \cdot \Delta x_k \quad (3.9)$$

Here k refers to the specific segment going from 1 to s and i refers to the frequency point being evaluated going from point 1 to n which is the last point in the segment. A discussion of the effects on the accuracy of the calculation of the (s, r, N) parameter set is given in section 3.4.1.1.

3.4 Algorithm testing

The algorithm was initially tested on simulated impedance data and then applied to experimentally measured impedance data from a large sample of cherry tomatoes, as detailed below. Hereafter, the subscript k – k refers to any result from the algorithm.

3.4.1 Simulated Data

Simulated data for the single-dispersion Cole impedance model shown in Fig. 3.1(a) was generated with component values $R_\infty = 1 \text{ k}\Omega$, $R_1 = 500 \Omega$, $C_1 = 0.2 \mu F$ and $\alpha_1 = 0.9$. For the double-dispersion model shown in Fig. 3.1(b) the component values for the simulated datasets were $R_1 = 100 \Omega$, $R_2 = 200 \Omega$, $C_2 = 0.5 \mu F$ and $\alpha_2 = 1$. The generated datasets were logarithmically distributed to cover the frequency range 100Hz to 1MHz with 100 points per decade where the natural logarithm of the impedance magnitude $\ln(|Z(\omega)|)$ was fitted and transformed using the proposed algorithm outlined above with $(s, r, N) = (25, 100, 10^4)$. The calculated phase $\phi_{k-k}(\omega)$ was compared to the original phase $\phi(\omega)$ and both are shown in Fig. 3.3(a). Note that the single-dispersion and double-dispersion datasets are given by black and red lines, respectively. Additionally, both the real and imaginary parts of the impedance were also obtained from the calculated phase using the equations

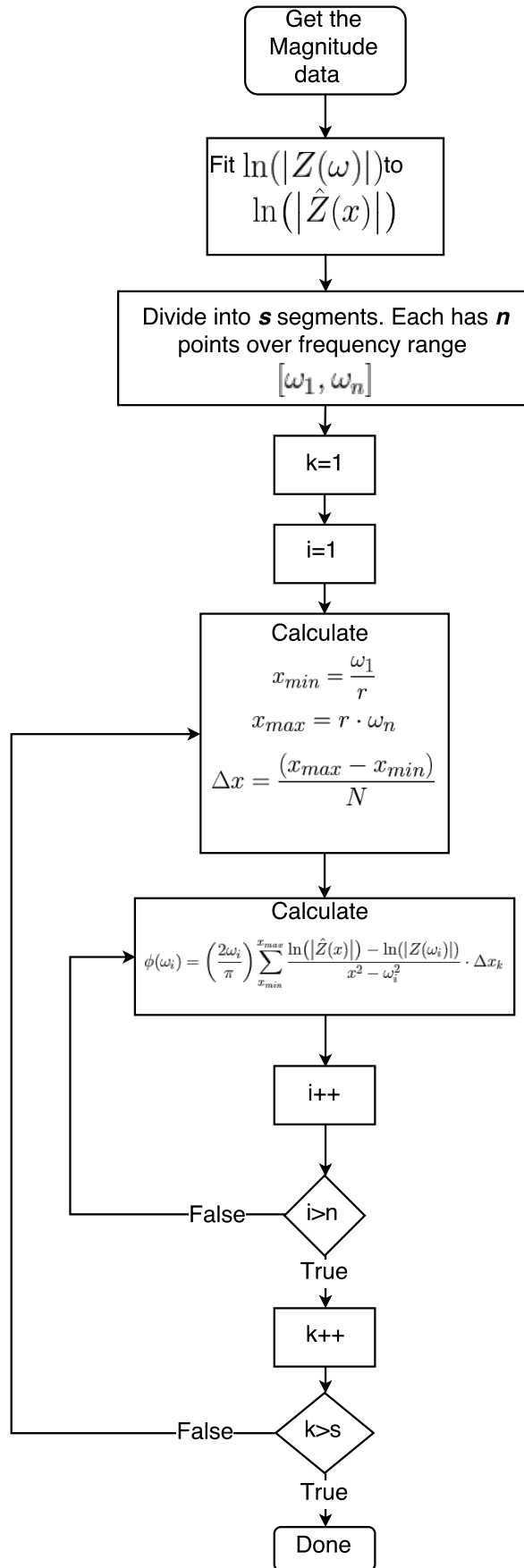


Figure 3.2: K-K modified transform algorithm flowchart

$$R_{k-k}(\omega) = |Z(\omega)| \cdot \cos(\phi_{k-k}(\omega)) \quad (3.10)$$

$$I_{k-k}(\omega) = |Z(\omega)| \cdot \sin(\phi_{k-k}(\omega)) \quad (3.11)$$

For further comparison with the simulated datasets, the Nyquist plot using the real and imaginary components from (3.10) and (3.11) is shown in Fig. 3.3(b). Again, the single-dispersion and double-dispersion datasets are given by black and red lines, respectively. The relative error $\delta_\phi(\omega)$ of the phase calculated using equation (3.12), is shown in Fig. 3.3(c).

$$\delta_\phi(\omega) = \left| \frac{\phi_{k-k}(\omega) - \phi(\omega)}{\phi(\omega)} \right| \times 100\% \quad (3.12)$$

3.4.1.1 Parameter tuning

The right choice of (s, r, N) is important for the accurate application of this algorithm. For a better understanding of the effect of these parameters, the double dispersion model using the same circuit parameter values mentioned previously was re-simulated over a wider frequency from 1Hz to 10MHz. The algorithm was applied with different sets of parameters (s, r, N) to quantify how each parameter affects the results. From these simulations, which are shown in Fig. 3.4, the summarized effects include:

- i) The effect of N is demonstrated in Fig. 3.4(a) for three different values of N ($N = 10^3, 10^4, 10^5$) fixing $s = 25$ and $r = 100$. Here, the relative error in phase is limited to a maximum of 20%. From the figure, it is seen that the value of $N = 10^4$ limits the relative error below 10% over the entire frequency range (100Hz-10MHz). Further increase of N above 10^4 increases the computation time without significantly improving accuracy.
- ii) The number of segments s defines the number of points being integrated with the

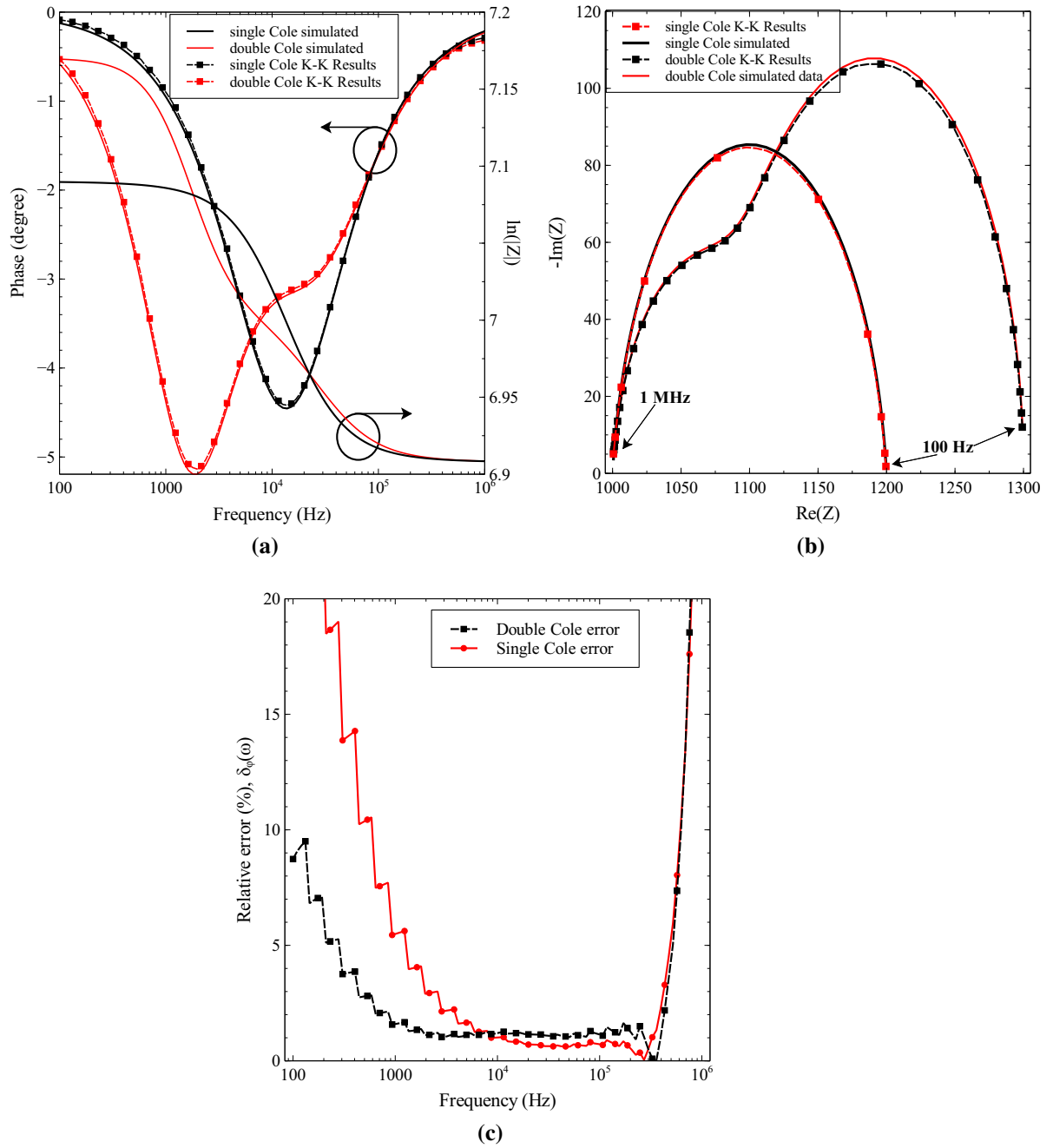


Figure 3.3: Comparison of computer simulated Cole-Cole impedance data original versus that obtained using the proposed modified K-K algorithm (a) Bode plot, (b) Nyquist plot and (c) relative error $\delta_\phi(\omega)$ in the extracted phase information. Reprinted by permission from [Springer Nature and Copyright Clearance Center]: [Springer Nature] [Circuits, Systems, and Signal Processing] [Extraction of phase information from magnitude-only bio-impedance measurements using a modified Kramers–Kronig transform, A. Al-Ali, A. Elwakil, B. Maundy, and T. Freeborn], [2017].

same Δx ; which gives the transform the ability to follow the phase transitions precisely. The results in Fig. 3.4(b) are given for three different values of s ($s = 4, 10, 25$) with fixed $N = 10^4$ and $r = 100$. These results indicate clearly that larger values of s while reducing the relative phase error $\delta_\phi(\omega)$ at low frequencies (approximately 5% error for $s = 25$), they degrade the phase error at high frequencies. Selecting $s = 4$ for example will ensure a relative phase error below 20% over the frequency range (100Hz-1MHz) while choosing $s = 25$ ensures a relative phase error below 20% over the frequency range (10Hz-300kHz). Due to the importance of low frequencies in bio-impedance measurements, we select $s = 25$.

- iii) It is clear from Fig. 3.4(c), performed with three different values of r ($r = 10, 100, 1000$) for fixed $N = 10^4$ and $s = 25$) that higher values of r improve the low frequency relative phase error but degrade it at high frequencies. Given these values of N and s we select $r = 100$ which can cover the range (100Hz-10MHz) with less than 20% phase error.

3.4.1.2 The Tails Problem

The tails problem describes the significant increase in error that may occur at very low or very high frequencies. This problem is significant when the impedance being measured has poles or zeros at those extreme frequencies. To visualize this problem better, the double-dispersion Cole model used in the previous example was re-simulated with the following parameters: $R_\infty = 1\text{ k}\Omega$, $R_1 = 900\text{ }\Omega$, $R_2 = 500\text{ }\Omega$, $C_1 = 100\text{ }\mu\text{F}$, $C_2 = 1\text{ nF}$, $\alpha_1 = 0.5$, $\alpha_2 = 0.9$. These parameter values yield characteristic time constants $\tau_{1,2} = (R_{1,2}C_{1,2})^{1/\alpha_{1,2}}$ which set the characteristic frequencies of the model at $f_{c1} = 1/2\pi\tau_1 = 19.64\text{ Hz}$ and $f_{c2} = 1/2\pi\tau_2 = 1.596\text{ MHz}$. Using the magnitude data in the two different frequency ranges (10Hz-1MHz) and (1Hz-10MHz) the phase information was extracted from both responses using the proposed algorithm. The Bode and Nyquist plots of ideal simulations and algorithm extracted simulations are shown in Figs. 3.5(a) and 3.5(b), respectively. The ideal

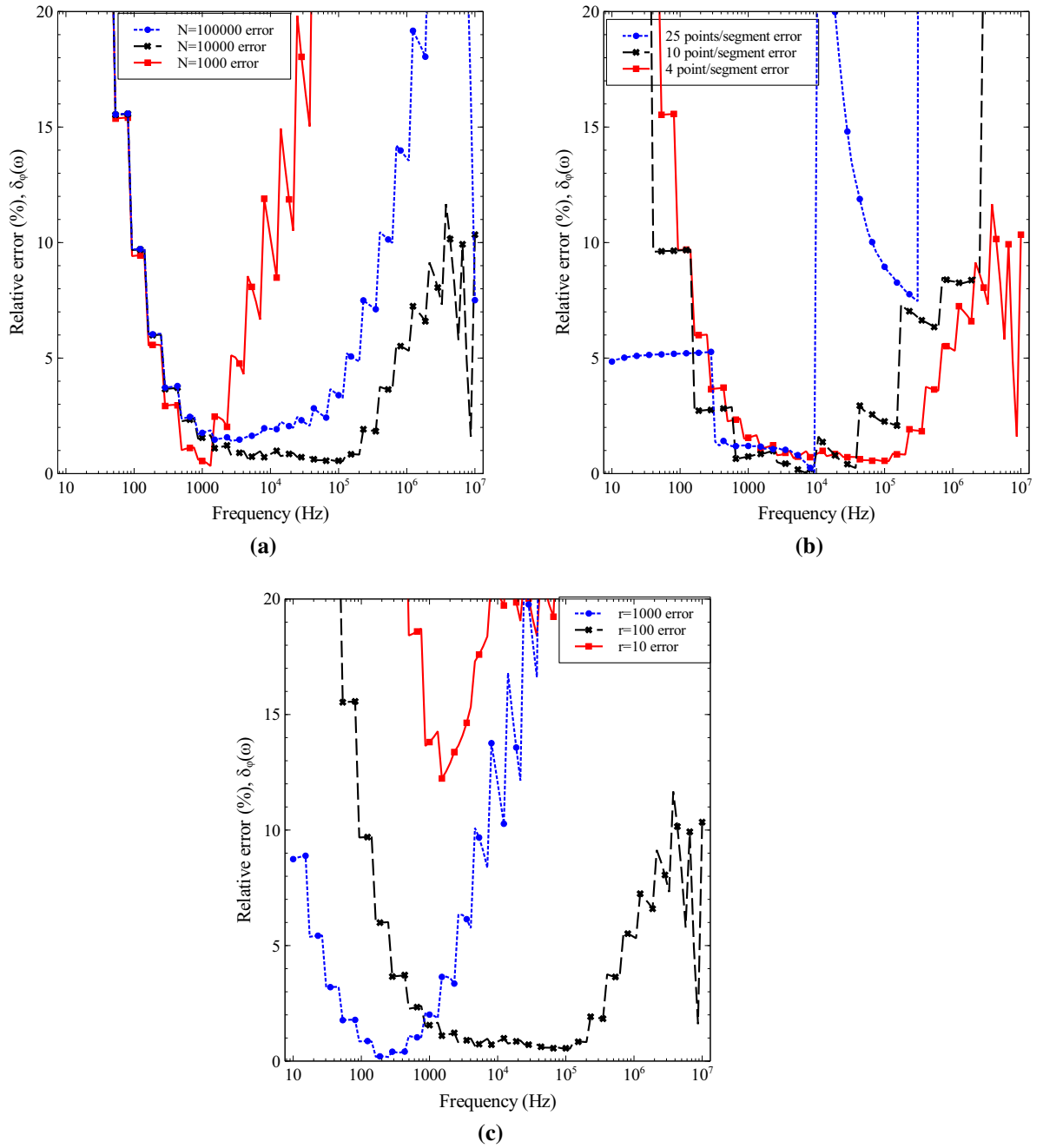


Figure 3.4: Relative error $\delta_\phi(\omega)$ analysis for (a) changing values of N , (b) changing values of s and (c) changing values of r . Reprinted by permission from [Springer Nature and Copyright Clearance Center]: [Springer Nature] [Circuits, Systems, and Signal Processing] [Extraction of phase information from magnitude-only bio-impedance measurements using a modified Kramers–Kronig transform, A. Al-Ali, A. Elwakil, B. Maundy, and T. Freeborn], [2017].

simulations are presented as solid lines with the algorithm extracted simulations presented as squares. From Fig. 4(c), the algorithm extracted simulations show a greater deviation from the ideal at high frequencies for both datasets. It should be noted that this deviation is greatest for the extraction from the 10 Hz to 1 MHz dataset; which was expected since $f_{c2} = 1.6\text{MHz}$ is out of the 10Hz-1MHz range. The error using the proposed algorithm is reduced significantly when the wider frequency range (1Hz-10MHz) is used for the identical data as shown in Fig. 3.5(c). In the proposed algorithm, the tails problem is reduced by integrating each segment alone on a specific frequency range. Using this approach, only segments close to the end-frequencies are affected in cases when the impedance datasets have critical frequencies close to these end frequencies. Since the location of the critical frequencies of a measured impedance are not known a-priori, this implies that in any hardware solution, the magnitude data should always be collected over the widest possible frequency range to minimize the likelihood of the tails problem and ensure the computed phase is accurate. Alternatively, one can safely assert that the computed phase is accurate over the frequency range which is one decade below the highest scanned frequency and one decade above the lowest scanned frequency. That is, if the impedance magnitude was measured over the frequency range (1Hz-10MHz) for example, then the tails problem does not affect the calculated phase in the range (10Hz-1MHz).

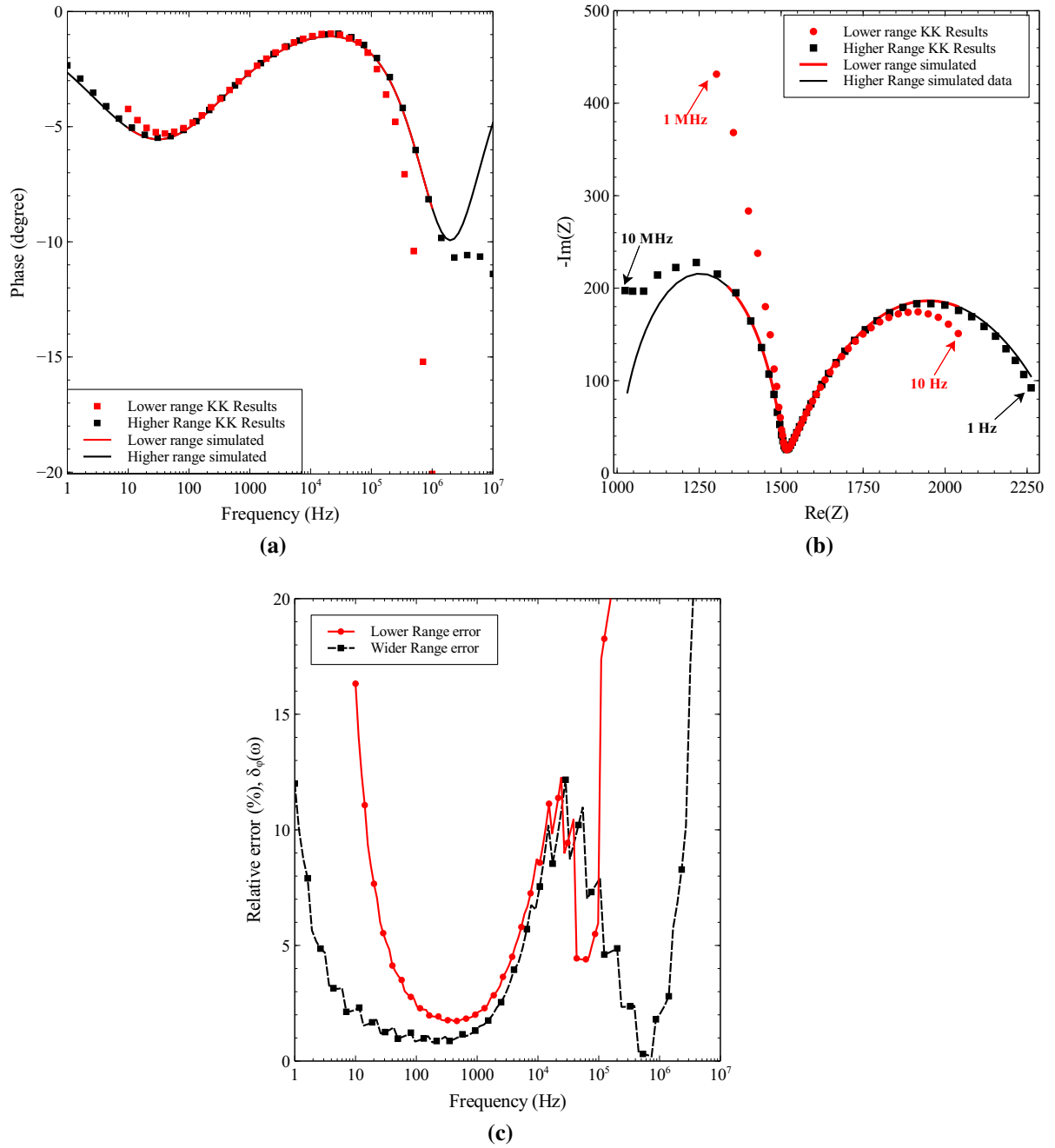


Figure 3.5: Demonstration of the tails problem in a double-dispersion Cole impedance model which has its critical frequencies located approximately at 20Hz and 1.6MHz when simulated for 2 different frequency ranges (10Hz-1MHz and 1Hz-10MHz) via (a) Bode Plot, (b) Nyquist plot and (c) relative error $\delta_\phi(\omega)$. Reprinted by permission from [Springer Nature and Copyright Clearance Center]: [Springer Nature] [Circuits, Systems, and Signal Processing] [Extraction of phase information from magnitude-only bio-impedance measurements using a modified Kramers–Kronig transform, A. Al-Ali, A. Elwakil, B. Maundy, and T. Freeborn], [2017].

3.4.1.3 Noise analysis

Testing the algorithm with noisy data is important because ideal datasets are not representative of situations under which this algorithm will be applied and different hardware designs are expected to have different noise levels. To generate the noisy datasets, the double-dispersion Cole impedance model was simulated from 1Hz-10MHz using the same parameter values given in the previous section with white Gaussian noise added. The Gaussian white noise was added using MATLABs “AWGN” function using SNR values of 40, 60 and 80dB, respectively. These noisy datasets are shown in Fig. 3.6(a). The computed phase using the proposed algorithm is plotted in Fig. 3.6(b) and the relative error, $\delta_\phi(\omega)$ is also shown in Fig. 3.6(c). It is seen that δ_ϕ is very low in the range 100Hz-1MHz for SNR values up to 45dB. Lower values of SNR significantly increase the phase error. However, it is important to mention that in actual hardware setups, the magnitude measurements are far less susceptible to noise than phase measurements, and hence impedance magnitude datasets with high SNRs can be achieved.

3.4.2 Cherry Tomato Experimental Data

The proposed algorithm was further tested using measurements from four cherry tomato samples using a two-electrode configuration. The first set of measurements were done over the frequency range 10Hz to 2MHz, while the second set of measurements, which represents the same sample tomatoes after 4 days from the first measurement, was done over the frequency range 1Hz to 2MHz. The data was obtained as 150 points of magnitude and phase using the precision N4L PSM 1735 Impedance analyzer [34] with a 100mV applied voltage signal. The magnitude data was used to calculate the phase (using the proposed algorithm) which was then compared to the experimentally measured phase as shown in Figs. 3.7(a) and 3.8(a). In both figures, the measured data for each sample is given as a solid line, while the algorithm extracted phase is given as diamonds. Also, using equations (3.10) and (3.11) applied both to the measured phase and the calculated phase,

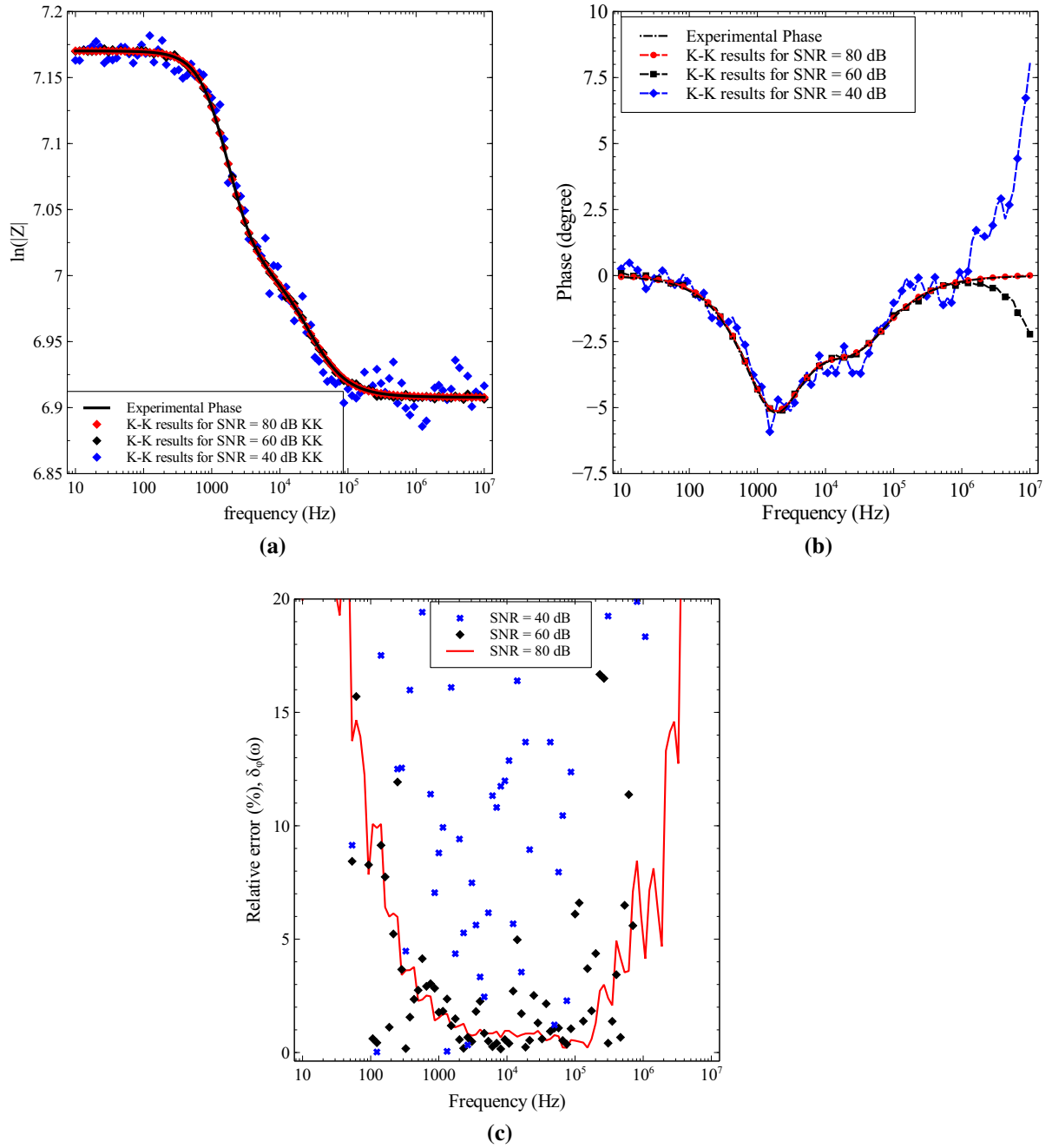


Figure 3.6: Noisy magnitude data testing (a) the input magnitude with different SNR levels and (b) the computed phase compared to the ideal value (c) relative error $\delta_\phi(\omega)$.

Reprinted by permission from [Springer Nature and Copyright Clearance Center]: [Springer Nature] [Circuits, Systems, and Signal Processing] [Extraction of phase information from magnitude-only bio-impedance measurements using a modified Kramers–Kronig transform, A. Al-Ali, A. Elwakil, B. Maundy, and T. Freeborn], [2017].

the Nyquist plots for both sets are shown in Figs. 3.7(b) and 3.8(b), respectively. For clarity, results for 4 samples only from each set are plotted.

It is clear from Fig. 3.7(a) that the impedance of the fresh tomatoes in the first set does have a critical frequency located between 1MHz and 2MHz and therefore the computed phase using the algorithm deviates from the measured phase above 1MHz for some samples (sample#2 and to a lesser extent sample#1). It is also clear from the same figure that all samples have another critical frequency located between 50Hz and 100Hz and therefore as expected, the computed phase starts to deviate from that experimentally measured close to that frequency range. In Fig. 3.8(a), the second set impedance data shows no significant change in the high frequency behavior. However, at the low frequency an extra critical low-frequency inflection point shows up for all of the samples. For sample#1 and sample#2, this critical point is clearly located between 1Hz and 10Hz where the computed phase deviates noticeably from that measured while for sample#3 and sample#4, this critical frequency is located somewhere between 10Hz and 20Hz and therefore the phase deviation is less. Given that for this second set the measurements were collected from a lower frequency 1Hz instead of 10Hz, we notice the existence of critical frequencies in the impedance at the lower frequency range. Furthermore, close inspection of Fig. 3.8(a) indicates that sample#3 is expected to undergo another phase inflection at a critical frequency below 1Hz. Based on the algorithm performance compared to the precise impedance measurements, a portable impedance device to monitor fresh cherry tomatoes using the impedance magnitude-only requires scanning the frequency range from 10Hz-2MHz to ensure the algorithm performs accurately. However, if the purpose of the portable device is to monitor the aging effect on these tomatoes then it will be necessary to widen the frequency scan range to 1Hz-2MHz since it is clear from Figs. 3.7 and 3.8 that the aging effect appears at the lower frequencies. Of course, if the cost in time and hardware can be tolerated, it would be possible to address both purposes by adopting a wider frequency scan range (say 0.1Hz-10MHz) and ensure optimum accuracy. Note however, that portable devices deployed in field will most likely

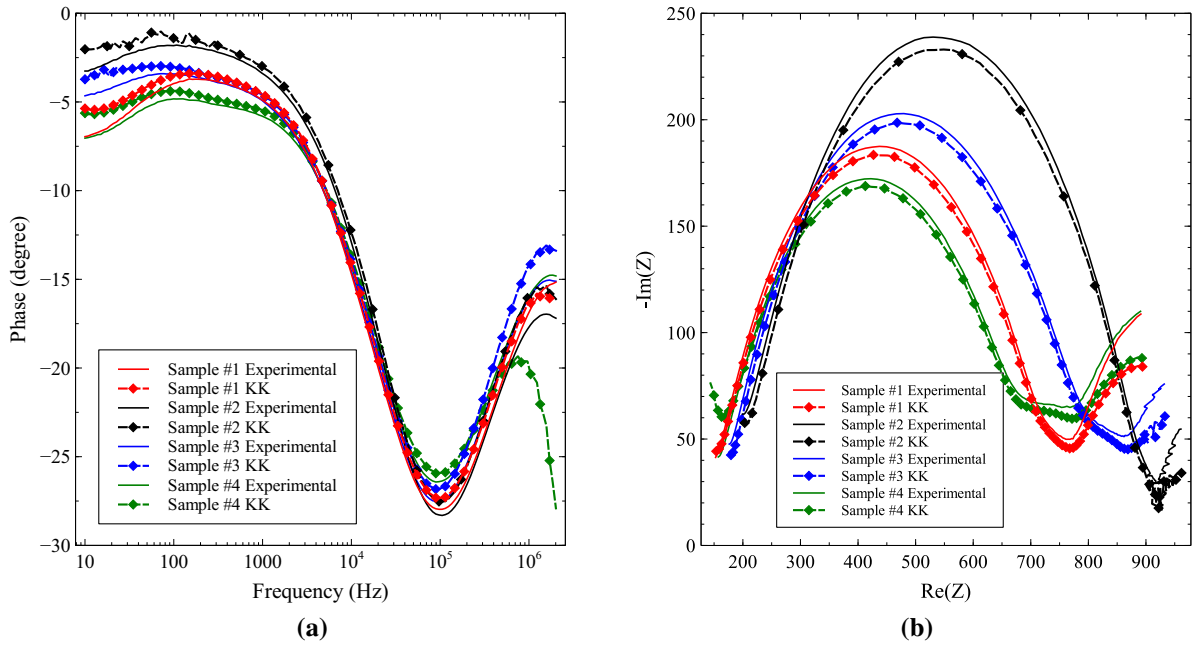


Figure 3.7: Results from the first (fresh) cherry tomato data set (a) phase information and (b) Nyquist plot. Reprinted by permission from [Springer Nature and Copyright Clearance Center]: [Springer Nature] [Circuits, Systems, and Signal Processing] [Extraction of phase information from magnitude-only bio-impedance measurements using a modified Kramers–Kronig transform, A. Al-Ali, A. Elwakil, B. Maundy, and T. Freeborn], [2017].

be battery operated and optimization of the measurement time extends the battery life time.

Finally, it is usually the case that following the performance of bio-impedance measurements a circuit model is targeted and optimization techniques are then applied to fit the measured magnitude and phase to this specific model. For example, assume fitting the measured tomatoe impedance data to a double-dispersion Cole model is a target. Using the freely available EIS software package [32] equipped with a number of optimization methods, we performed best fitting on sample #1 from the fresh tomatoes data set and sample #2 from the aging date set to obtain the results reported in Table. 3.1. A plot of the fitted curves alongside the actual measured impedance data is given in Figs. 3.9(a) and 3.9(b) for both samples respectively. The same optimization EIS technique was then fed with the measured impedance magnitude but with the computed phase using the proposed algo-

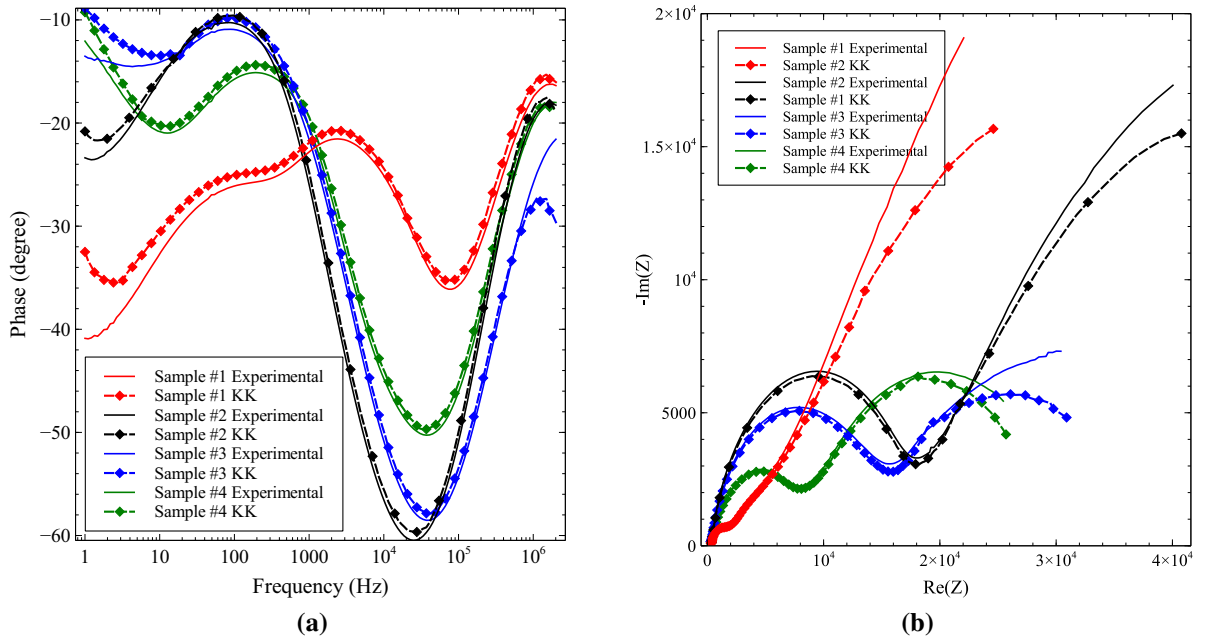


Figure 3.8: Results from cherry tomato second (aging) data set (a) phase information and (b) Nyquist plot. Reprinted by permission from [Springer Nature and Copyright Clearance Center]: [Springer Nature] [Circuits, Systems, and Signal Processing] [Extraction of phase information from magnitude-only bio-impedance measurements using a modified Kramers–Kronig transform, A. Al-Ali, A. Elwakil, B. Maundy, and T. Freeborn], [2017].

rithm. The fitting results are also plotted in the same Figs. 3.9(a) and 3.9(b). These figures show the actual measured impedance in solid red the EIS best fitting of this impedance in solid black while the K-K computed impedance is shown in dashed red and its best EIS fitting in dashed black. It is noted that while EIS optimization was not able to minimize the error in K-K computed data at low frequencies for sample#1 (see Fig. 3.9(a)), it was able to minimize it for sample#2, see Fig 3.9(b). The reason is that sample#1 impedance measurements were performed starting at 10Hz while sample#2 impedance data measurements were performed starting at 1Hz. In conclusion, the wider the frequency range over which the magnitude of the impedance is measured, the less the error that will result in the computed K-K phase.

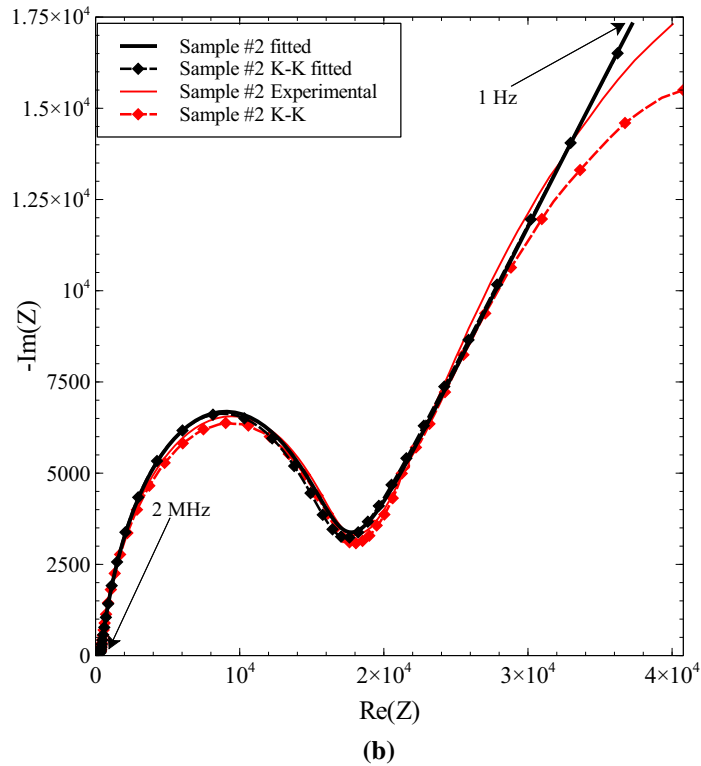
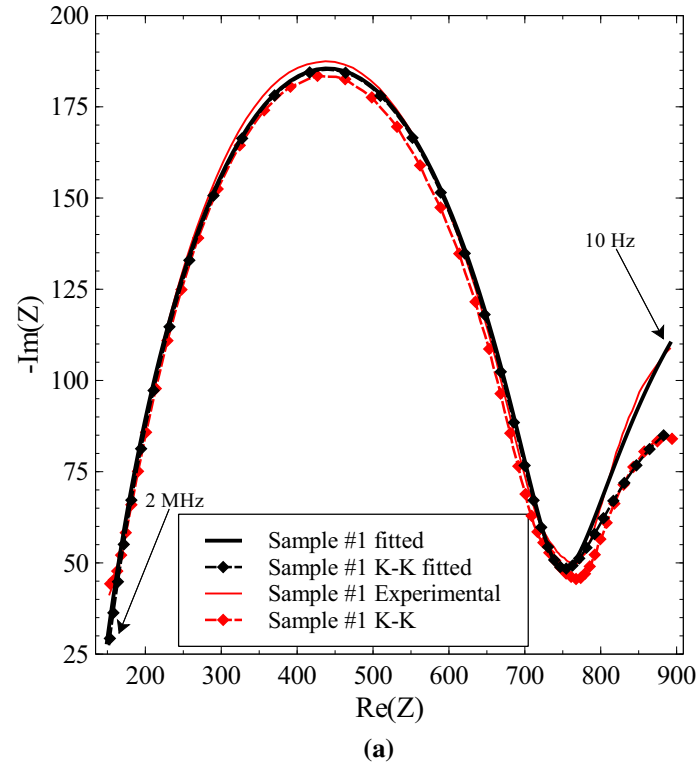


Figure 3.9: Comparison of data fitting to a double dispersion impedance model using precisely measured impedance data and the K-K constructed data for two tomato samples (a) sample #1 from the fresh tomatoe set and (b) sample #2 from the aging set. Reprinted by permission from [Springer Nature and Copyright Clearance Center]: [Springer Nature] [Circuits, Systems, and Signal Processing] [Extraction of phase information from magnitude-only bio-impedance measurements using a modified Kramers–Kronig transform, A. Al-Ali, A. Elwakil, B. Maundy, and T. Freeborn], [2017].

Table 3.1: Comparison of the parameters of a double-dispersion Cole-Cole model fitting of two tomato samples. Reprinted by permission from [Springer Nature and Copyright Clearance Center]: [Springer Nature] [Circuits, Systems, and Signal Processing] [Extraction of phase information from magnitude-only bio-impedance measurements using a modified Kramers–Kronig transform, A. Al-Ali, A. Elwakil, B. Maundy, and T. Freeborn], [2017].

Sample	$R_{\infty}(\Omega)$	$R_1(\Omega)$	$R_2(\Omega)$	$C_1(\mu)$	$C_2(\mu)$	α_1	α_2
Sample #1							
Experimental	132.8	606.5	603.0	437.4	0.3517	0.5348	0.6945
K-K transform	136.3	592.4	428.1	475.6	0.3243	0.50126	0.7013
Sample #2							
Experimental fit	270.8	15140	1×10^6	0.0185	15.72	0.8588	0.4377
K-K transform results fit	280.07	14780	0.972×10^6	0.0162	16.47	0.8699	0.4325

3.5 Summary

A phase extraction method based on the modified K-K algorithm was proposed and tested with different sets of data to obtain the phase information from the measured magnitude. The application to bio-impedance data of cherry tomatoes in the ranges 1Hz-2MHz and 10Hz-2MHz was demonstrated and the errors induced by narrowing the frequency range clearly studied. The results reported are an important step towards the realization of cheap and portable bio-impedance sensor devices that reduce the necessary measurement hardware by eliminating phase measurements without sacrificing the accuracy of measurements, or introducing assumptions regarding the impedance model of the measured tissue.

CHAPTER 4

Proposed Impedance Analyzer Design and Implementation

4.1 Introduction

As it was mentioned in the introduction of this thesis, the primary objective of this work is to design a portable bio-impedance analyzer with simple hardware, so it can be easily deployed in the field and conduct continuous measurements. Eliminating the need for the hardware phase measurement by using the K-K transform algorithm to extract the phase from the magnitude reduced the design complicity.

In this chapter, the details of the proposed design which was previously shown in Fig. 1.1 will be discussed. Starting with the magnitude detection circuit before going through the processing and control which is done through the microcontroller and the Python code. Additionally, the implementation of the proposed design is discussed.

4.2 The magnitude detection

Measuring the magnitude as a function of the frequency can be done in several ways such as using instrumentation amplifiers and gain detector chip like the AD8302 as in the work proposed in [81, 82]. The AD8302 chip can detect the gain between any two signals using log amplifiers and produces a DC voltage representing the gain in dB with a sensitivity of 30mV/dB with an input range -60 dBm to 0 dBm [83]. However, after testing the chip it showed a high error in frequencies below 20Hz and displayed calibration problems at high frequencies. To avoid the limitations of using a single chip solution like the AD8302 and

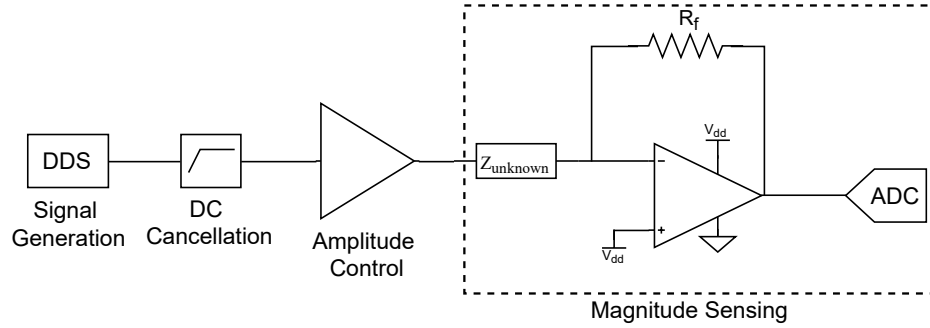


Figure 4.1: Magnitude detection hardware design

be able to cover the full frequency range 1Hz to 10MHz, a new technique based on the basic non-inverting amplifier design was proposed.

Figure 4.1 shows the overall design of the hardware design which starts initially with generating a voltage signal (excitation signal) followed by a DC cancellation stage and amplitude control of the signal. Finally, the magnitude is measured using the newly proposed technique which is based on a simple gain amplifier. The details of the design first published in [84] will be discussed in the following sub-sections.

4.2.1 Signal generation

To generate an accurate and precise signal, we chose to use a Direct Digital Synthesizer (DDS). The best choice for our design was the AD9850 chip from Analog Devices [85]. This chip has a 32-bit tuning word which provides a resolution of 0.0291 Hz with a 125 MHz clock and maximum frequency of 62.5MHz. Those ratings and being compatible and easy to interface with the microcontroller we chose made it the best choice for our design. However, the AD9850 produces a signal with a constant DC offset of 0.5V and an amplitude of $1V_{p-p}$. To control those two specifications we needed the following two stages of DC cancellation and Amplitude control.

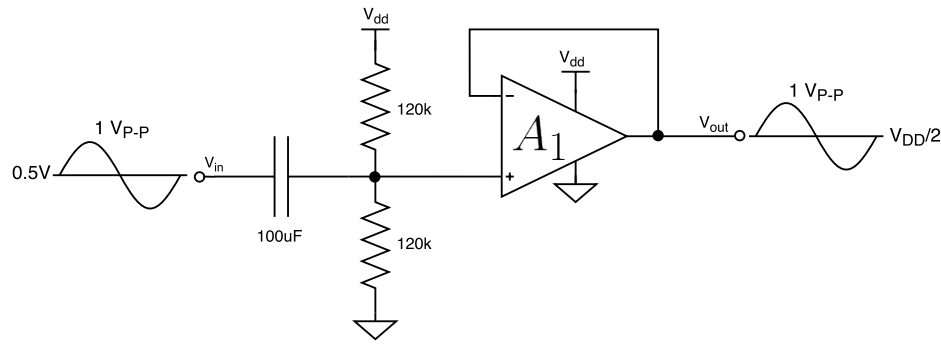


Figure 4.2: DC cancellation circuit design

4.2.2 DC Cancellation

Keeping the DC offset constant across the unknown impedance is a crucial issue for some bio-impedance tests, since it is necessary to avoid DC polarization at the measured impedance. This could happen when the DC voltage is different on the two ends of $Z_{unknown}$ in Fig. 4.1 [51]. Figure 4.2 shows the DC cancellation schematic which starts with a coupling capacitor that makes an RC high pass filter with a cutoff frequency $f_c = \frac{1}{2\pi RC} = 26.53 \text{ mHz}$. The cut-off frequency was chosen this low so that at 1 Hz the gain of the filter would be -0.003 dB at a phase of 1.5° and at 100 mHz the gain of the filter would be -0.3 dB at a phase of around 15° , which provides the circuit the ability to have an excitation frequency as low as 1 Hz without affecting the excitation signal amplitude. It should be noted that if the filter cutoff was chosen to be at 100 mHz then at 1 Hz the gain of the filter would be -0.04 dB at a phase of 5.7° which would affect the excitation signal. This low cut-off ensures the cancellation of the DC offset before setting it to $\frac{V_{dd}}{2}$ using voltage division. Setting the offset to $\frac{V_{dd}}{2}$ ensures that the signal will have this same DC voltage over the entire analog front end and to be able to get the highest dynamic range of the Op-Amps and the analog to digital converter (ADC). This stage is followed by a buffer to isolate it from the amplification stage.

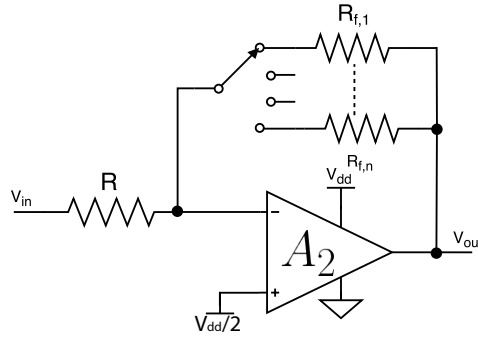


Figure 4.3: Amplitude control circuit design

4.2.3 Amplitude control

When conducting bio-impedance measurements of fruits, generally speaking they are not sensitive to the excitation signal amplitude. However, in bio-impedance tests like the ones done on humans and other biological tissues require very low excitation voltages to keep it safe [51]. This makes controlling the amplitude necessary for any impedance analyzer to be able to work for different applications and in various fields. While programmable gain amplifiers (PGA) are built to conduct amplitude control, we could not find a commercial PGA that could satisfy the system requirements of gain steps while working over the whole frequency range. In this work, a simple non-inverting amplifier with switched feedback resistors was used to control the amplitude of the excitation signal as shown in Fig. 4.3, where the output will have a gain A_v calculated as follows

$$A_v = \frac{V_{out_{A1}}}{V_{in_{A1}}} = -\frac{R_{f1,n}}{R} \quad (4.1)$$

where n is the number of the feedback resistor and switching between those n resistors can give us any excitation voltage that we need.

4.2.4 Magnitude Sensing Amplifier

To understand how the magnitude sensing amplifier works, we have to start with the basic inverting amplifier circuit shown Fig. 4.4. Analyzing the circuit would give us the following well known inverting amplifier gain equation

$$\left| \frac{V_{outA2}}{V_{inA2}} \right| = \frac{R_{f2}}{|Z_{unknown}|} \quad (4.2)$$

where $|V_{inA2}|$ is the input signal amplitude to this stage, $|V_{outA2}|$ is the output signal amplitude from this stage, R_{f2} is the switched feedback resistor and $|Z_{unknown}|$ is the magnitude of the unknown impedance which we intend to measure. Re-arranging equation (4.2) to solve $|Z_{unknown}|$ yields,

$$|Z_{unknown}| = R_{f2} \cdot \left| \frac{V_{inA2}}{V_{outA2}} \right| \quad (4.3)$$

While both R_{f2} and V_{inA2} can be controlled by the microcontroller, $|V_{outA2}|$ is the only unknown parameter that needs to be measured to obtain the magnitude of $Z_{unknown}$.

With V_{inA2} set to be constant through out the sweep in most cases, the value of the feedback resistor R_{f2} is the only value that we can control to cover a high impedance range. The choice of the feedback resistor R_{f2} determines the maximum and minimum unknown impedance that can be measured as follows

$$|Z_{unknown}|^{max} = R_{f2} \cdot \left| \frac{V_{inA2}}{V_{outA2,min}} \right| \quad (4.4)$$

$$|Z_{unknown}|^{min} = R_{f2} \cdot \left| \frac{V_{inA2}}{V_{outA2,max}} \right| \quad (4.5)$$

Where $V_{outA2,min}$ is the minimum amplitude output voltage that can be read by the ADC and $V_{outA2,max}$ is the maximum amplitude voltage which won't saturate both the ADC and the Op-Amp. In the proposed design the feedback resistor can be automatically switched using

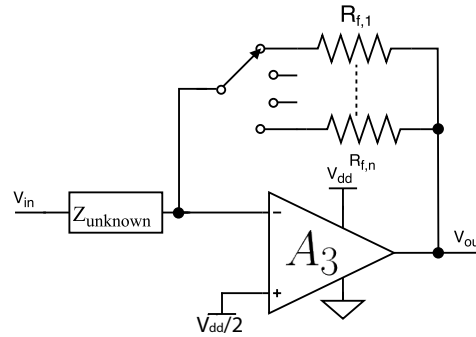


Figure 4.4: Magnitude sensing circuit design

the microcontroller to cover any impedance range of interest. This was done by using a switch in the Op-Amp feedback loop as shown in Fig. 4.4.

4.2.5 Analog to digital conversion (ADC)

The ADC marks the end of the magnitude detection hardware where the output voltage signal $v_{out_{A2}}$ is digitized to get the amplitude $|V_{out_{A2}}|$. The ADC also controls the frequency range that can be covered using this device. In the proposed design, the internal ADC of the microcontroller was used. However, with a maximum sampling frequency of 500kHz the frequency range would be limited to 100 kHz, since at least 5 points per period are needed to get a good fitting for the sampled signal. This was solved by using under-sampling to sample signals over 100kHz up to 10MHz. The idea of under-sampling states that you need to sample the signal with at least double its bandwidth instead of double its maximum frequency, where the bandwidth of the signal can be controlled by the number of cycles being sampled. Using this technique simplified the overall system design and reduced the cost since it eliminates the need for an external high sampling ADC which in addition to being much more expensive it would require special printed circuit board (PCB) design and a field-programmable gate array (FPGA) to control it.

4.3 Processing and Control

The proposed design is controlled by the microcontroller unit (MCU) which excites the signal through the DDS, sets the values of R_{f1} and R_{f2} through the switches and digitize the output signal. A personal computer (PC) utilizing a python code communicates with the MCU to set the parameters (f, R_{f1}, R_{f2}). Also, the PC reads the digitized signal to process it and then calculate the unknown impedance magnitude $|Z_{unknown}|$ and extract the phase using the K-K transform afterwards.

4.3.1 Microcontroller code

The microcontroller is one of the main parts of the proposed design. The flowchart in Fig. 4.5 shows the sequence in which the microcontroller code works. It starts by getting a command through the serial port to either set the value of one of the two feedback resistors or generate the excitation signal at the specified frequency. The microcontroller then decides to either use over-sampling to sample the signals under 100kHz or use under-sampling to sample signals over 100kHz and up to 10MHz and set the sampling frequency accordingly to assure that at least one period of the output signal v_{outA2} is being sampled. Finally, the microcontroller code collects 1024 samples then conveys it over to the PC where further processing is done using the Python code.

4.3.2 Python Code

The python code was written using jupyter notebook which is a web application that allows you to create a document from your code and add some visualization. In this work a python code was written using this web application to do the processing of the data after getting it from the microcontroller, and it also controls the frequency sweep as shown in the flowchart in Fig. 4.6. The code initializes the sweep by connecting to the microcontroller through the serial interface, and then it sets the values of the feedback resistors R_{f1}, R_{f2} through the

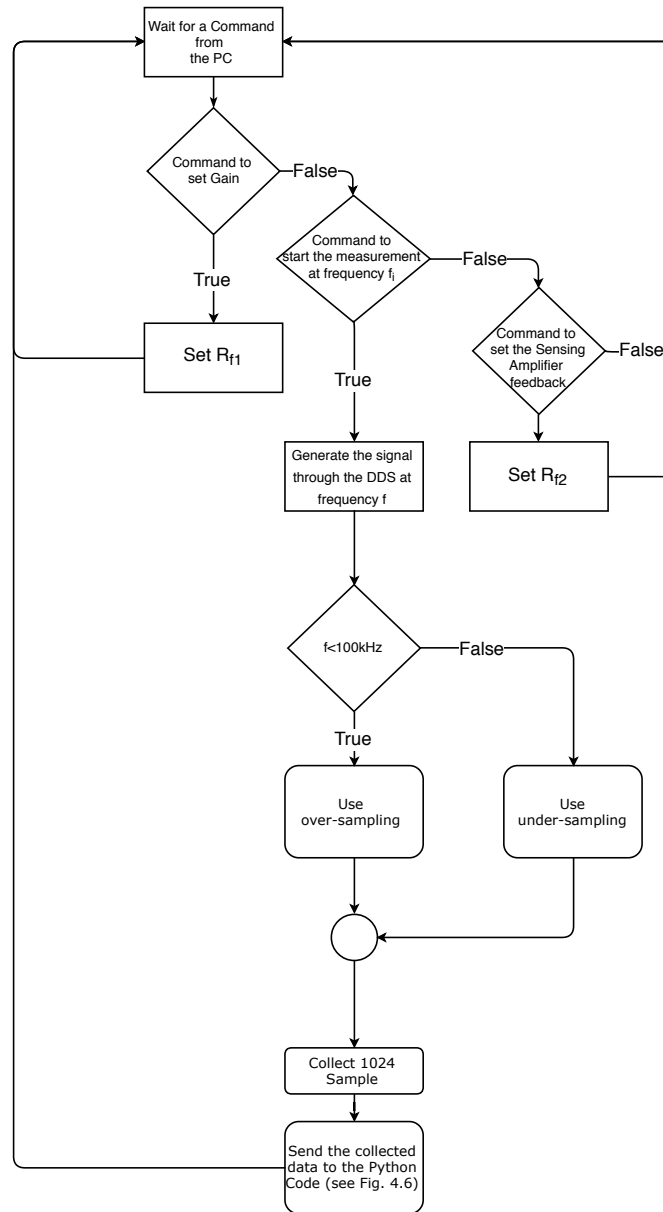


Figure 4.5: Microcontroller code flowchart

microcontroller to set the gain and the impedance range of operation. Afterwards, it starts sweeping the frequencies using a predefined frequency array. At each frequency point, the Python code gets the digitized signal from the microcontroller and fits it to a sine wave using an open source fitting algorithm (LMFIT) from [86]. The digitized signal gets fitted to the following equation

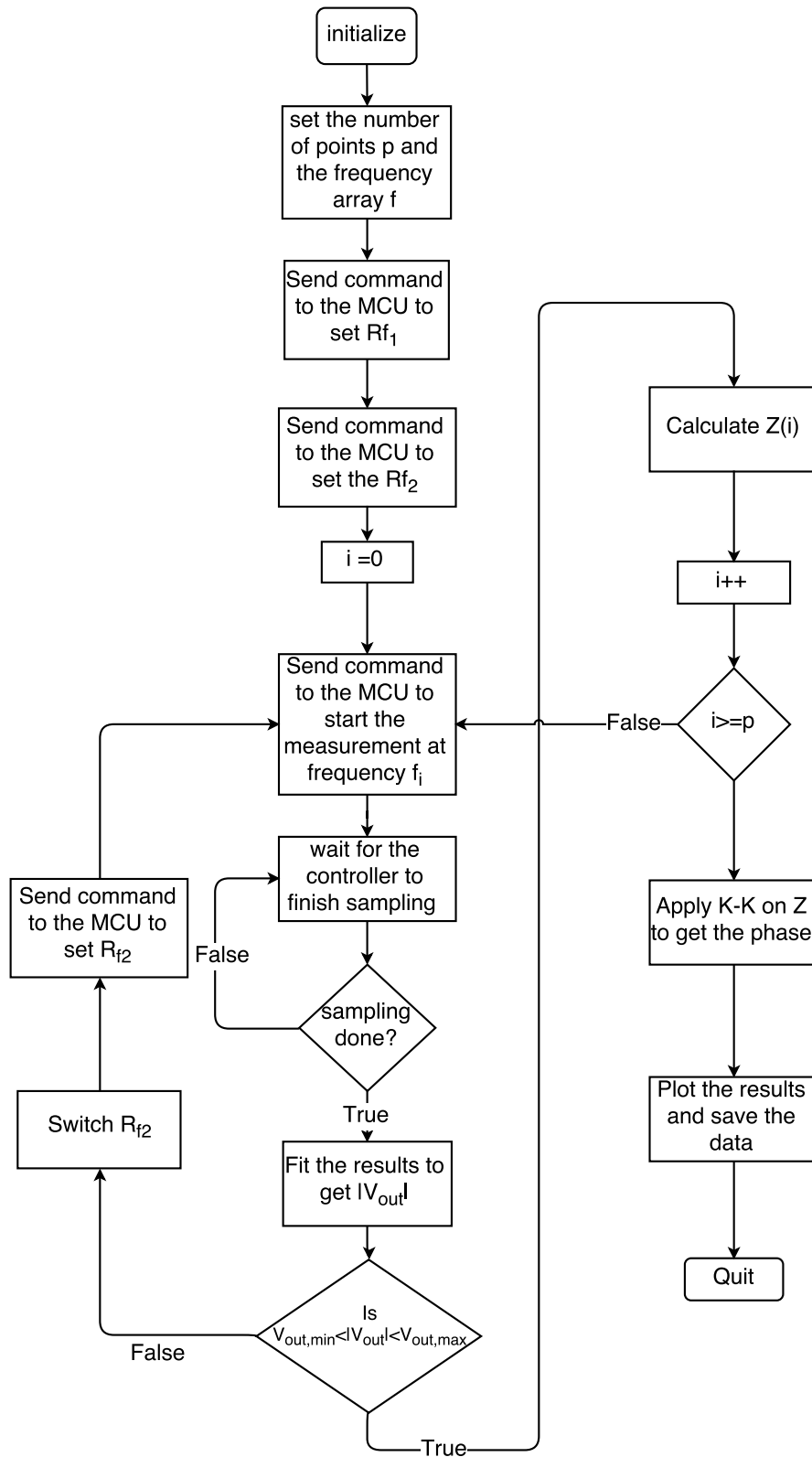


Figure 4.6: Python code flowchart

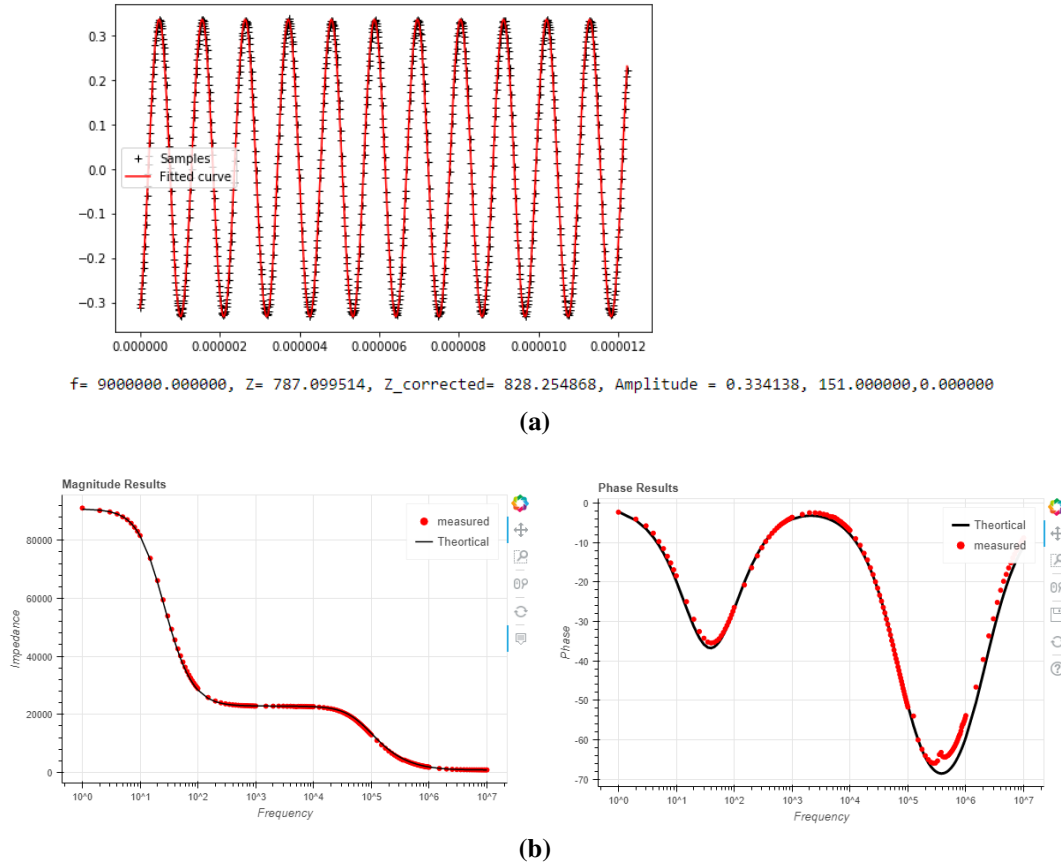
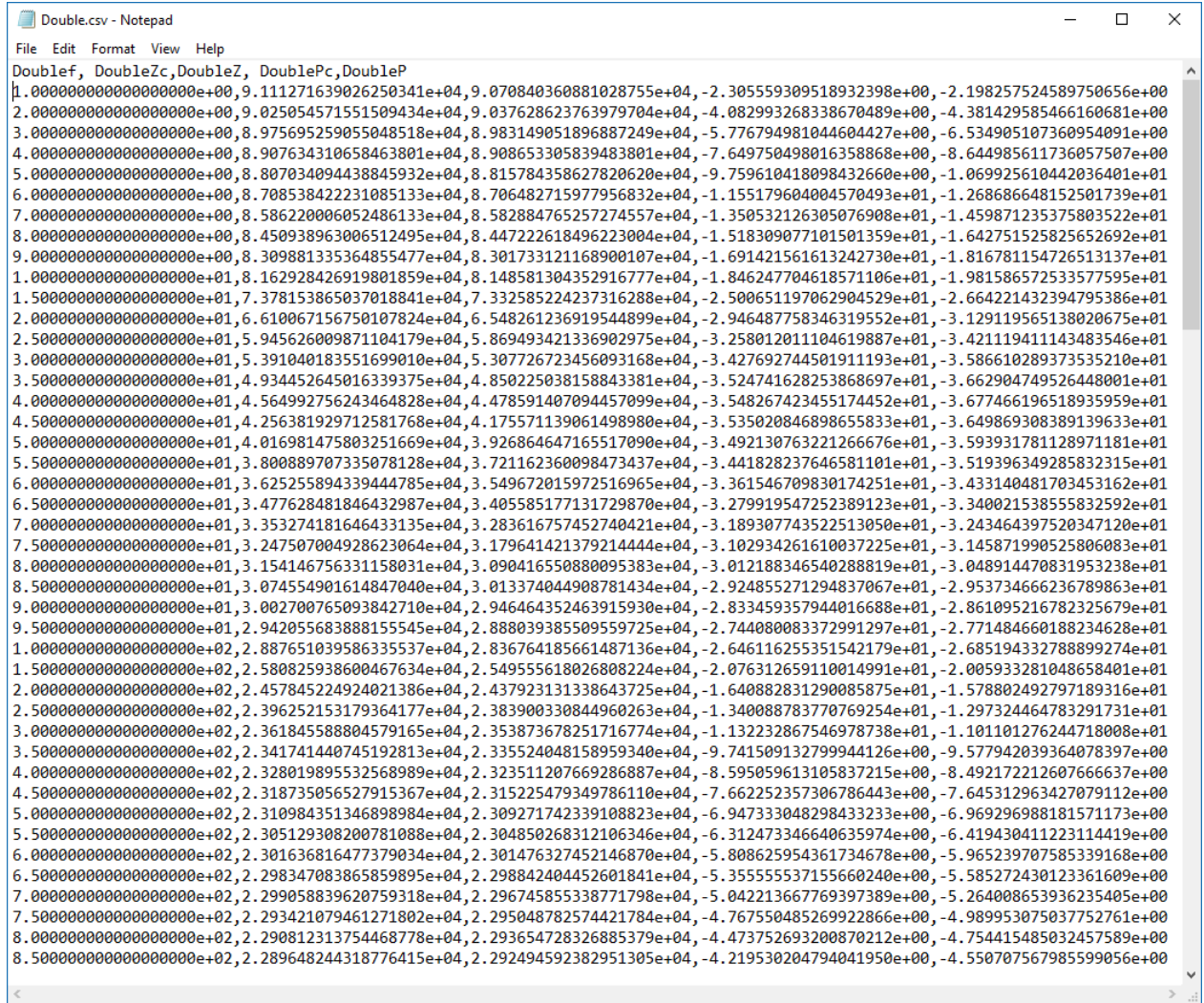


Figure 4.7: Python code results (a) sampled v_{outA2} signal and (b) Magnitude and phase results

$$x(t) = A \cdot \sin(f_i \cdot t + \phi) + DC \quad (4.6)$$

where the fitted signal amplitude A represents the output voltage of the sensing amplifier $|V_{outA2}|$. This value determines whether to switch the value of R_{f2} and/or calculate the impedance value as it was mentioned in the subsection 4.2.4. During the sweep at each frequency point f_i the fitted data and the extracted magnitude is shown for the user as in Fig. 4.7(a). Then after the sweep, the python code applies the K-K transform to the impedance magnitude array to extract the phase of the measured magnitude as it was previously discussed in section 3.3. Finally, the impedance magnitude and phase gets plotted for the user to see the results (see Fig. 4.7(b)) which are then saved into a text file as it is shown in Fig. 4.8.



```

Double.csv - Notepad
File Edit Format View Help
Doublef, DoubleZc, DoubleZ, DoublePc, DoubleP
1.0000000000000000e+00,9.111271639026250341e+04,9.070840360881028755e+04,-2.305559309518932398e+00,-2.198257524589750656e+00
2.0000000000000000e+00,9.025054571551509434e+04,9.037628623763979704e+04,-4.082993268338670489e+00,-4.381429585466160681e+00
3.0000000000000000e+00,8.975695259055048518e+04,8.983149051896887249e+04,-5.776794981044604427e+00,-6.534905107360954091e+00
4.0000000000000000e+00,8.907634310658463801e+04,8.908653305839483801e+04,-7.649750498016358868e+00,-8.644985611736057507e+00
5.0000000000000000e+00,8.807034094438845932e+04,8.815784358627820620e+04,-9.759610418098432660e+00,-1.069925610442036401e+01
6.0000000000000000e+00,8.708538422231085133e+04,8.706482715977956832e+04,-1.155179604004570493e+01,-1.268686648152501739e+01
7.0000000000000000e+00,8.586220006052486133e+04,8.582884765257274557e+04,-1.350532126305076908e+01,-1.459871235375803522e+01
8.0000000000000000e+00,8.450938963006512495e+04,8.447222618496223004e+04,-1.518309077101501359e+01,-1.64275152582562692e+01
9.0000000000000000e+00,8.309881335364855477e+04,8.301733121168900107e+04,-1.691421561613242730e+01,-1.816781154726513137e+01
10.0000000000000000e+01,8.162928426919801859e+04,8.148581304352916777e+04,-1.846247704618571106e+01,-1.981586572533577595e+01
11.0000000000000000e+01,7.378153865037018841e+04,7.332585224237316288e+04,-2.500651197062904529e+01,-2.664221432394795386e+01
12.0000000000000000e+01,6.610067156750107824e+04,6.548261236919544899e+04,-2.946487758346319552e+01,-3.129119565138020675e+01
13.0000000000000000e+01,5.945626009871104179e+04,5.869493421336092975e+04,-3.258012011104619887e+01,-3.421119411143483546e+01
14.0000000000000000e+01,5.391040183551699010e+04,5.307762723456093168e+04,-3.427692744501911193e+01,-3.586610289373535210e+01
15.0000000000000000e+01,4.934452645016339375e+04,4.850225038158843381e+04,-3.524741628253868697e+01,-3.662904749526448001e+01
16.0000000000000000e+01,4.564992756243464828e+04,4.478591407094457099e+04,-3.548267423455174452e+01,-3.677466196518935959e+01
17.0000000000000000e+01,4.256381929712581768e+04,4.175571139061498980e+04,-3.535020846898655833e+01,-3.649869308389139633e+01
18.0000000000000000e+01,4.016981475803251669e+04,3.926864647165517090e+04,-3.492130763221266676e+01,-3.593931781128971181e+01
19.0000000000000000e+01,3.800889707335078128e+04,3.721162360098473437e+04,-3.441828237646581101e+01,-3.519396349285832315e+01
20.0000000000000000e+01,3.625255894339444785e+04,3.549672015972516965e+04,-3.361546709830174251e+01,-3.433140481703453162e+01
21.0000000000000000e+01,3.477628481846432987e+04,3.405585177131729870e+04,-3.279919547252389123e+01,-3.34002153855582592e+01
22.0000000000000000e+01,3.353274181646433135e+04,3.283616757452740421e+04,-3.189307743522513050e+01,-3.243464397520347120e+01
23.0000000000000000e+01,3.247507004928623064e+04,3.179641421379214444e+04,-3.102934261610037225e+01,-3.145871990525806083e+01
24.0000000000000000e+01,3.154146756331158031e+04,3.090416550880095383e+04,-3.012188346540288819e+01,-3.048914470831953238e+01
25.0000000000000000e+01,3.074554901614847040e+04,3.013374044908781434e+04,-2.924855271294837067e+01,-2.953734666236789863e+01
26.0000000000000000e+01,3.002700765093842710e+04,2.946464352463915930e+04,-2.833459357944016688e+01,-2.861095216782325679e+01
27.0000000000000000e+01,2.942055683888155545e+04,2.888039385509559725e+04,-2.744080083372991297e+01,-2.771484660188234628e+01
28.0000000000000000e+02,2.887651039586335537e+04,2.836764185661487136e+04,-2.646116255351542179e+01,-2.685194332788899274e+01
29.0000000000000000e+02,2.580825938600467634e+04,2.549555618026808224e+04,-2.076312659110014991e+01,-2.005933281048658401e+01
30.0000000000000000e+02,2.457845224924021386e+04,2.437923131338643725e+04,-1.640882831290085875e+01,-1.578802492797189316e+01
31.0000000000000000e+02,2.396252153179364177e+04,2.383900330844960263e+04,-1.340088783770769254e+01,-1.297324464783291731e+01
32.0000000000000000e+02,2.361845588804579165e+04,2.353873678251716774e+04,-1.132232867546978738e+01,-1.101101276244718008e+01
33.0000000000000000e+02,2.341741440745192813e+04,2.335524048158959340e+04,-9.741509132799944126e+00,-9.577942039364078397e+00
34.0000000000000000e+02,2.328019895532568989e+04,2.323511207669286887e+04,-8.595059613105837215e+00,-8.492172212607666637e+00
35.0000000000000000e+02,2.318735056527915367e+04,2.315225479349786110e+04,-7.662252357306786443e+00,-7.645312963427079112e+00
36.0000000000000000e+02,2.310984351346898984e+04,2.309271742339108823e+04,-6.947333048298433233e+00,-6.969296988181571173e+00
37.0000000000000000e+02,2.305129308200781088e+04,2.304850268312106346e+04,-6.312473346640635974e+00,-6.419430411223114419e+00
38.0000000000000000e+02,2.301636816477379034e+04,2.301476327452146870e+04,-5.808625954361734678e+00,-5.96523970758339168e+00
39.0000000000000000e+02,2.298347083865859895e+04,2.298842404452601841e+04,-5.35555537155660240e+00,-5.585272430123361609e+00
40.0000000000000000e+02,2.299058839620759318e+04,2.296745855338771798e+04,-5.042213667769397389e+00,-5.264008653936235405e+00
41.0000000000000000e+02,2.293421079461271802e+04,2.295048782574421784e+04,-4.767550485269922866e+00,-4.989953075037752761e+00
42.0000000000000000e+02,2.290812313754468778e+04,2.293654728326885379e+04,-4.473752693200870212e+00,-4.754415485032457589e+00
43.0000000000000000e+02,2.289648244318776415e+04,2.292494592382951305e+04,-4.219530204794041950e+00,-4.550707567985599056e+00

```

Figure 4.8: The saved CSV file

4.3.3 Calibration Process

Calibration is necessary to ensure accurate results. The calibration process is done to account for the switched resistors non-ideality. Although the switched resistors are expected to have a linear response with a constant impedance (equal to the resistor value) over the whole frequency range, in reality it was discovered that the resistors would cut-off at various frequencies depending on their value and tolerance [87]. On the other hand, having a switch in the amplifier feedback makes the non-inverting amplifier shown in Fig. 4.4 act as an integrator because the switches add parasitic capacitance to the feedback loop. The

calibration process is done using the following equation

$$Z_c(f) = \frac{R_c(f)}{\hat{R}_c(f)} \cdot Z(f) \quad (4.7)$$

where $Z_c(f)$ is the calibrated impedance, $R_c(f)$ is the actual impedance of the calibration resistor measured using a commercial impedance analyzer (see Fig. 4.9), $Z(f)$ is the measured impedance result of equation (4.3) and $\hat{R}_c(f)$ is the measured impedance of the calibration resistor R_c using our device (the result of equation (4.3) taking R_c as $Z_{unknown}$). The values of $R_c(f)$ shown in Fig. 4.9 show that the resistors are non-ideal as expected and they cut-off at a certain frequency due to their non-linearity. The calibration is usually done with a resistor value equal to the feedback resistor to calibrate with the amplifier having a gain of 1. Figure 4.10 shows the calibration process for the feedback resistor $R_{f_2} = 2.2k\Omega$ using a calibration resistor $R_c = 2.2k\Omega$. At first the actual impedance of the calibration resistor was obtained using the precision N4L PSM1735 impedance analyzer and saved as $R_c(f)$. Afterwards the same calibration resistor was placed in $Z_{unknown}$ in Fig. 4.4 to be measured. The obtained readings (the result of equation (4.3)) are saved as $\hat{R}_c(f)$ to be used in the calibration of the magnitude results while using this feedback resistor afterwards. Figure 4.11 shows with calibration the effect of correcting the results of a $3.3k\Omega$ resistor measured with our design with $R_{f_2} = 2.2k\Omega$. Any measurements done at frequencies above the cut-off would have some higher error, although this error was reduced by completing the calibration process for each feedback resistor. It is important to mention that the calibration process and its data is saved on the PC and done using the python code.

4.4 Implementation

The proposed design was implemented on a breadboard first to test and choose the components, and then a printed circuit board (PCB) was designed and manufactured. In this section, the details of the chosen components will be discussed before going through the

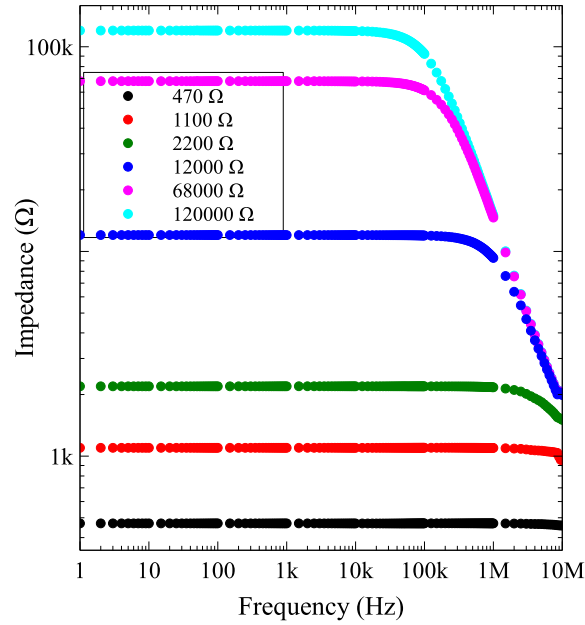


Figure 4.9: Calibration resistors actual values $R_c(f)$ measured using the precision N4L PSM1735 impedance analyzer

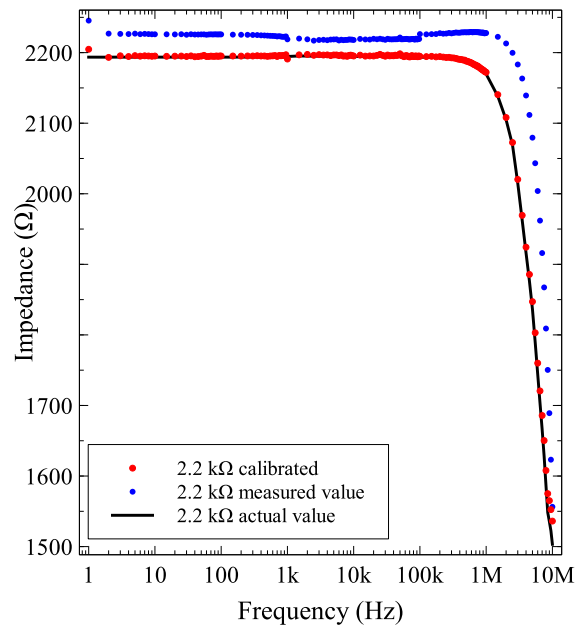


Figure 4.10: Calibration process done for $R_{f_2} = 2.2k\Omega$ with $R_c = 2.2k\Omega$

PCB design and implementation.

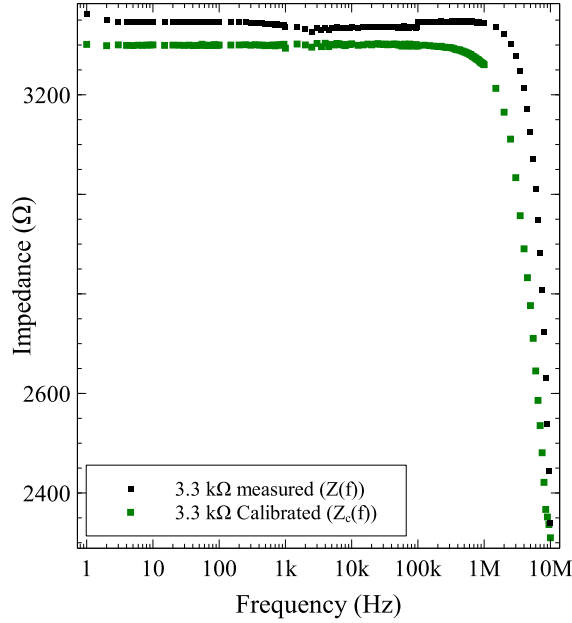


Figure 4.11: Calibration process being applied while $Z_{unknown}$ is a $3.3k\Omega$ resistor

4.4.1 Analog and Digital Components

The proposed design is controlled by an ARM® Cortex®-M4F Microcontroller [87] which is a fast controller with a clock speed of 180 MHz and two 16-bit SAR ADCs that can reach a sampling frequency of 500 kHz. In the implementation of the design, we used the Teensy 3.6 controller board which has the ARM® Cortex®-M4F in its core. This board which is shown in Fig. 4.12 was used since it can be programmed using the Arduino integrated development environment (IDE) which is an open source widely used IDE. Also, as it was discussed in subsection 4.2.1 the AD9850 was chosen as the signal generator in this design, and for the design implementation the AD9850 module which is shown in Fig. 4.13 was used. The module has all the necessary external components, can be easily interfaced with the microcontroller and simply be operated using a 3.3V single supply.

For the Op-Amps, the OPA3355 package was used from Texas Instruments [88]. It has three Op-Amps with high bandwidth and can be operated with a single 3.3V supply which is exactly what is needed for this design. Switching the feedback resistors was done using the TS5A3357 analog switches [89] from Texas Instruments. One was used to switch

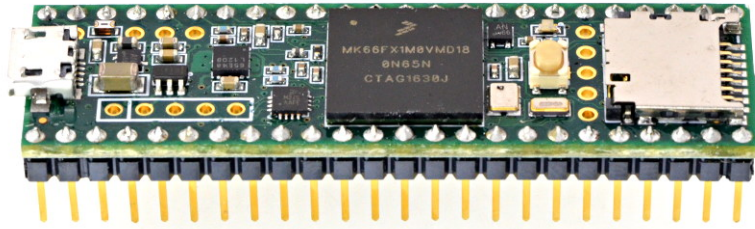


Figure 4.12: The teensy microcontroller module

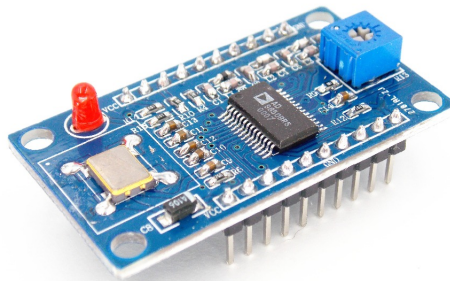


Figure 4.13: The AD9850 DDS module

between 3 resistors and two in parallel were used to switch between 6 resistors for R_{f1} and R_{f2} , respectively. The switches can also work with a 3.3V single supply just like the other components in the circuit which improved the portability of the design by making it possible to use an external battery as a power source.

4.4.2 Printed Circuit Board (PCB)

After testing the proposed design with the chosen components from the previous section on a breadboard, a printed circuit board (PCB) was designed based on the schematics shown Fig. 4.14 using EAGLE software from Autodesk. The double-sided (two layer) PCB layout was then designed. The final PCB design which is shown in Fig. 4.15 was manufactured in China by PCBGOGO (see Fig. 4.16) and then assembled at the university laboratories (see Fig. 4.17).

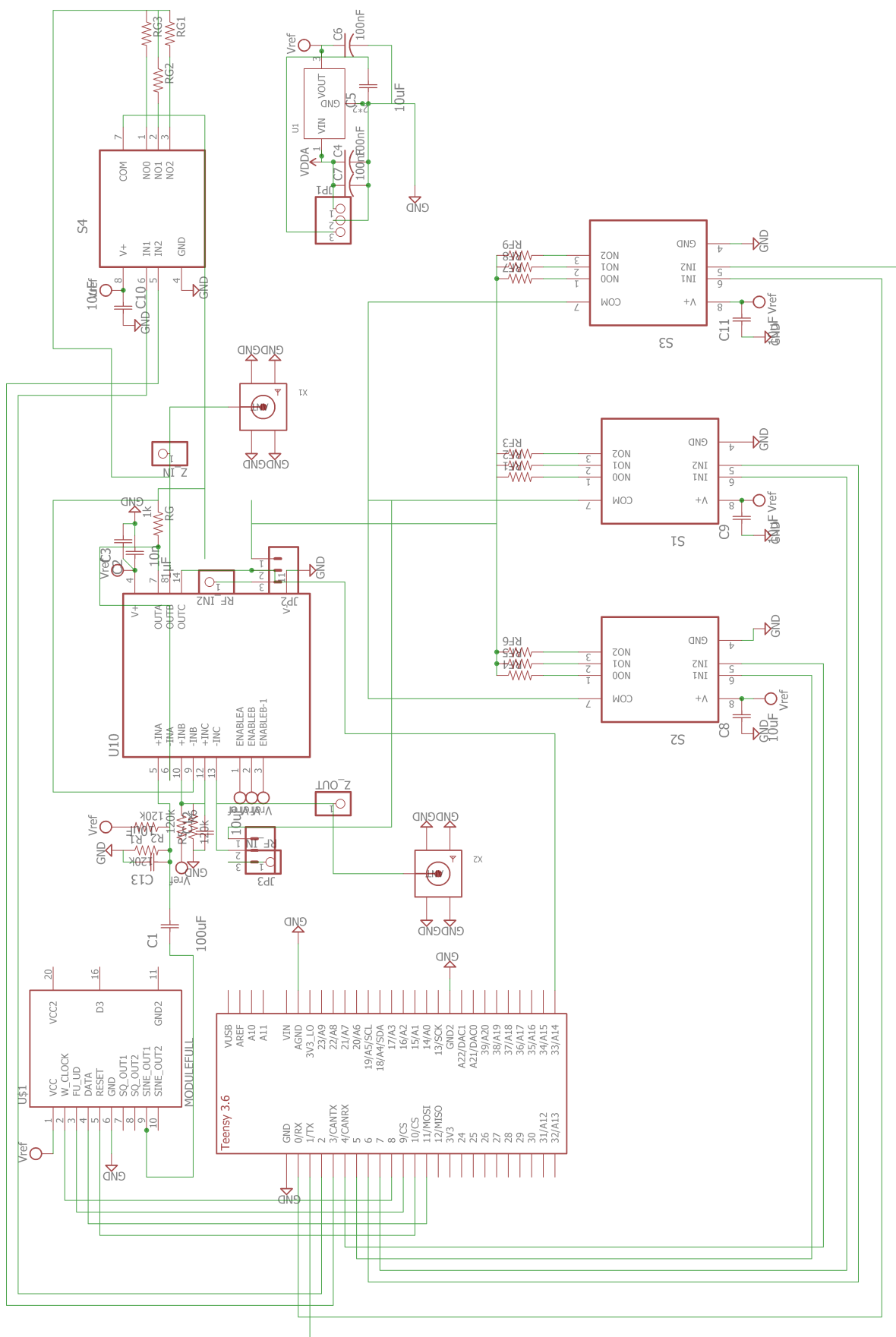


Figure 4.14: PCB schematics design

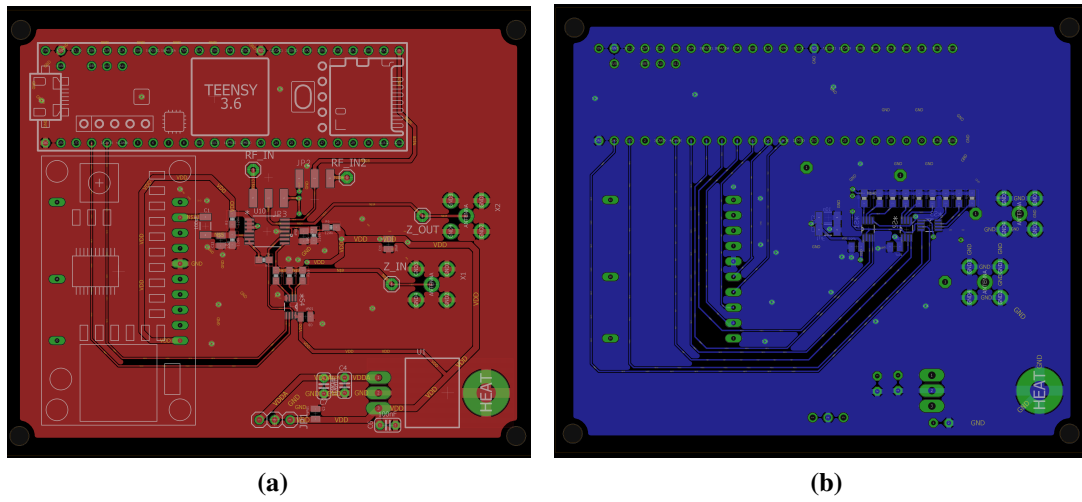


Figure 4.15: Double sided PCB layout (a) top (b) bottom layers

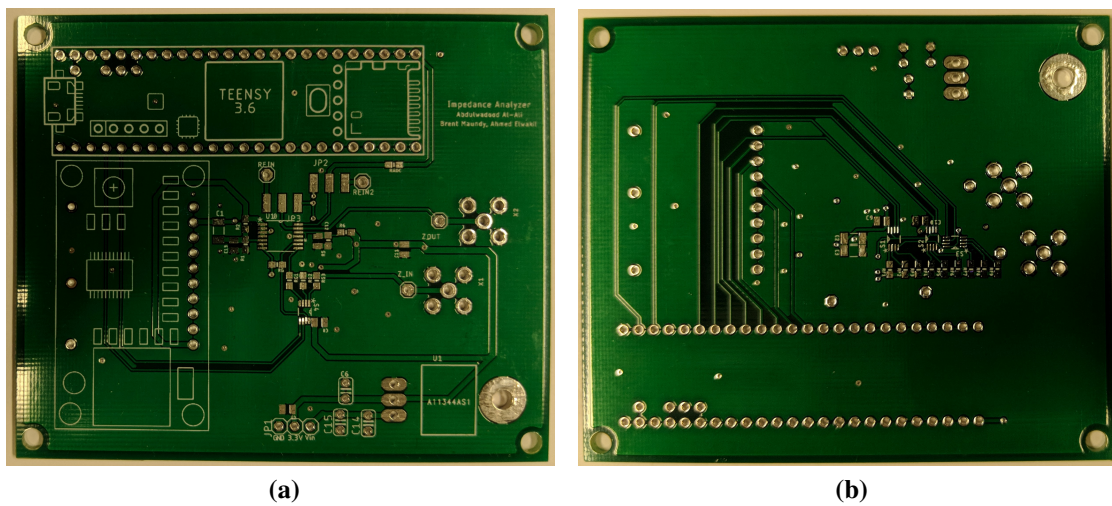


Figure 4.16: Manufactured PCB (a) top (b) bottom layers

4.4.3 Power Consumption

The power consumption of the device is very important for the designed to be portable and work in the field. The choice of the components was made to have the lowest possible power consumption while matching the needed specifications. The current consumption according to the parts datasheets was found to be $79.69mA$ as detailed in Table. 4.1. However, the implemented PCB was drawing a current of $88mA$ in the sweep mood, and $52mA$ while waiting for a command from the microcontroller. The rating of the proposed sys-

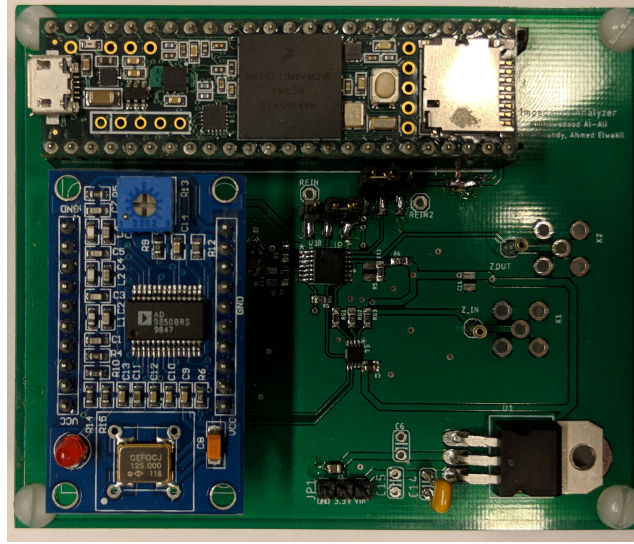


Figure 4.17: Assembled PCB

Table 4.1: Power consumption

Part	Part model	Quantity used	Supply Voltage	Supply current	Total current
DDS	AD9850	1	3.3	46.69mA	46.69mA
Op-Amps	OPA355	3 (one package)	3.3	11mA	33mA
Switches	TS5A3357	3	3.3	10 μ A	30 μ A
				Total:	79.69mA

tem is very reasonable taking into consideration that the device will work for few minutes (four minutes for one sweep) to take its reading and then shutdown till the next measurement. The system testing was done using a lithium-ion power bank with 5V output that was regulated to 3.3V on the PCB.

4.4.4 Total Cost

The low cost of the device was a crucial aspect of the design as we aim for a low-cost device that can give comparable results to the expensive devices available commercially. The detailed cost of a single unit is shown in Table. 4.2 which sums up to around \$95 CAD which is still very cheap in comparison with the expensive devices in the market. More than 50% of the total cost is taken by the microcontroller and the DDS modules. Those two modules were used for prototyping, and they can be redesigned to fit the need of the

Table 4.2: Cost of a single unit

Part	Part model	Part price (CAD)	Quantity	Total price (CAD)
Microcontroller	Teensy 3.6	\$54.07	1	\$54.07
DDS	AD9850 Module	\$20.97	1	\$20.97
Op-Amps	OPA3355	\$6.53	1	\$6.53
Resistors & Capacitors	-	\$0.33	20	\$6.60
Switches	TS5A3357	\$1.36	3	\$4.08
PCB Manufacturing	-	\$1.25	1	\$1.25
Regulator	LD1117V33	\$0.81	1	\$0.81
			Total:	\$94.31

system which would reduce the cost significantly.

4.5 Summary

In this chapter, the full detailed design of the proposed impedance analyzer was discussed in details by going through both the software and the hardware aspects of it, before discussing the implementation of the device. The power consumption and the cost of the device were also discussed. It is clear from the previous sections that the device matches the requirements of a simple, low-cost and low-power design that is needed to be used in the field.

CHAPTER 5

Experimental Results

5.1 Introduction

The proposed impedance analyzer was tested in two stages, first on a Breadboard to check the compatibility of the parts then the assembled PCB as shown in Fig. 4.17 was tested. The testing for each stage was done first using some passive components and then with some fruit samples to highlight the device ability to do bio-impedance measurements in comparison with some of the commercial impedance analyzers.

The following sections will discuss each stage results and show the overall performance of the analyzer. Finally, an application to Strawberry ageing and its effect on the bio-impedance is presented.

5.2 Breadboard Tests

Testing the device on a breadboard before finalizing the design was essential to ensure compatibility and to test it before sending the PCB out for manufacturing. The testing was done on a limited frequency range 1Hz to 100kHz due to the limitations of the breadboard where the effect of the breadboard capacitance will appear on the results above this frequency. Some passive components were used first to show that the device would produce accurate results, before using some Apples to show that the device can work to obtain a high-quality bio-impedance data.

5.2.1 Passive Components Measurements

The proposed design was first tested using the well known Cole-Cole models of Fig. 3.1(a) and Fig. 3.1(b). The single-dispersion model used the following values $R_\infty = 470\Omega$, $R_1 = 2200\Omega$, $C_1 = 1\mu F$ with $\alpha_1 = 1$ and the double dispersion model was obtained by adding $R_2 = 570\Omega$, $C_2 = 0.1\mu F$ with $\alpha_2 = 1$. The experimental results in this section were obtained over the range $1Hz$ to $100kHz$ with an excitation amplitude $V_{in} = 150mV$ and R_f being switched between 2 resistors ($12k\Omega$ and $2.2k\Omega$). The results for the single-dispersion model are shown in Fig. 5.1 while the results for the double dispersion model are shown in Fig. 5.2. The results are in excellent agreement with the theoretical values, but the error can be seen to be increasing above $60kHz$ especially in the double dispersion-Cole model. This was caused by the limited sampling frequency of the ADC ($500kHz$). This limitation reduces the accuracy of the fit which in turn affects the measured impedance magnitude values.

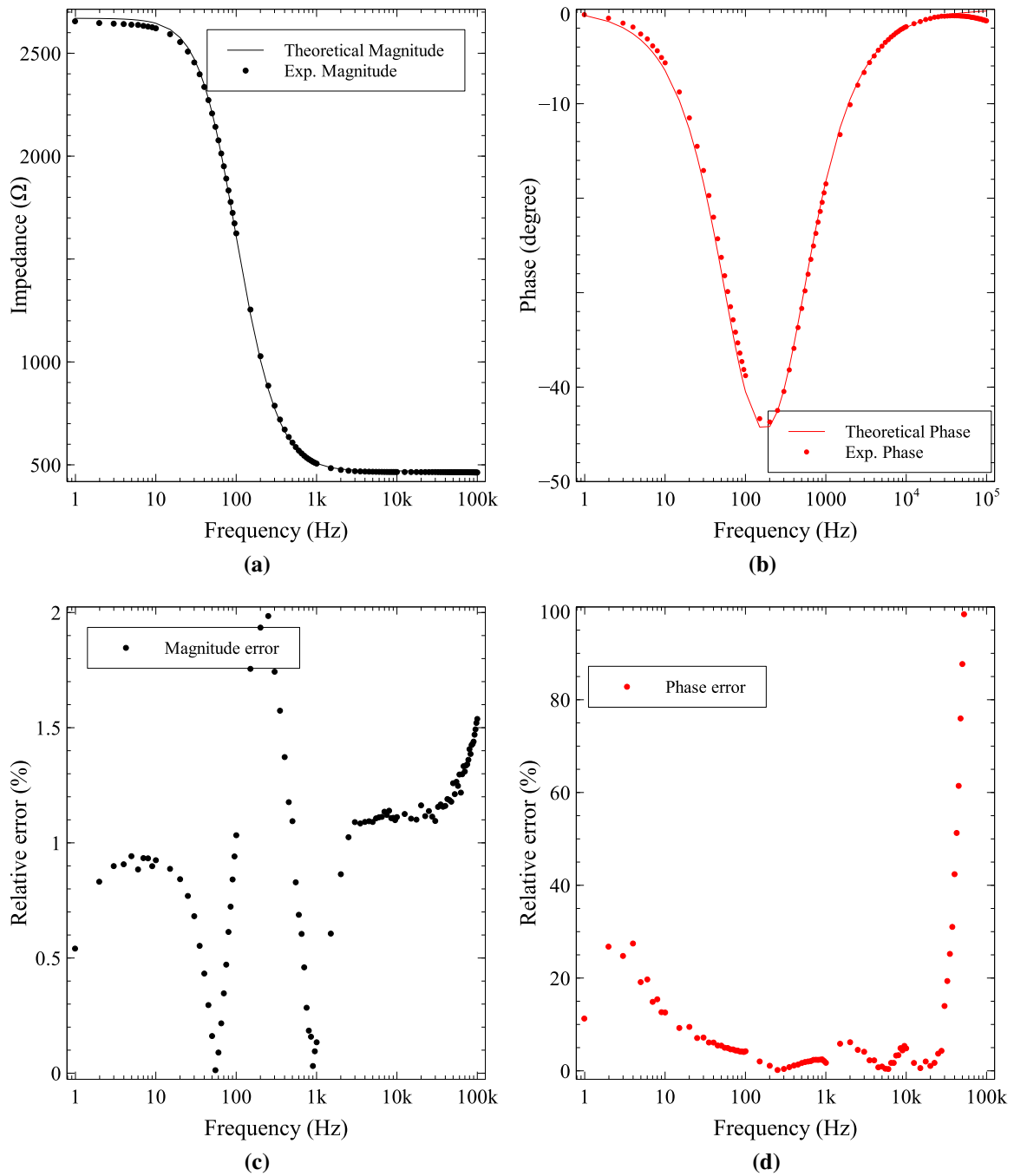


Figure 5.1: Single-dispersion Cole-Cole model testing with passive components with the values $R_{\infty} = 470\Omega$, $R_1 = 2200\Omega$ and $C_1 = 1\mu F$. (a) Impedance magnitude plot (b) Impedance phase plot (c) Magnitude error and (d) Phase error.

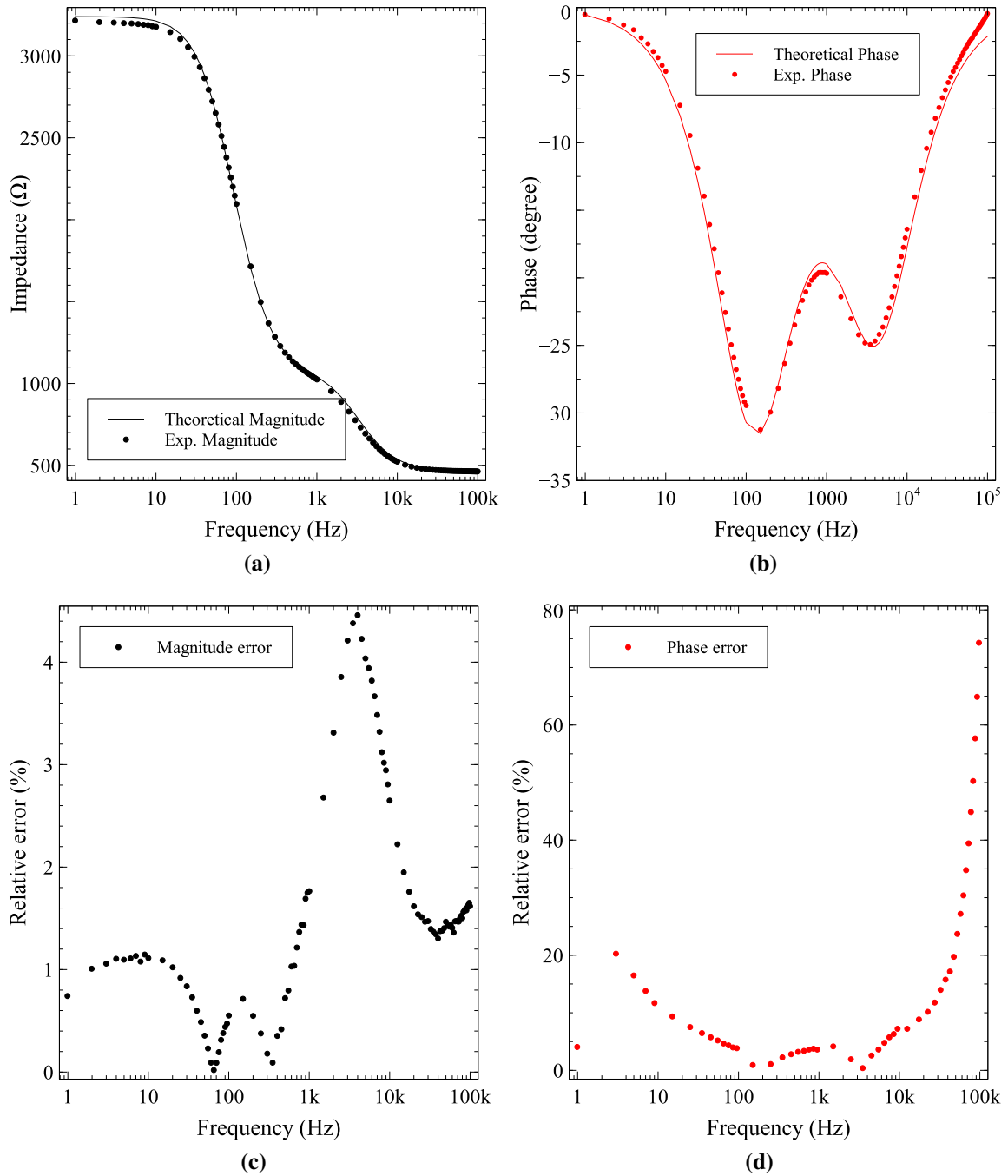


Figure 5.2: Double-dispersion Cole-Cole model testing with on shelf components with $R_{\infty} = 470 \Omega$, $R_1 = 2200 \Omega$, $C_1 = 1 \mu F$, $R_2 = 570 \Omega$, $C_2 = 0.1 \mu F$. (a) Impedance magnitude plot (b) Impedance phase plot (c) Magnitude error (d) Phase error.

Table 5.1: Comparison of the parameters of a double-dispersion Cole-Cole model fitting of the two Apple samples

Sample	$R_\infty(\Omega)$	$R_1(\Omega)$	$R_2(\Omega)$	$C_1(\mu)$	$C_2(\mu)$	α_1	α_2
Green Apple (#1)							
Experimental Fit	0	19552	1.4252×10^6	0.021884	0.02906	0.7862	0.38814
IM6 Fit	826.8	19552	1.1399×10^6	0.021884	0.02906	0.7862	0.38814
Red Apple (#2)							
Experimental Fit	233.95	27619	54669	0.025378	2.9759	0.73987	0.79187
IM6 Fit	1571.7	24560	70734	0.016007	3.5961	0.80774	0.69765

5.2.2 Apple Measurements

The design was further tested with two different apples (#1 is a green apple, and #2 is a red apple). They were both tested in the same range but with four feedback resistors ($326\text{ k}\Omega$, $120\text{ k}\Omega$, $47\text{ k}\Omega$ and $15\text{ k}\Omega$) to cover a wider impedance range. The Apples were also measured using a professional impedance analyzer (BAS-Zahner IM6) [35]. The results are shown in Fig. 5.3 also show good accuracy especially for Apple #2 while Apple #1 magnitude has some error at the low frequencies. However, both apples have an error in the phase at the edges of the frequency ranges. This is due to the so-called tails problem in the phase extraction algorithm [80]. The tails problem is caused by the existence of poles/zeros below and/or above the covered frequency range [68]. From the results in Fig. 5.3 we can see that there is a pole at frequencies lower than 1 Hz and a zero near 100 kHz which causes the error at those two ends.

Finally, to validate that the measurements are meaningful despite the error in phase, the free EIS software package from [32] was used to fit the data from both our proposed design and the IM6 impedance analyzer to the double-dispersion Cole-Cole model. The Nyquist plots for apple #1 and #2 are shown in Figs. 5.4(a) and 5.4(b), respectively. From the plotted data the fitted parameters are shown in Table. 5.1. The proposed design results give close parameters values to those obtained by the professional device (BAS-Zahner IM6 [35]).

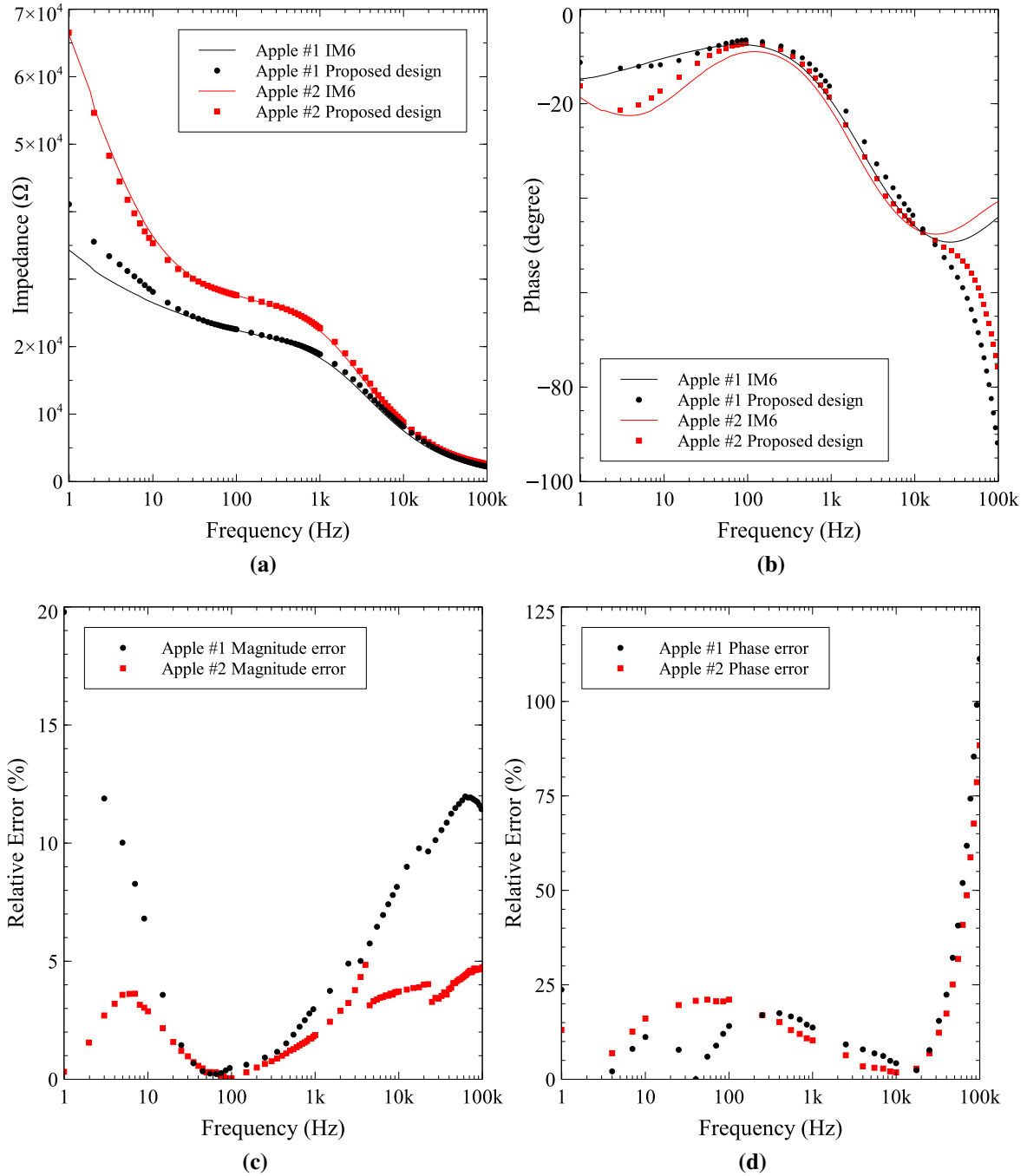
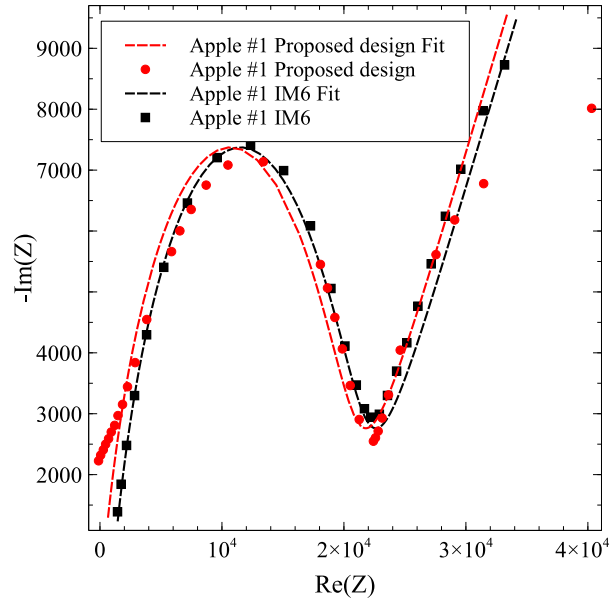
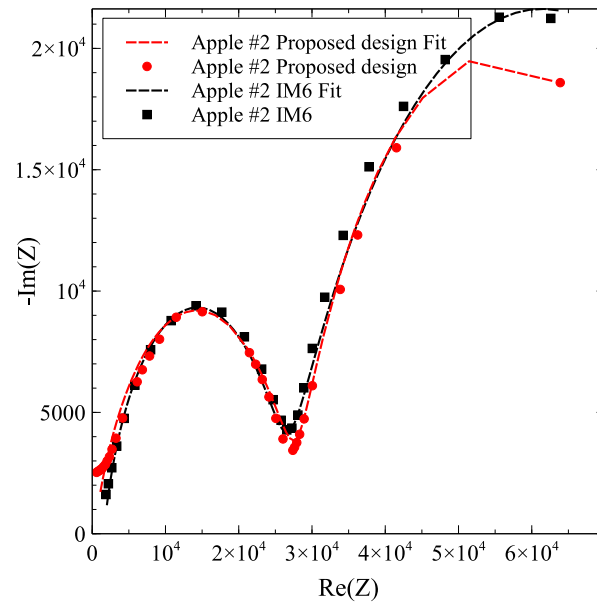


Figure 5.3: Testing for bio-impedance using two different apples using the proposed hardware design. (a) Impedance magnitude plot (b) Impedance phase plot (c) Magnitude error (d) Phase error.



(a)



(b)

Figure 5.4: Comparison of data fitting to a double dispersion model using precisely measured impedance data and the proposed design for the two apples (a) Green Apple #1 and (b) Red Apple #2.

5.3 PCB Testing

The final designed PCB which was discussed in the previous chapter extended the frequency range up to 10MHz after utilizing the under-sampling technique and a more compact design that can work with high frequencies. The excitation voltage in this section was fixed to $1V_{p-p}$ except for impedances under 200Ω where the excitation voltage was switched to $500mV_{p-p}$ to avoid the ADC and Op-Amp saturation. Using this excitation voltage and resistor $R_{f_2} = \{0.5k\Omega, 1k\Omega, 2.2k\Omega, 12k\Omega, 68k\Omega, 120k\Omega\}$ a wide impedance range 100Ω - $280k\Omega$ was achieved.

5.3.1 Passive Components Measurements

The PCB was first tested using two different double-dispersion models, the first one had the following values $R_\infty = 820\Omega$, $R_1 = 68k\Omega$, $C_1 = 0.12\mu F$, $R_2 = 15k\Omega$, $C_2 = 0.1nF$ with $\alpha_1 = \alpha_2 = 1$ and the second one was obtained by using $R_\infty = 220\Omega$, $R_1 = 47k\Omega$, $C_1 = 15nF$, $R_2 = 15k\Omega$, $C_2 = 1nF$ with $\alpha_1 = \alpha_2 = 1$. The experimental results were obtained over the range $1Hz$ to $10MHz$ with an excitation amplitude $V_{in} = 500mV$ and R_{f_2} being switched between 6 resistors as mentioned before. The results for the first model are shown in Fig. 5.5 while the results for the second model is shown in Fig. 5.6. The results are in excellent agreement with the theoretical values, but the error in the phase can be seen to be increasing in the first and last decades which once again is related to *the tails problem* especially in the second model.

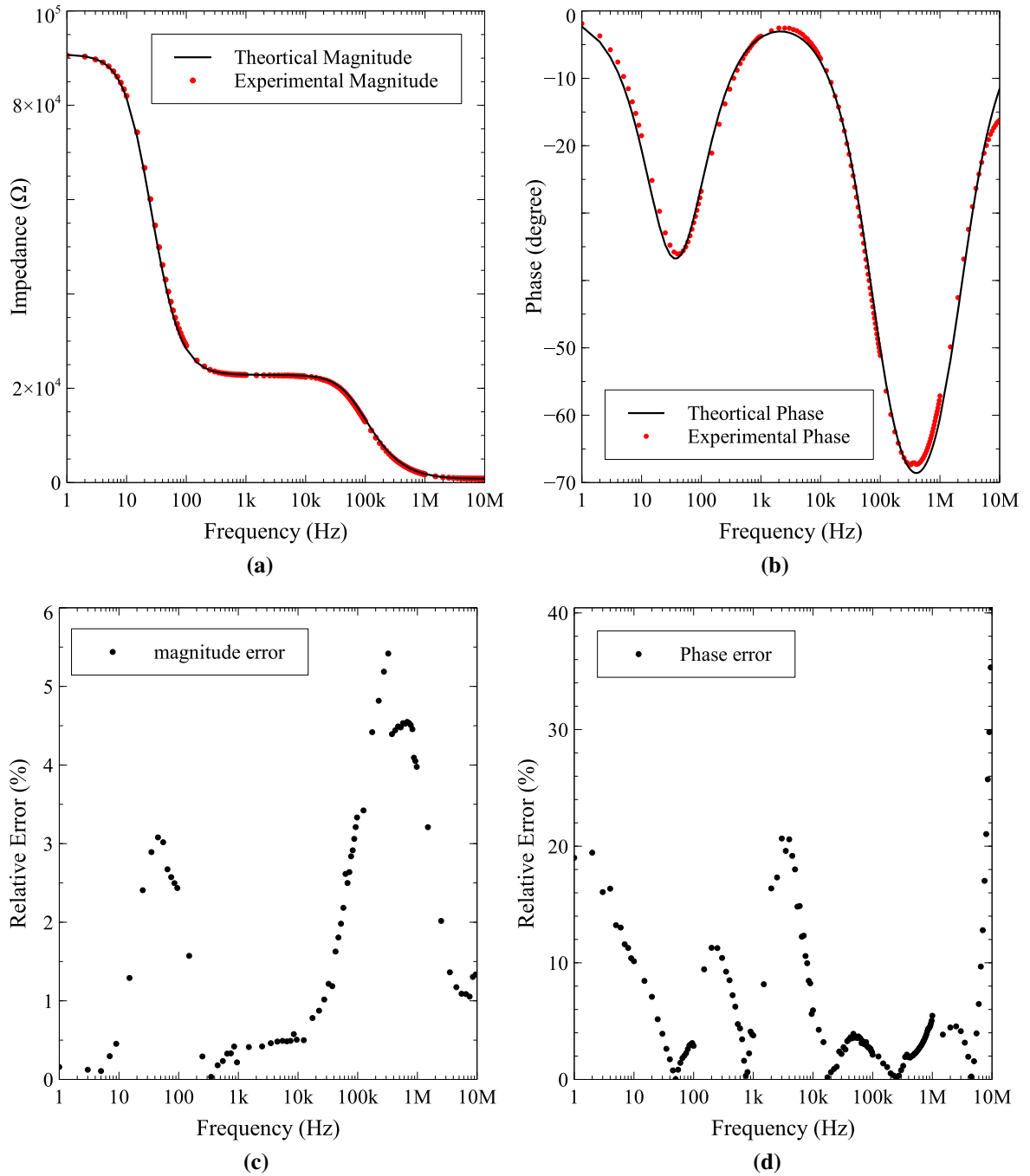


Figure 5.5: Testing with on shelf components double-dispersion Cole-Cole model with $R_\infty = 820 \Omega$, $R_1 = 68 k\Omega$, $C_1 = 0.12 \mu F$, $R_2 = 15 k\Omega$, $C_2 = 0.1 nF$. (a) Impedance magnitude plot (b) Impedance phase plot (c) Magnitude error (d) Phase error.

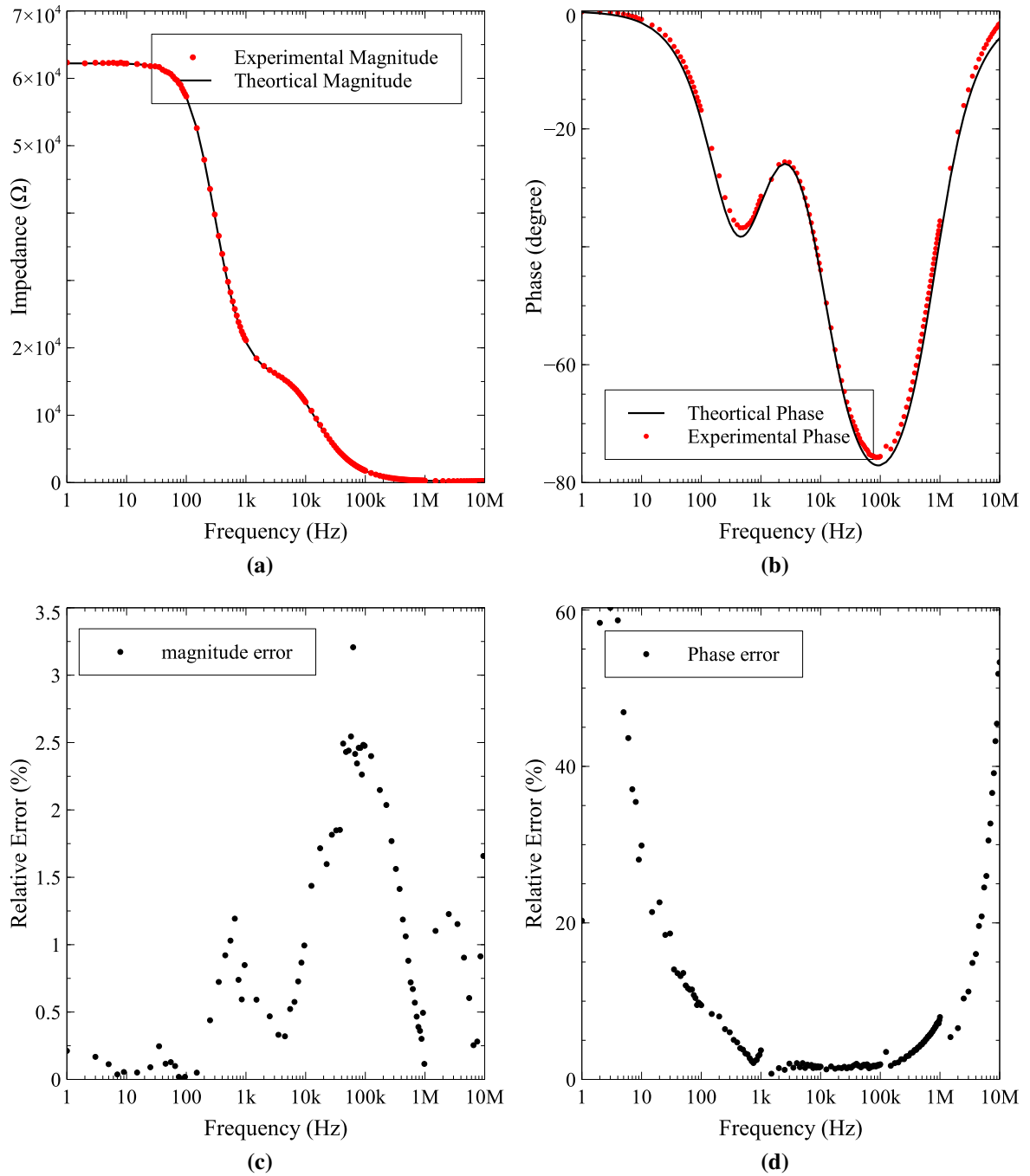


Figure 5.6: Testing with on shelf components double-dispersion Cole-Cole model with $R_\infty = 220 \Omega$, $R_1 = 47 k\Omega$, $C_1 = 15 nF$, $R_2 = 15 k\Omega$, $C_2 = 1 nF$. (a) Impedance magnitude plot (b) Impedance phase plot (c) Magnitude error (d) Phase error.

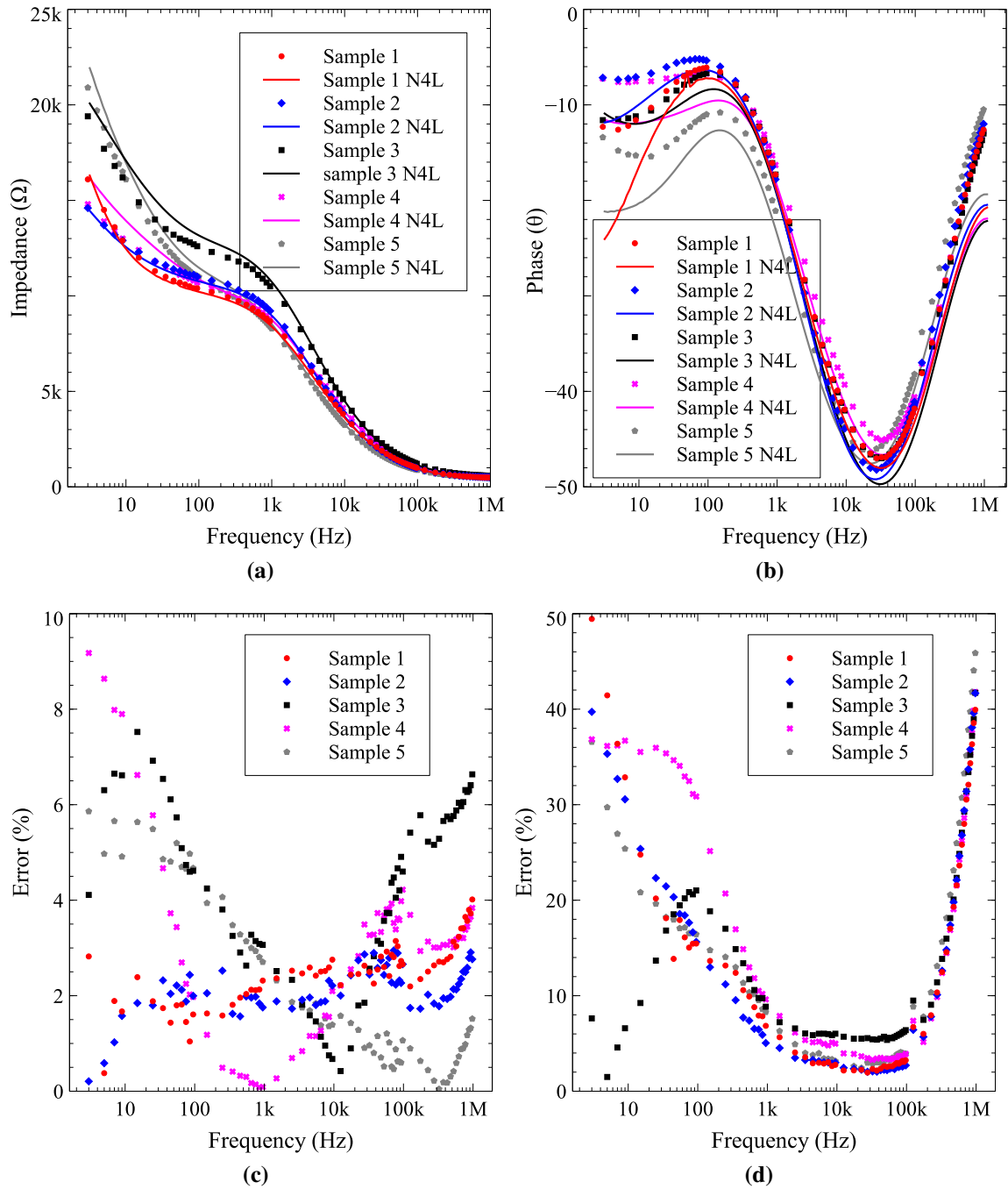


Figure 5.7: Day one results from the proposed design and the N4L impedance analyzer
 (a) Impedance magnitude plot (b) Impedance phase plot (c) Magnitude error (d) Phase error.

5.3.2 Strawberry Measurements

Fresh strawberries were purchased from a local supermarket, and their impedance was measured immediately after purchase using our portable device; which uses the two-electrode configuration. Also, measurements using the precision N4L PSM1735 impedance analyzer [34] were taken as a reference as shown in Fig. 5.7. The measured magnitude and phase were taken from 3Hz to 1MHz under fresh conditions using our portable device and the N4L device. The relative error in the magnitude between our device and the N4L was less than 10% in all samples (see Fig. 5.7(c)). However, the phase error reached its maximum of 40% at the tail frequencies of 3Hz and 1MHz, while it remains below 20% in the entire 10Hz-500kHz range (see Fig. 5.7(d)). The Tails magnitude error which also affects the extracted phase at low frequencies can be related to the fact that the electrodes can move while changing the test instrument which has some effect on the results as it was discussed in [90] where it was shown that the electrode placement on the fruit (Apples in their experiments) does affect the magnitude results.

5.4 Application to Strawberry Ageing

The ageing of fruits and vegetables is an important factor that affects their freshness conditions. Strawberries, in particular, are known to have a very short on-shelf lifetime even under well-controlled storage conditions.

To test the ageing effect of strawberries the fresh samples from subsection 5.3.2 were then left in the open air before being re-tested after 24 hours and again after 48 hours with the electrode placement maintained in the same position as shown in Fig. 5.8. The Nyquist plots in Fig. 5.9 show a clear difference in the impedance due to the ageing effect particularly at the low frequencies.

To quantitatively assess the ageing effect, the measured impedance was fitted to a

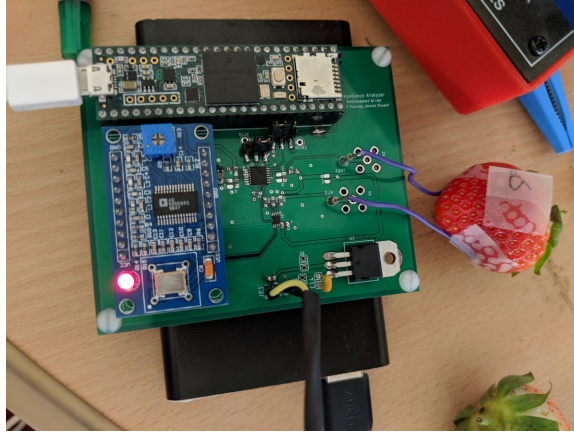


Figure 5.8: A picture of the portable device with one fruit sample being tested.

double-dispersion Cole-Cole circuit model with impedance given by

$$Z(s) = R_{\infty} + \frac{R_1}{1 + s^{\alpha_1} R_1 C_1} + \frac{R_2}{1 + s^{\alpha_2} R_2 C_2} \quad (5.1)$$

This model, shown in Fig. 3.1(b), has seven parameters, which were determined by using the Newton optimization algorithm built in the EIS software package [32]. Note that $s^{\alpha} = (j\omega)^{\alpha} = \omega^{\alpha} (\cos(\alpha\pi/2) + j \sin(\alpha\pi/2))$. The Nyquist plots for sample#4 and sample#5 along with the best fit model are shown in Fig. 5.10 comparing the fresh situation to the 24-hours and 48-hours ageing situations. The suitability of the double-dispersion Cole-Cole model is clear from the goodness of the fit to the data and the extracted model parameters are reported in Table 5.2. From these values, it is clear that all three resistors R_{∞} , R_1 and R_2 increase significantly due to ageing. At the same time, the pseudo-capacitance C_2 significantly decreases with ageing with the dispersion coefficient α_1 also showing a decreasing trend. Dispersion coefficient α_2 appears to peak after 24 hours and then decrease. These preliminary results confirm that the ageing effect can be detected by bio-impedance measurements.

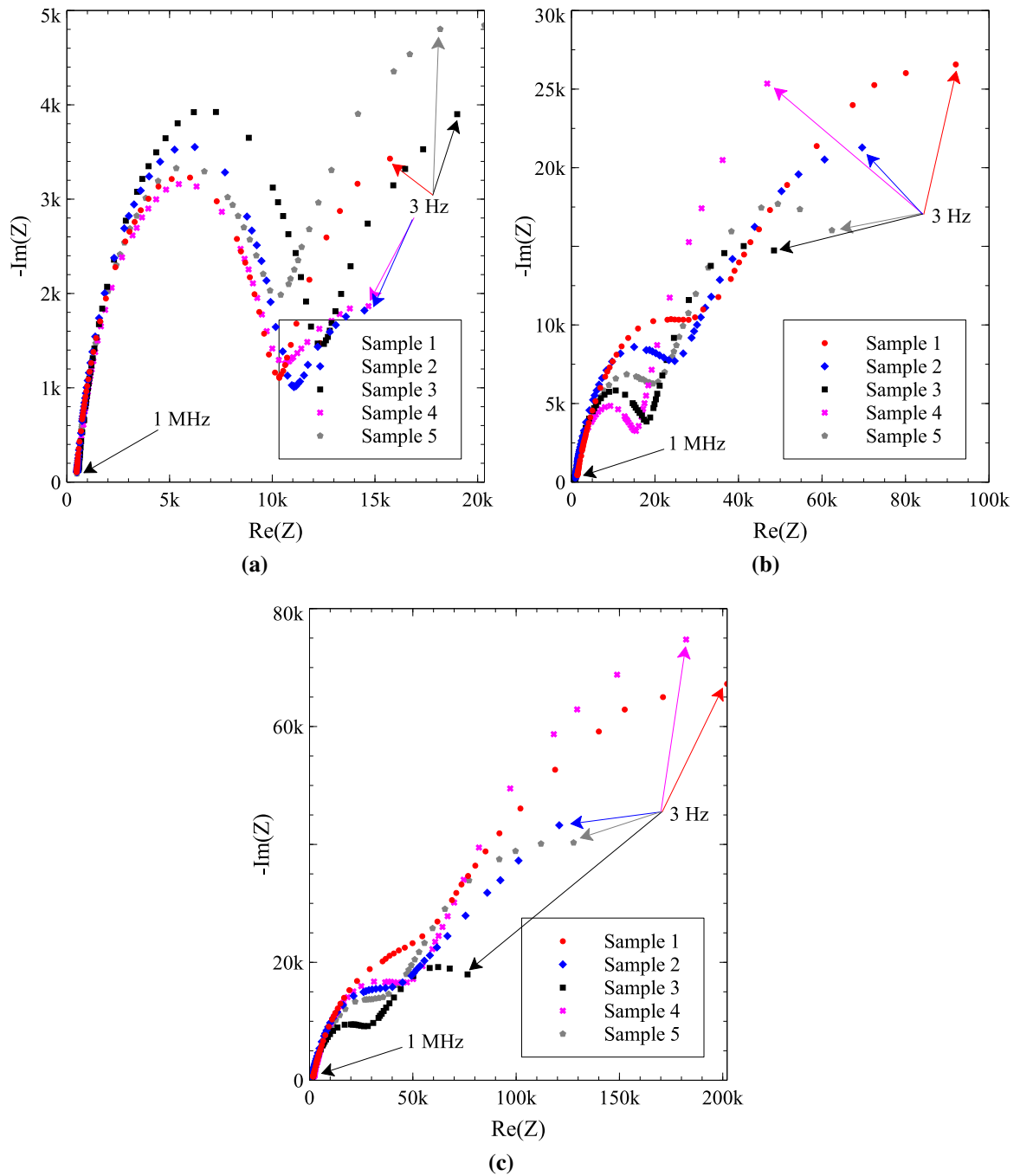


Figure 5.9: Nyquist plots for the five samples in (a) day 1 (b) day 2 (c) day 3

5.5 Summary

The proposed bio-impedance analyzer was tested with some passive components, and it showed a good agreement with the theoretical values. Additionally, the device was tested

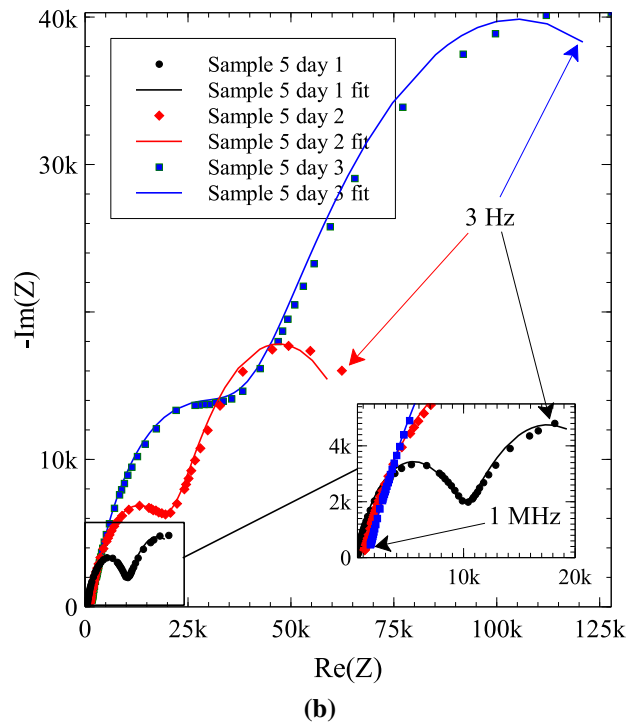
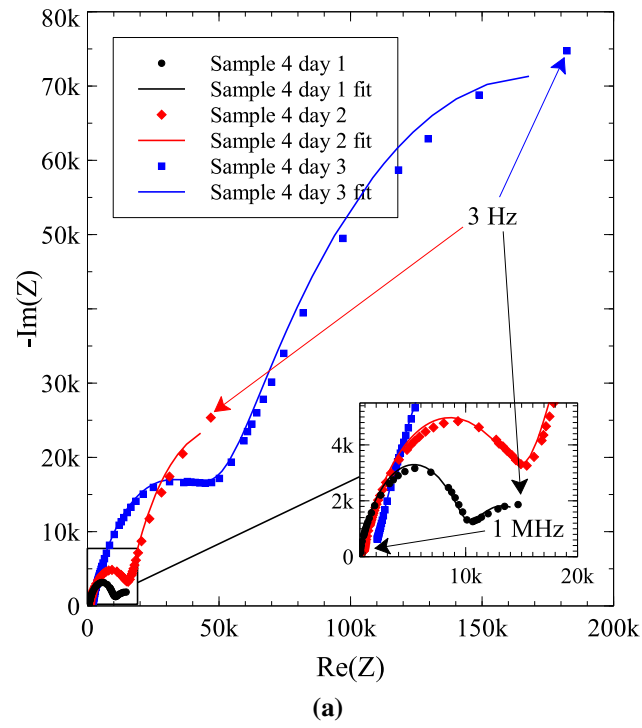


Figure 5.10: Nyquist plots for (a) sample#4 and (b) sample#5 with their fitted model results showing the ageing effect over the three days.

Table 5.2: Comparison of the parameters of a double-dispersion Cole–Cole model fitting of sample 4 results over the 3 days

	$R_{\infty}(\Omega)$	$R_1(\Omega)$	$R_2(\Omega)$	$C_1(n)$	α_1	$C_2(\mu)$	α_2
Sample #4							
fresh	497.38	9356.1	7214.1	48.663	0.76117	20.151	0.58087
24 hours	813.69	14617	70095	45.626	0.73286	2.0634	0.76226
48 hours	1796.2	46862	243.7k	29.308	0.69309	0.59168	0.6709
Sample #5							
fresh	459.74	9479.7	15567	61.55	0.76724	6.3752	0.69008
24 hours	1001.1	20350	52872	73.496	0.68712	1.141	0.74376
48 hours	1419.0	36986	136.28k	54.761	0.67398	0.7529	0.6648

with Apples and Strawberries, and the results showed a good accuracy with two different and precise commercial Impedance analyzers. The device was then used to monitor the ageing effect of some strawberry samples over a period of 3 days. A clear trend is present in the results from the three days, and it shows that bio-impedance can be of great use in agriculture and food quality and hence the magnitude only technique can be used for this application.

CHAPTER 6

Conclusions and future work

6.1 Conclusion

The main objective of this thesis was to design a portable low power and low-cost impedance analyzer that can be used in the field for online monitoring for fruits and food quality control. This was done in three stages. At first, a phase extraction algorithm based on the Kramers-Kronig transform was presented and tested. Afterward, a simple magnitude measurement hardware that utilizes the previously presented K-K transform algorithm for phase extraction was designed and implemented. Finally, the entire system design was tested with both passive components and fruits.

The phase extraction algorithm simplifies the system design as it removes the main complexity of the hardware, namely the phase measurement and uses intensive software to extract it from the magnitude which can be easily measured. The algorithm which was presented in chapter 3 takes the magnitude data and then extracts the phase using a modified Kramers-Kronig transform. The proposed algorithm was tested with some simulated and experimental magnitude data, and the results showed the ability of the proposed algorithm to be used for bio-impedance measurement with a new technique that would simplify the hardware significantly.

The magnitude only measurement hardware was designed ensuring low-power and low-cost design. Although, many magnitude detection techniques can be found in the literature a new simplified design based on the simple idea of the inverting amplifier was proposed, where the input was known and monitoring the output was enough to extract the unknown

Table 6.1: Proposed design specifications

Frequency range	1 Hz-10 MHz
Impedance Range	100 Ω – 280k Ω
Excitation Amplitude	0.5, 1, 2 V_{pp}
Magnitude error	$\leq 10\%$
Phase error	$\leq 20\%$
Power Dissipation	293.7 mW
Total Cost	\$95

impedance which was controlling the gain of the amplifier. The proposed system design was then implemented in a breadboard before finalizing it on a PCB. The device's final cost of the device was around \$95 CAD which satisfies the low-cost requirement of the design in comparison with the commercial devices in the market. With a power consumption of around 293.7 mW at 3.3V, the device portability was achieved by using a portable power bank. Table 6.1 shows the full design specifications¹.

Finally, the device testing was done on two stages, starting by testing some passive components and some fruits with the design implemented on a breadboard, before repeating the same procedure to test the assembled PCB. Finally, application oriented measurements were done where some strawberries were tested to show that the ageing effect can be studied using Bio-impedance measurements done by this device. The device testing showed an acceptable error in comparison with two commercially available precise impedance analyzers, which makes it a good alternative especially for bio-impedance measurements that need to be done continuously in the field.

6.2 Future Work

Although the device displayed very good results and some improvements to what's already available in the literature especially in its simple design. Further improvement can always be done for better results and a more reliable design.

The work can be improved in the following points:

¹The phase error is for the mid-frequency range ignoring the tails error which can't be quantified.

- Phase extraction algorithm: further work can be done to improve the algorithm results by probably using an optimization routine. Its goal would be determine the best parameters combination that can be used to reduce the phase error especially at the tails. Also, investigating the K-K transform from a mathematical perspective could show some ways of improving the approximation that was used to evaluate the transform.
- Hardware design: putting the whole analog front-end of the design on a single chip, would reduce the error, the total power consumption and the cost of the final device. Also, it could give us some flexibility to expand the impedance range to be able to cover the very low and very high impedances that might be needed for some applications.
- Post-Processing: adding a feature to fit the impedance data to some predefined models and export the modeled parameters would be a great addition to this system since it would eliminate the need to use any external processing softwares, such as the EIS software package [32] .
- Graphical User Interface (GUI): For the device to be more user friendly a GUI can be designed for a better user experience.

6.3 System Vision

The proposed work presented a low-power, low-cost impedance analyzer that can produce comparable results to the expensive and bulky commercial devices. Such a device can be used for research proposes where portable and cost-efficient device is needed. Additionally, the device demonstrated interesting bio-impedance measurements in fruits, which can be related to fruit growth, ripeness and ageing. A provisional patent application has been filed to the US patent office through Innovate Calgary, and further work is being performed to study the feasibility of commercializing such a device. The device can also be embedded

in an intelligent system offering some useful information to a user who doesn't have any basic knowledge of how does it work, perhaps in some agriculture and food characterization applications

BIBLIOGRAPHY

- [1] J. R. Macdonald, "Impedance spectroscopy," *Annals of Biomedical Engineering*, vol. 20, pp. 289–305, May 1991. 1
- [2] M. Simic, "Realization of complex impedance measurement system based on the integrated circuit AD5933," in *21st Telecommunications Forum (TELFOR)*, pp. 573–576, Nov. 2013. 1
- [3] L. Breniuc, V. David, and C.-G. Haba, "Wearable impedance analyzer based on AD5933," in *Electrical and Power Engineering (EPE), 2014 Int. Conf. and Exposition on*, pp. 585–590, Oct 2014. 1
- [4] E. Barsoukov and J. Macdonald, *Impedance Spectroscopy: Theory, Experiment, and Applications*. John Wiley & Sons, 2 ed., Jul 2005. 5, 10, 11, 12
- [5] L. Callegaro, "The metrology of electrical impedance at high frequency: a review," *Measurement Science and Technology*, vol. 20, p. 022002, Dec 2008. 6
- [6] D. Tsunami, J. McNames, A. Colbert, S. Pearson, and R. Hammerschlag, "Variable frequency bioimpedance instrumentation," in *Engineering in Medicine and Biology Society, 2004. IEMBS '04. 26th Annual International Conference of the IEEE*, vol. 1, pp. 2386–2389, Sep 2004. 6
- [7] J.-P. Morucci, V. Max E, B. Riguard, C. J. Felice, C. J. Felice, and C. J. Felice, *Bioelectrical Impedance Techniques in Medicine*, vol. 24. Critical Reviews in Biomedical Engineering, Feb 1996. 6

- [8] A. Väinölä and T. Repo, "Impedance spectroscopy in frost hardness evaluation of rhododendron leaves," *Annals of Botany*, vol. 86, pp. 799–805, Oct 2000. 6
- [9] T. Repo, Z. G. R. A., and R. Rikala, "The electrical impedance spectroscopy of scot pine (*pinus sylvestris* L.) shoots in relation to cold acclimation," *Faculty of Forestry, University of Joensuu, Joensuu, Finland, Journal of Experimental Botany*, Dec 2000. 6
- [10] H. Fukuma, K. Tanaka, and I. Yamaura, "Measurement of impedance of columnar botanical tissue using the multielectrode method," *Department of Management, Shinshu Junior College, Negano, Japan, Electronics and Communications in Japan*, Feb 2001. 6
- [11] M. Grossi and B. Riccò, "Electrical impedance spectroscopy (eis) for biological analysis and food characterization: a review," *Journal of Sensors and Sensor Systems*, vol. 6, p. 303, Aug 2017. 7, 8, 9, 12
- [12] M. Anas, N. Nurun, A. Norali, and M. Normahira, "Non-invasive blood glucose measurement," in *Biomedical Engineering and Sciences (IECBES), 2012 IEEE EMBS Conference on*, pp. 503–507, IEEE, Dec 2012. 7
- [13] D. Kamat, D. Bagul, and P. Patil, "Blood glucose measurement using bioimpedance technique," *Advances in Electronics*, vol. 2014, Dec 2014. 7
- [14] P. Aberg, I. Nicander, J. Hansson, P. Geladi, U. Holmgren, and S. Ollmar, "Skin cancer identification using multifrequency electrical impedance-a potential screening tool," *IEEE transactions on biomedical engineering*, vol. 51, pp. 2097–2102, Dec 2004. 7
- [15] T. Anh-Nguyen, B. Tiberius, U. Pliquet, and G. A. Urban, "An impedance biosensor for monitoring cancer cell attachment, spreading and drug-induced apoptosis," *Sensors and Actuators A: Physical*, vol. 241, pp. 231–237, May 2016. 7

- [16] A. A. Bakr, A. G. Radwan, A. H. Madian, and A. S. Elwakil, "Aging effect on apples bio-impedance using AD5933," in *Advances in Computational Tools for Engineering Applications (ACTEA), 2016 3rd International Conference on*, pp. 158–161, IEEE, Jul 2016. 7
- [17] J. R. González-Araiza, M. C. Ortiz-Sánchez, F. M. Vargas-Luna, and J. M. Cabrera-Sixto, "Application of electrical bio-impedance for the evaluation of strawberry ripeness," *International Journal of Food Properties*, vol. 20, pp. 1044–1050, Oct 2016. 7
- [18] E. Borges, A. Matos, J. Cardoso, C. Correia, T. Vasconcelos, and N. Gomes, "Early detection and monitoring of plant diseases by bioelectric impedance spectroscopy," in *2012 IEEE 2nd Portuguese Meeting in Bioengineering (ENBENG)*, pp. 1–4, IEEE, Feb 2012. 7
- [19] H. Lizhi, K. Toyoda, and I. Ihara, "Dielectric properties of edible oils and fatty acids as a function of frequency, temperature, moisture and composition," *Journal of Food Engineering*, vol. 88, pp. 151–158, Sep 2008. 7
- [20] F. R. Harker and J. H. Maindonald, "Ripening of nectarine fruit (changes in the cell wall, vacuole, and membranes detected using electrical impedance measurements)," *Plant physiology*, vol. 106, pp. 165–171, Sep 1994. 7
- [21] K. Toyoda, "Impedance spectroscopic analysis in agricultural products," in *Developments in Food Engineering*, pp. 143–145, Springer, Jan 1994. 7
- [22] X. Zhao, H. Zhuang, S.-C. Yoon, Y. Dong, W. Wang, and W. Zhao, "Electrical impedance spectroscopy for quality assessment of meat and fish: A review on basic principles, measurement methods, and recent advances," *Journal of Food Quality*, vol. 2017, Jul 2017. 7

- [23] A. M. Lopes, J. T. Machado, and E. Ramalho, "On the fractional-order modeling of wine," *European Food Research and Technology*, vol. 243, pp. 921–929, June 2017. 7
- [24] A. M. Lopes, J. T. Machado, E. Ramalho, and V. Silva, "Milk characterization using electrical impedance spectroscopy and fractional models," *Food Analytical Methods*, pp. 1–12, Oct 2017. 7
- [25] M. Mabrook and M. Petty, "Effect of composition on the electrical conductance of milk," vol. 60, pp. 321–325, 12 2003. 7
- [26] O. G. Martinsen and S. Grimnes, *Bioimpedance and bioelectricity basics*. Academic press, Mar 2008. 8
- [27] V. Muralidharan, "Warburg impedance - basics revisited," *Anti-Corrosion Meth & Material*, vol. 44, pp. 26–29, Feb 1997. 8
- [28] K. S. Cole and R. H. Cole, "Dispersion and absorption in dielectrics i. alternating current characteristics," *The Journal of Chemical Physics*, vol. 9, pp. 341–351, Apr 1941. 9
- [29] A. Elwakil, "Fractional-order circuits and systems: An emerging interdisciplinary research area," *Circuits and Systems Magazine, IEEE*, vol. 10, pp. 40–50, Nov 2010. 9
- [30] W. Glockle and T. Nonnenmacher, "A fractional calculus approach to self-similar protein dynamics," *Biophys. J.*, vol. 68, pp. 46–53, Jan 1995. 9
- [31] I. S. Jesus, J. Tenreiro Machado, and J. Boaventure Cunha, "Fractional electrical impedances in botanical elements," *Journal of Vibration and Control*, vol. 14, pp. 1389–1402, Sep 2008. 9

- [32] A. Bondarenko and G. Ragoisha, *Inverse problem in potentiodynamic electrochemical impedance*. Nova Science Publishers: New York, Feb 2005. 9, 34, 61, 69, 75
- [33] B. Sanchez, R. Bragos, and G. Vandersteen, "Influence of the multisine excitation amplitude design for biomedical applications using impedance spectroscopy," in *Engineering in Medicine and Biology Society, EMBC, 2011 Annual International Conference of the IEEE*, pp. 3975–3978, Aug 2011. 11, 12
- [34] U. Newton 4th LTD, *IAI Impedance Analysis Interface user manual*, 2015. 13, 31, 68
- [35] I. Data, "Electrochemical impedance spectroscopy using the bas-zahner im6 and im6e impedance analyzers," *Current Separations*, vol. 17, p. 54, Jan 1998. 13, 61
- [36] D. Jamaludin, S. A. Aziz, D. Ahmad, and H. Z. Jaafar, "Impedance analysis of Labisia Pumila plant water status," *Information Processing in Agriculture*, vol. 2, pp. 161–168, Oct 2015. 13
- [37] E. J. Rose, D. Pamela, and K. Rajasekaran, "Apple vitality detection by impedance measurement," *Int. J. of Advanced Research in Computer Science and Software Engineering*, vol. 9, pp. 144–148, Mar 2013. 13
- [38] F. Seone, I. Mochino-Herranz, J. Ferreira, L. Alvarez, R. Buendia, D. Ayllon, C. Llerena, and R. Gil-Pita, "Wearable biomedical measurement systems for assessment of mental stress of combatants in real time," *Sensors*, vol. 14, pp. 7120–7141, Apr 2014. 13
- [39] Y.-H. Kim, J.-S. Park, and H.-I. Jung, "An impedimetric biosensor for real-time monitoring of bacterial growth in a microbial fermentor," *Sensors and Actuators B: Chemical*, vol. 138, pp. 270–277, Apr 2009. 13
- [40] A. Devices, *1 MSPS, 12-Bit Impedance Converter, Network Analyzer AD5933 Datasheet*, May 2013. Rev. E. 13

- [41] C. J. Chen, J. T. Liu, S.-J. Chang, M.-W. Lee, and J.-Z. Tsai, "Development of a portable impedance detection system for monitoring the growth of mouse 1929 cells," *Journal of the Taiwan Institute of Chemical Engineers*, vol. 43, pp. 678–684, Sep 2012. 13, 15
- [42] T. Schwarzenberger, P. Wolf, M. Brischwein, R. Kleinhans, F. Demmel, A. Lechner, B. Becker, and B. Wolf, "Impedance sensor technology for cell-based assays in the framework of a high-content screening system," *Physiol. Meas.*, vol. 32, pp. 977–993, Jul 2011. 15
- [43] M.-H. Wang, M.-F. Kao, and L.-S. Jang, "Single hela and mcf-7 cell measurement using minimized impedance spectroscopy and microfluidic device," *Rev. Sci. Instrum.*, vol. 82, p. 064302, Jun 2011. 15
- [44] J. Broeders, S. Duchateau, B. Van Grinsven, W. Vanaken, M. Peeters, T. Cleij, R. Thoelen, P. Wagner, and W. De Ceuninck, "Miniaturised eight-channel impedance spectroscopy unit as sensor platform for biosensor applications," *Phys. Status Solidi A*, vol. 208, pp. 1357–1363, May 2011. 15
- [45] P. Bogonez-Franco, A. Bayes-Genis, J. Rosell, and R. Bragos, "Performance of an implantable impedance spectroscopy monitor using zigbee," *J. Phys.: Conf. Ser.*, vol. 224, p. 012163, Apr 2010. 15
- [46] J. Ferreira, F. Seoane, A. Ansedé, and R. Bragos, "Ad5933-based spectrometer for electrical bioimpedance applications," *J. Phys.: Conf. Ser.*, vol. 224, p. 012011, Apr 2010. 15
- [47] C. Margo, J. Katrib, M. Nadi, and A. Rouane, "A four-electrode low frequency impedance spectroscopy measurement system using the ad5933 measurement chip," *Physiol. Meas.*, vol. 34, pp. 391–405, Apr 2013. 15

- [48] A. Melwin and K. Rajasekaran, "Implementation of bioimpedance instrument kit in ARM7," *International Journal of Advanced Research in Computer Science and Software Engineering*, vol. 34, pp. 391–405, May 2013. 15
- [49] G. Lentka and J. Hoja, "Interface circuit for impedance sensors using two specialized single-chip microsystems," *Sensors and Actuators A: Physical*, vol. 163, pp. 191–197, Sep 2010. 15
- [50] J. Hoja and G. Lentka, "A family of new generation miniaturized impedance analyzers for technical object diagnostics," *Metrology and Measurement Systems*, vol. 20, pp. 43–52, Mar 2013. 15
- [51] K. Chabowski, T. Piasecki, A. Dzierka, and K. Nitsch, "Simple wide frequency range impedance meter based on AD5933 integrated circuit," *Metrology and Measurement Systems*, vol. 22, pp. 13–24, Feb 2015. 16, 40, 41
- [52] A. A. Al-Ali, A. S. Elwakil, A. Ahmad, and B. J. Maundy, "Design of a portable low-cost impedance analyzer," in *10th Joint Int. Conf. on Biomedical Engineering Systems and Technologies (BIOSTEC 2017) and Biomedical Electronics and Devices (BIODEVICES-2017)*, vol. 1, pp. 104–109, Feb. 2017. 16
- [53] T. Radil, P. M. Ramos, and A. C. Serra, "DSP based portable impedance measurement instrument using sine-fitting algorithms," in *2005 IEEE Instrumentation and Measurement Technology Conference Proceedings*, vol. 2, pp. 1018–1022, May 2005. 16
- [54] T. Radil, P. M. Ramos, and A. C. Serra, "Impedance measurement with sine-fitting algorithms implemented in a DSP portable device," *IEEE Transactions on Instrumentation and Measurement*, vol. 57, pp. 197–204, Jan 2008. 16

- [55] P. M. Ramos and F. M. Janeiro, "Implementation of DSP based algorithms for impedance measurements," in *IEEE Int. Conf. Signal Processing and Communications, ICSPC2007*, pp. 816–819, Nov 2007. 16
- [56] T. Piasecki, K. Chabowski, and K. Nitsch, "Design, calibration and tests of versatile low frequency impedance analyser based on ARM microcontroller," *Measurement*, vol. 91, pp. 55–161, Sep 2016. 16
- [57] V. Valente and A. Demosthenous, "Wideband fully-programmable dual-mode CMOS analogue front-end for electrical impedance spectroscopy," *Sensors*, vol. 6, pp. 1159–1179, Jul 2016. 16
- [58] C. T.-S. Ching and W.-Y. Chih, "Design and evaluation of an affordable and programmable mobile device, capable of delivering constant current and high voltage electric pulses of different waveforms for biomedical and clinical applications," *Sensors and Actuators B: Chemical*, vol. 194, pp. 361–370, Apr 2014. 16
- [59] C. T.-S. Ching, T.-P. Sun, W.-T. Huang, S.-H. Huang, C.-S. Hsiao, and K.-M. Chang, "A circuit design of a low-cost, portable and programmable electroporation device for biomedical applications," *Sensors and Actuators B: Chemical*, vol. 166, pp. 292–300, May 2012. 16
- [60] B. Maundy, A. Elwakil, and A. Allagui, "Extracting the parameters of the single-dispersion Cole bioimpedance model using a magnitude-only method," *Comput. Electron. Agric.*, vol. 119, pp. 153–157, Nov. 2015. 18
- [61] T. J. Freeborn, B. Maundy, and A. S. Elwakil, "Extracting the parameters of the double-dispersion Cole bioimpedance model from magnitude response measurements," *Medical & Biological Engineering & Computing*, vol. 52, pp. 749–758, Sep 2014. 18

- [62] S. Papezova, "Signal processing of bioimpedance equipment," *Sensors and Actuators B: Chemical*, vol. 95, pp. 328–335, Oct 2003. 18
- [63] D. D. Macdonald and M. Urquidi-Macdonald, "Application of Kramers-Kronig transforms in the analysis of electrochemical systems I. polarization resistance," *Journal of the Electrochemical Society*, vol. 132, pp. 2316–2319, Jun 1985. 18, 20
- [64] M. Urquidi-Macdonald, S. Real, and D. D. Macdonald, "Application of Kramers-Kronig transforms in the analysis of electrochemical systems II. transformations in the complex plane.," *Journal of the Electrochemical Society*, vol. 133, pp. 2018–2024, Oct 1986. 18, 20, 21, 22
- [65] S. L. Hahn, *Hilbert Transforms in Signal Processing*. Artech House, 1996. 19
- [66] R. d. L. Kronig, "On the theory of dispersion of X-rays," *Journal of the Optical Society of America*, vol. 12, no. 6, pp. 547–557, 1926. 19
- [67] F. W. King, *Hilbert transforms*, vol. 2. Cambridge University Press Cambridge, 2009. 19
- [68] M. Urquidi-Macdonald, S. Real, and D. D. Macdonald, "Applications of Kramers-Kronig transforms in the analysis of electrochemical impedance data III. stability and linearity," *Electrochimica Acta*, vol. 35, pp. 1559–1566, Oct 1990. 20, 61
- [69] H. Shih and F. Mansfeld, "Should the Kramers-Kronig transforms be used for the validation of experimental impedance data," *Corrosion*, vol. 45, no. 4, pp. 325–328, 1989. 20
- [70] H. Shih and F. Mansfeld, "Concerning the use of the Kramers-Kronig transforms for the validation of impedance data," *Corrosion Science*, vol. 28, no. 9, pp. 933–938, 1988. 20

- [71] W. Ehm, H. Gohr, R. Kaus, B. Roseler, and C. Schiller, “The evaluation of electrochemical impedance spectra using a modified logarithmic Hilbert transform,” *ACH-Models in Chemistry*, vol. 137, pp. 145–157, Jan 2000. 20
- [72] V. A. Tyagal and G. Y. Kolbasove, “Use of the Kreamers-Kronig experssions for the analysis of low-frequency impedance,” *Journal of the Electrochemical Society*, vol. 8, pp. 54–56, 1972. 20
- [73] J. M. Esteban and M. E. Orazem, “On the application of the Kramers-Kronig relations to evaluate the consistency of electrochemical impedance data,” *Journal of the Electrochemical Society*, vol. 138, pp. 67–76, Jan 1991. 20
- [74] H. W. Bode, “Relations between attenuation and phase in feedback amplifier design,” *Bell Labs Technical Journal*, vol. 19, pp. 421–454, Jul 1940. 21
- [75] H. W. Bode *et al.*, “Network analysis and feedback amplifier design,” 1945. 21
- [76] P. Grosse and V. Offermann, “Analysis of reflectance data using the Kramers–Kronig relations,” *Appl. Phys. A*, vol. 52, pp. 38–144, Feb 1991. 21
- [77] T. Pritz, “Unbounded complex modulus of viscoelastic materials and the Kramers–Kronig relations,” *J. Sound Vib.*, vol. 279, pp. 687–697, Jan 2005. 21
- [78] V. Shtrauss, “FIR Kramers–Kronig transformers for relaxation data conversion,” *Signal Processing*, vol. 86, pp. 2887–2900, Oct 2006. 21
- [79] C. Leon, J. Martin, J. Sanatamaria, J. Skarp, G. Gonzalez-Diaz, and F. Sanchez-Quesada, “Use of Kramers–Kronig transforms for the treatment of admittance spectroscopy data of p-n junctions containing traps,” *J. Appl. Phys.*, vol. 79, pp. 7830–7836, May 1996. 21
- [80] A. Al-Ali, A. Elwakil, B. Maundy, and T. Freeborn, “Extraction of phase information from magnitude-only bio-impedance measurements using a modified

- Kramers–Kronig transform,” *Circuits, Systems, and Signal Processing*, vol. DOI: 10.1007/s00034-017-0727-y, pp. 1–16, Dec 2017. 21, 61
- [81] E. Mylotta, E. Kutschera, and R. Widenhorn, “Supplemental material: Bia device description,” 38
- [82] Y. Yang and J. Wang, “A design of bioimpedance spectrometer for early detection of pressure ulcer,” in *Engineering in Medicine and Biology Society, 2005. IEEE-EMBS 2005. 27th Annual International Conference of the*, pp. 6602–6604, IEEE, Sep 2005. 38
- [83] A. Devices, *AD8302 LF to 2.7 GHz RF IF Gain and Phase Detector*, Jul 2002. Rev. A. 38
- [84] A. A. Al-Ali, B. J. Maundy, and A. S. Elwakil, “Design and implementation of a bio-impedance analyzer based on the kramers-kronig transform,” in *2018 IEEE International Symposium on Circuits and Systems (ISCAS) (Accepted)*, May 2018. 39
- [85] A. Devices, *AD9850 CMOS 125 MHz Complete DDS Synthesizer*, Feb 2004. 39
- [86] M. Newville, T. Stensitzki, D. B. Allen, and A. Ingargiola, “LMFIT: Non-Linear Least-Square Minimization and Curve-Fitting for Python,” Sep 2014. 45
- [87] S. Freescale, *Kinetis K66 Sub-Family 180 MHz ARM® Cortex®-M4F Microcontroller.*, Jan 2016. 48, 51
- [88] B. brown Products from Texas instruments, *OPA3355 200MHz, CMOS OPERATIONAL AMPLIFIER WITH SHUTDOWN*, Jan 2004. 51
- [89] T. instuments, *TS5A3357 SINGLE 5- \hat{I} © SP3T ANALOG SWITCH 5-V/3.3-V 3:1 MULTIPLEXER/DEMULTIPLEXER*, Dec 2007. 51

- [90] T. J. Freeborn, A. S. Elwakil, and B. J. Maundy, “Electrode location impact on cole-impedance parameters using magnitude-only measurements,” in *IEEE 59th Int. Midwest Symposium on Circuits and Systems (MWSCAS)*, vol. 1, pp. 21–24, IEEE, Jul 2016. 68

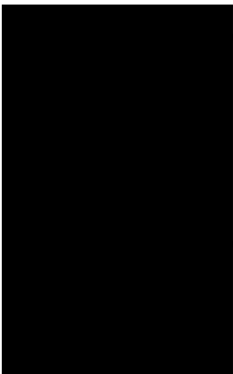
APPENDIX A

Appendix 1

SPRINGER NATURE LICENSE
TERMS AND CONDITIONS

Apr 16, 2018

This Agreement between Abdulwadood Alali ("You") and Springer Nature ("Springer Nature") consists of your license details and the terms and conditions provided by Springer Nature and Copyright Clearance Center.

License Number	4331110608642
License date	Apr 16, 2018
Licensed Content Publisher	Springer Nature
Licensed Content Publication	Circuits, Systems and Signal Processing
Licensed Content Title	Extraction of Phase Information from Magnitude-Only Bio-impedance Measurements Using a Modified Kramers-Kronig Transform
Licensed Content Author	A. A. Al-Ali, A. S. Elwakil, B. J. Maundy et al
Licensed Content Date	Jan 1, 2017
Type of Use	Thesis/Dissertation
Requestor type	academic/university or research institute
Format	print and electronic
Portion	full article/chapter
Will you be translating?	no
Circulation/distribution	>50,000
Author of this Springer Nature content	yes
Title	Design and Implementation of a Magnitude Only Bio-Impedance Analyzer
Instructor name	Brent Maundy
Institution name	University of Calgary
Expected presentation date	Apr 2018
Requestor Location	
Billing Type	
Billing Address	
Total	0.00 CAD

Terms and Conditions

Springer Nature Terms and Conditions for RightsLink Permissions
Springer Customer Service Centre GmbH (the Licensor) hereby grants you a non-exclusive, world-wide licence to reproduce the material and for the purpose and